Statistical study of the errors arising from plasma reconstruction using inverse equilibrium for the TCV tokamak.

By: Mikhail Kibalchenko

Project supervisor: Jean-Marc Moret

23/06/2005

In the TCV tokamak the plasma shapes for each shot are reconstructed by inverse equilibrium using the magnetic measurements. The quality and the reliability of the results produced depend substantially on a good knowledge of the experimental errors. In this project these errors were studied statistically by taking the differences between the direct measurements and the fitted values generated by the inverse equilibrium. The results were used to propose modifications to the parameterisation of the inverse equilibrium. Modifications were made by removing some sensors from the reconstruction, and applying specific weights to each sensor. The z position in the plasma's magnetic axis was found to vary by as much as 0.5 cm compared to the standard reconstruction.

Dans le TCV tokamak la forme de plasma pour chaque shot est déduite de l'équilibre inverse en utilisant les mesures du champ magnétique. La qualité et la fiabilité des résultats qu'elle produit dépend intimement d'une bonne connaissance des erreurs expérimentales. Dans ce travail ces erreurs ont été déduites de l'écart entre les mesures et les valeurs fournies par l'équilibre inverse. Pour la modification de l'équilibre inverse, quelques senseurs ont été enlevés, et les poids des senseurs ont été changés. La nouvelle position z de l'axe magnétique a été changée au maximum de 0.5 cm en comparaison avec l'équilibre standard.

Table of contents

1. Introduction

A tokamak: toroidalnaya kamera & magnitnay katushka (Russian) consists of magnetic coils wound around a torus shaped vacuum vessel. Gas is pumped inside the vessel and heated until the electrons become free of the atoms such that the resultant ionised gas (plasma) contains only ions and electrons. The toroidal [section 2.1] current is induced inside the plasma to create a poloidal [section 2.1] magnetic field around the plasma to help keep the plasma stable. The toroidal magnetic field from the external coils combines with the poloidal magnetic field from the current inside the plasma to keep the plasma magnetically confined inside the vacuum vessel.

Many experiments are carried out in tokamaks worldwide. The aim is to research plasma sufficiently to be able to build a reliable power producing system. Lithium with deuterium could be used as the gas and long enough confinement in the ionised state would lead to ignition and production of very large amounts of energy, a process which is called thermonuclear fusion.

The aim of the TCV (tokamak à configuration variable) tokamak is to search for improvement in plasma performance by studying different shapes of plasma. To serve this purpose the vacuum vessel has an almost rectangular cross-section with a large number of diagnostics and coils to measure and control the plasma shape [Figure 1]. This enables the production of highly elongated plasmas as well as highly complicated plasma configurations, for example plasma with two magnetic axes. Research into plasma heating by methods of Electron Cyclotron Resonance Heating (ECRH) and current inductance in the plasma by Electron Cyclotron Current Drive (ECCD) is also undertaken at TCV.

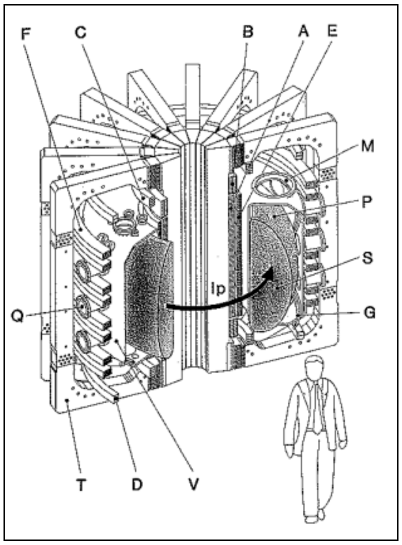

Figure 1: TCV cross-section[1]:

A: Ohmic transformer coil, B-F: poloidal field coils for plasma shaping, G: internal poloidal field coil for fast position control, M: large port for maintenance access, Q: diagnostic ports, P: highly elongated plasma with current Ip , S: hot central region of the plasma, T: toroidal field coils, V: vacuum vessel.

---

[1] Picture and caption from CRPP website (http://crppwww.epfl.ch/tcv/parameters.html)

For each successful TCV experiment (shot) the data from all diagnostics systems is stored. By solving the Magneto Hydro Dynamic (MHD) equations using the magnetic measurements, the plasma equilibrium inside the vacuum vessel is reconstructed. The reconstruction provides us with the shape of the plasma from which plasma properties can be calculated.

The solution to the plasma equilibrium reconstruction using the magnetic measurements is not unique since the equation to be solved is non-linear and mathematically ill conditioned and also because measurements are subject to errors.

A more accurate solution can be found by including measurements of other physical quantities, for example by using diamagnetic measurements to derive the plasma pressure [1], using soft X-ray emissions from the plasma [2], or Faraday rotation measurements through the plasma [5]. These however are very complex and are difficult to achieve and thus are not systematically used.

The aim of this project is to attempt to improve the reconstruction accuracy by fine tuning of the reconstruction code. The quality and reliability of the reconstructed results depend intimately on a good knowledge of the experimental errors in the magnetic measurements. To get a better understanding of these errors, I will be studying the differences between the measurements and the reconstructed data from many shots already carried out at the TCV. This will help me to propose modifications to the inverse equilibrium reconstruction.

Section 2 introduces the technical details necessary for this project. Section 3 presents and discusses the work carried out. And section 4 concludes on this project.

2. Technical Details

2.1 Sensor details

TCV is equipped with a large number of diagnostics. In this project the data were used only from the magnetic sensors described below. There are two field orientations within the tokamak vessel. The toroidal field is a circular vector field about the z-axis of the vessel (the current, Ip, in Figure 1 is running toroidally). The poloidal field is a vector field around the cross-section of the vessel with a component along the z-axis of the vessel. The magnetic field due to the toroidal current Ip in Figure 1 would be a poloidal field. The vessel is donut shaped, with the empty space inside the donut referred to as inner board and the outer area of the donut referred to as outer board.

2.1.1 Current sensors in the poloidal field coils

Flexible control over the shape of the plasma is achieved by sixteen coils that follow a toroidal path around the vacuum vessel. Eight are positioned inner board of the vessel and eight outer board of the vessel labelled E1 to E8 and F1 to F8 respectively [Figure 2]. The current in the coils induces a poloidal magnetic field which shapes the plasma. Coil A powered by the power supply OH1 creates an electric field inside the vessel that inductively drives the current within the plasma. Coils B1, B2, C1, C2, D1 and D2 [Figure 2] powered in series by OH2 power supply cancel out the small magnetic field inside the vessel created by coil A. Surrounding these coils, another 16 coils running poloidally around the vacuum vessel produce the toroidal magnetic field needed to confine the plasma [labelled T in Figure 1]. LEM modules are used to measure the coil currents [3]. The current sensors have a typical measurement error of 50 A [3].

2.1.2 Poloidal magnetic field probes

The study of a wide range of plasma shapes requires a high density of magnetic sensors with a good spatial coverage. 38 magnetic probes positioned evenly inside the vessel chamber [Figure 2] measure the component of the poloidal magnetic field. TCV has four such 38 probe arrays positioned 90° toroidally from each other. The probes are in sector 3 and opposite sector 11, sector 7 and opposite sector 15. The signals from sector 3 and 11 are averaged and used for real-time control. Measurements from sector 3 are used in equilibrium reconstruction. Each probe consists of a single layer of 10 turns of wire wound around a moulded ceramic core [3]. Accuracy of 1 mT in the measurement of the poloidal magnetic field with a position error of a few mm has been achieved [3].

2.1.3 Poloidal magnetic flux loops

38 flux loops wound toroidally inner board and outer board of the vacuum vessel measure the poloidal magnetic flux going through the loop. Each flux loop is paired with a magnetic probe [Figure 2] to enable the calculation of the extrapolation of flux towards the plasma boundary [3]. Some loops have to bypass the ports around the vessel and therefore do not have a constant radius. Loops #10-12 and #28-30 are partial loops because of the presence of large ports at the top and the bottom of the vessel. These six loops do not measure the full poloidal flux but the flux difference between neighbouring loops [4]. The poloidal flux from loop #1 covering the inner board midsection of the vessel is subtracted from the other loops (except the six partial loops) to cancel out the dominating magnetic flux from the coil A that is on the inside of the vessel. This maintains good dynamic range in the amplifying electronics and data acquisition [4]. Accuracy of 0.5 mWb in the measurement of the poloidal magnetic flux has been achieved [3].

2.2 Inverse equilibrium reconstruction

After each shot it is necessary to reconstruct the equilibrium of the plasma from the sensor data. The reconstruction is necessary to calculate the properties of the plasma that was created.

At TCV an in-house equilibrium reconstruction algorithm is used, it is called “LIUQE”. The reconstruction is a complicated problem: firstly, mathematically it is a non-linear problem that is solved by an iterative method; secondly it is further complicated by the fact that measurements are subject to error, giving us no unique solution. The steps in the algorithm are outlined below [5], this procedure is called the inverse equilibrium reconstruction:

a) The cross-section of the tokamak vessel where plasma was supposed to be is divided into six sections. In each of these sections the current in the plasma is approximately fitted to agree with the magnetic measurements. This method is called fast magneto-static method [6], [7]. It gives a rough approximation of the plasma current distribution.

b) Knowing the plasma current distribution, the flux $\psi(R,Z)$, where $\psi(R,Z) \equiv RA_\varphi$ is the poloidal magnetic flux through a circle defined by point (R,Z), is found. The last closed flux surface (LCFS) is worked out by either finding the X-point of the plasma or finding the flux contour nearest to the vessel wall. The TT' and p' source functions are assumed to be sums of polynomials, where $T = T(\psi) \equiv RB_\varphi$ is related to current distribution, $T' = \frac{\partial T}{\partial \psi}$, $p = p(\psi)$ is the plasma pressure and $p' = \frac{\partial p}{\partial \psi}$ with φ describing a vector field in the toroidal direction. The LCFS is used as the boundary condition in the Grad-Shafranov equation [Equation 1] for the fitting of the coefficients for TT' and p'.

$$\mu_0 p' = -R^{-2}\frac{\partial^2 \psi}{\partial Z^2} - R^{-1}\frac{\partial}{\partial R}\left(R^{-1}\frac{\partial \psi}{\partial R}\right) - \frac{TT'}{R^2}$$

Equation 1: The Grad-Shafranov equation, derived from MHD equations

c) The fitted TT' and p' values are used to work out the toroidal plasma current density [Equation 2].

$$j_\varphi(R,Z) = Rp' + \frac{TT'}{\mu_0 R}$$

Equation 2: Toroidal plasma current density equation

d) From the plasma current distribution $j_\varphi(R,Z)$ other variables are calculated. The goodness of the reconstructed results is checked by calculating root square mean (RMS) error χ using the cost function [Equation 3].

$$\chi^2 = \sum_m \left(\frac{\hat{B}_m - B_m}{\Delta B_m}\right)^2 + \sum_f \left(\frac{\hat{\psi}_f - \psi_f}{\Delta \psi_f}\right)^2 + \sum_n \left(\frac{\hat{I}_n - I_n}{\Delta I_n}\right)^2$$

Equation 3: Cost function to calculate RMS

Where $\hat{B}_m$ is the fitted magnetic field value, B_m is the measured value, ΔB_m is the inverse of the weight given to that sensor, ψ_f is the magnetic flux and I_n is the current in the coils.

Steps b), c) and d) are repeated until χ reaches the desired conversion.

An example reconstruction can be seen in Figure 2 with flux contours reconstructed for shot #12868 at the time 0.72 seconds.

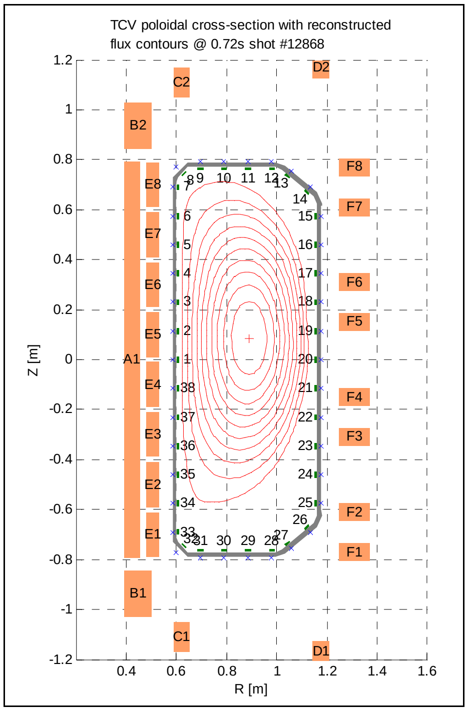

Figure 2: Poloidal cross-section of TCV's vacuum vessel showing current coils, poloidal flux loops (x) and poloidal magnetic probes as rectangles inside the vessel. The flux contours of the plasma have been reconstructed using LIUQE.

2.3 Database details

The data from all diagnostics systems for each successful TCV experiment (shot) are stored in MDS tree database. To analyse the errors for the purpose of this project, specific diagnostic measurements were converted into a Matlab database. The database contained data of 5804 shots for the following variables [Table 1].

Table 1: Variables in the Matlab database.

Variable	Description
BPOL_003	38 probes measuring poloidal magnetic field in sector 3 [T]
BPOL_011	38 probes measuring poloidal magnetic field in sector 11 [T]
B_FIELD_FIT	Fitted magnetic field for the 38 probes in sector 3 [T]
BERR	Weight for the magnetic field probes ΔB_m^{-1} [T]
IPOL	Current for the 16 poloidal coils and OH1, OH2 coils [A]
IPOL_FIT	Fitted current for the 16 poloidal coils and OH1, OH2 coils [A]
CERR	Weight for the current sensors ΔI_n^{-1} [kA]
RFLUX	Relative magnetic flux through the 37 loops [Wb]
PSI_FIT	Fitted magnetic flux for the 37 loops [Wb]
FERR	Weight for the flux loops $\Delta \psi_f^{-1}$ [Wb]
TIME	Time of each sample [s]
SHOT	Shot number

Each variable is a table, with different number of columns but the same number of rows. The columns represent each sensor and rows contain measurements for each time sample. SHOT table and TIME table are supplementary tables to link each measurement (row) from other tables to a shot number and a time instance. TIME table contains one column with a time instant in each row, such that if we take data from the 10th row in the BPOL_003 table, we can see at what time instant it occurs by looking at the 10th row of TIME table, and to which shot the time and the measurements correspond by looking at the same row in the SHOT table. Variables contain time samples separated by 0.05 seconds.

3. Analysis

3.1 Preliminary data outlook

The difference was taken between the measurements of the BPOL_003 probes, the RFLUX loops and the IPOL sensors with the corresponding fitted data B_FIELD_FIT, PSI_FIT and IPOL_FIT. These differences will also be referred to as errors between the experimental and fitted values. The difference was also taken between the BPOL_011 probes which measure the poloidal magnetic field in the 11th sector and the B_FIELD_FIT, which contains fitted poloidal magnetic field measurements for the BPOL probes in the 3rd sector. Physically and geometrically the data from BPOL_003 and BPOL_011 should be very similar and by taking the difference for 11th sector with the fitted 3rd sector it will be possible to see any asymmetries created due to measurement errors in the magnetic probes or other sources.

To get a general overview of the differences and to see the occurrence frequency of magnitudes of errors, the differences for each sensor were plotted on a histogram. To enable comparison between sensors, the range was fixed for sensors within each group by the maximum and minimum difference value in the group.

It was expected that the peaks in the histograms would be of a Gaussian distribution centred about zero. The assumption that the errors would follow a Gaussian distribution is based on the Central Limit Theorem which states that the mean of any set of variates with any distribution having a finite mean and variance tends to the Gaussian distribution.

The histograms for the 4 groups of sensors showed distributions roughly centred about zero mostly with one peak, but two or more peaks were also present. The range set by the minimum and the maximum values within each sensor group was much larger than expected with the reason for such a range not visible in the histograms. The reason was not visible because the frequencies about zero were much higher than the comparably tiny frequencies of differences that set the range. The difference in frequencies can be seen in Figure 3 for BPOL_003 probe #1 positioned in the middle of the inner wall of the vessel.

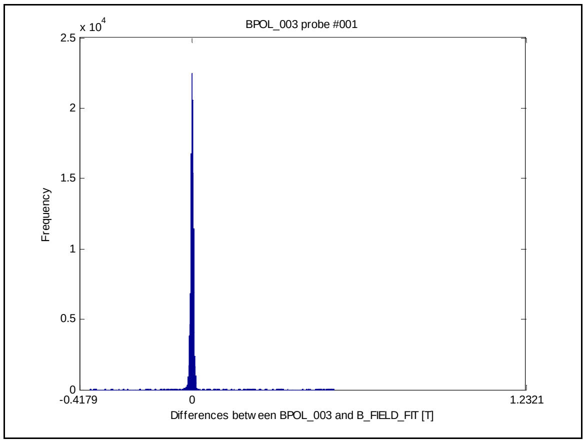

Figure 3: Histogram for the BPOL_003 #1 probe showing the large frequency of the peak and small not visible frequencies around the peak.

To see the smaller frequencies occurring further out from zero the graphs were re-plotted for all the 4 groups of sensors with y-scale reduced while keeping the x-scale range constant for each group. For all the sensor groups small frequencies of outliers were visible. Figure 4 shows the histogram with reduced y-scale for the BPOL_003 probe #1 clearly showing the relatively small frequencies of outliers present around the peak.

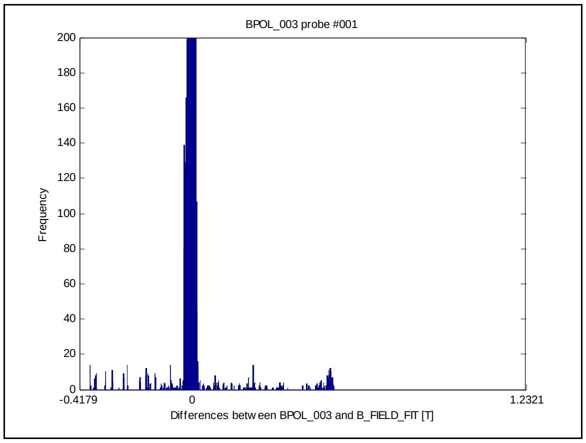

Figure 4: Histogram with reduced y-scale for the BPOL_003 #1 probe clearly showing the outliers around the peak.

In the BPOL_003 group of sensors, the probe #37 [Figure 5] had a very wide peak with a lot of noise around the peak. Comparing the histogram to the others in BPOL_003 it is rather clear that this probe is malfunctioning in the measurements that it takes.

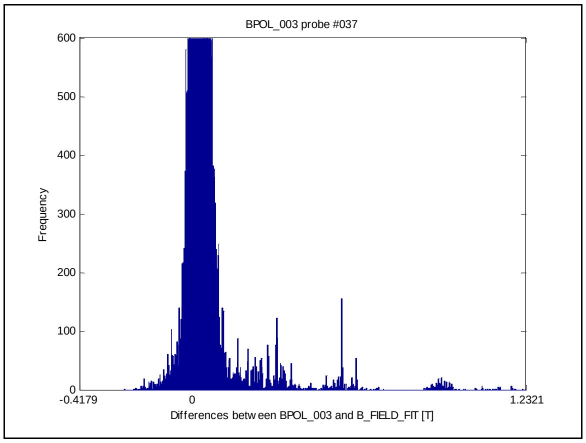

Figure 5: Histogram with reduced y-scale for the BPOL_003 #37 probe showing malfunction in the measurements by this probe.

For the RFLUX group of sensors, the partial loops #10-12 at the top of the vessel, and partial loops #28-30 at the bottom of the vessel show a very noisy distribution compared to the other loops in the group. Figure 6 compares the partial loop #12 with the complete loop #13. The reason for such a difference between the two signals is because 31 RFLUX loops are relative fluxes to loop #1. Subtracting loop #1 from the other loops (37 loops - 6 partial loops = 31 loops) subtracts the dominating magnetic flux signal from coil A which is used to induce the current inside the plasma. The partial loops are the only 6 loops from which loop #1 is not subtracted. The noisy difference is due to the added measurement of the flux from coil A and due to their complicated and far imperfect paths around the ports which they have to bypass.

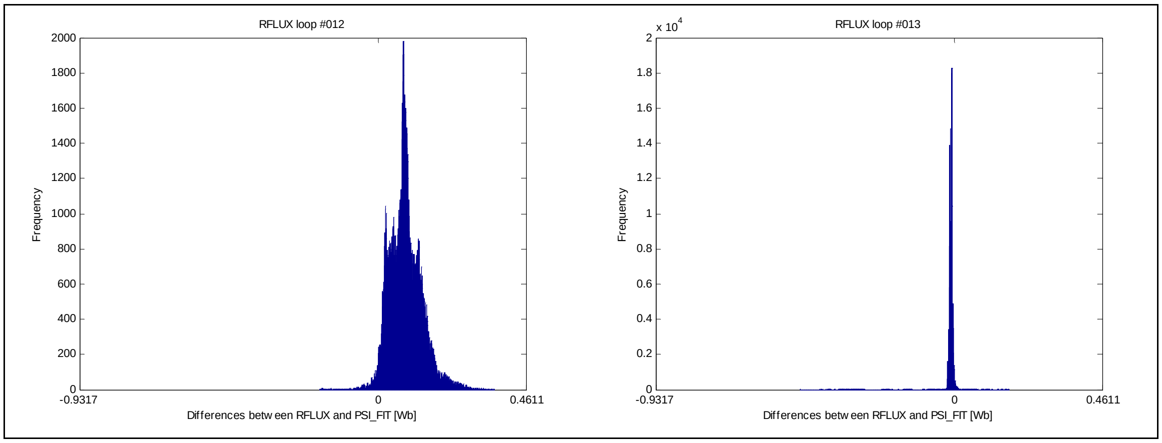

Figure 6: Comparison of the distributions for the partial loop #12 at the top of the vessel and the complete loop #13 next to it.

3.2 Data pre-processing

The low frequencies occurring around the main distributions seen in the magnified histograms were classified as outliers. A lot of outliers were found to be due to acquisition systems registering zeros, such that when the corresponding fitted values are subtracted, large differences occur. Other possible explanations for outliers could be electronic glitches and rare sensor failures. Outliers did not have a systematic pattern leading to a conclusion that they were due to random errors.

To be able to carry out accurate data analysis it was necessary as in every experiment to pre-process the data to remove any anomalous data. To remove outliers, database samples where the differences between experimental and fitted data more than 3 standard deviations away from the mean difference for each sensor were found and removed. After the data pre-processing the size of the database was reduced by 19% to contain data from 5346 shots.

3.3 Data outlook after pre-processing

The histograms were re-plotted with the x-axis range once again set by the minimum and the maximum values within a sensor group. On each plot the mean (μ) and the standard deviation (σ) were calculated and displayed to know exactly where the average of the distribution lies and what the spread is.

For the BPOL_003, BPOL_011, RFLUX and IPOL histograms the range was reduced by a factor of 4, 10, 2 and 36 respectively. The reason BPOL_003 was reduced less than the BPOL_011 is because of the malfunctioning probe #37 in BPOL_003, minimum and maximum values of which set the range for the whole BPOL_003 group. The RFLUX range was still dominated by the noisy signals from loops #10-12 and #28-30, which resulted in a small range reduction. The substantial range reduction for the IPOL could be due to the large currents inside the coils. The current reaches 7kA in the shaping coils and 23kA in the OH1 and OH2 coils. This could explain the small frequencies of very large differences.

The smaller range enabled a clearer view of the cases with multiple peaks. Histograms for BPOL_003 and BPOL_011 had almost half the sensors showing two peaks [Figure 7]. The RFLUX histograms had plots with at least 2 peaks as well as cases with more than 3 peaks. For IPOL sensors, only three histograms contained 2 peaks [Figure 8], while the rest showed close Gaussian distributions.

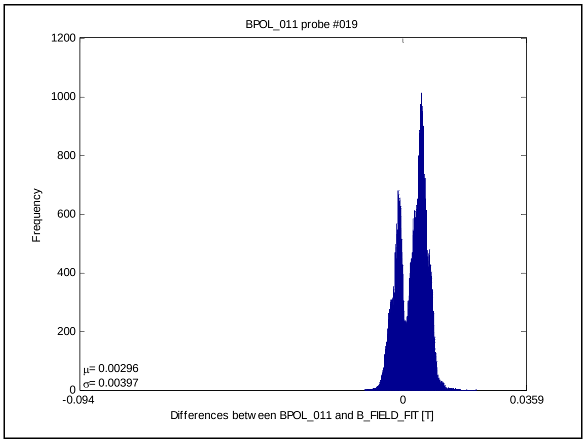

Figure 7: Magnetic probe #19 showing a typical 2 peaked example distribution for BPOL_011 after data pre-processing.

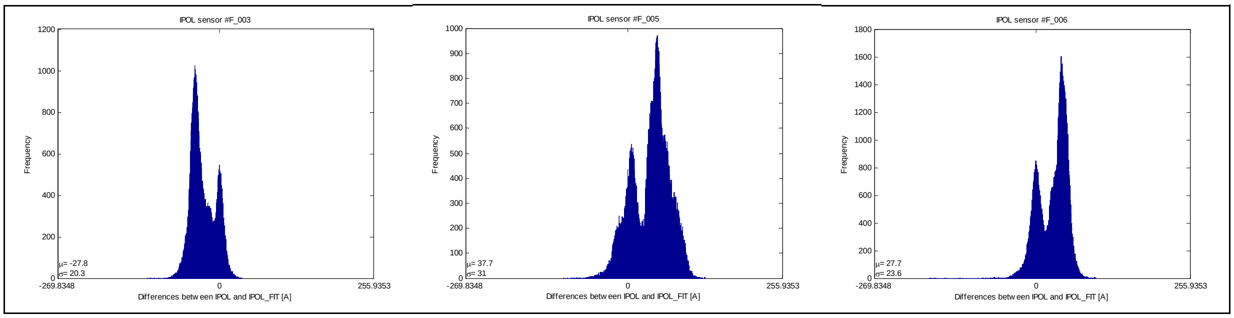

Figure 8: Only 3 histograms in IPOL group of sensors contained 2 peaked distributions.

To check the closeness of each distribution of differences to the assumed Gaussian distribution, a Gaussian curve [Equation 4] was superimposed onto each histogram using the calculated μ and σ values and scaled to the maximum frequency of the histogram. The 3rd and 4th normalised moments of a Gaussian, skewness [Equation 5] and kurtosis [Equation 6] were also calculated for each plot. Skewness characterises the asymmetry of the distribution about its mean. The positive value of skewness indicates distribution with an asymmetric tail extending towards positive values, and vice versa. Kurtosis measures the relative peakedness or flatness compared to a Gaussian distribution, positive kurtosis indicates a relatively peaked distribution, and vice versa.

$$y = y_{\max} e^{-(x-\mu)^2/(2\sigma^2)}$$

Equation 4: Gaussian distribution equation, where ymax is the maximum frequency.

$$F'(3) = \frac{\int y \times (x-\mu)^3 dx}{\sigma^3 \int y dx}$$

Equation 5: Normalised skewness equation.

$$F'(4) = \frac{\int y \times (x-\mu)^4 dx}{\sigma^4 \int y dx} - 3$$

Equation 6: Normalised kurtosis equation.

For an exact Gaussian distribution F'(3) and F'(4) are equal to zero. Analysing these values for all the sensors would allow us to see which have Gaussian distribution of errors and which do not.

For the BPOL_003 sensor group the probes have distributions with means centred about zeros, randomly varying between positive and negative values, all within |0.01| T [appendix Figure 29], which is rather large relative to the magnetic fields measured and to the measurement accuracy of 0.001 T. The standard deviations are of order 0.005 T. The skewness is close to zero for each probe, indicating an almost symmetrical distribution, randomly varying between slight negative or positive asymmetry. The values for kurtosis show that most of the probes have slightly more peaked distributions compared to a Gaussian, with 3 probes, #13, #18, #21, more peaked than the others [appendix Figure 30, all results in appendix Table 6]. Figure 9 shows an example for probes #10 (a Gaussian distribution) and #25 (a 2 peaked distribution).

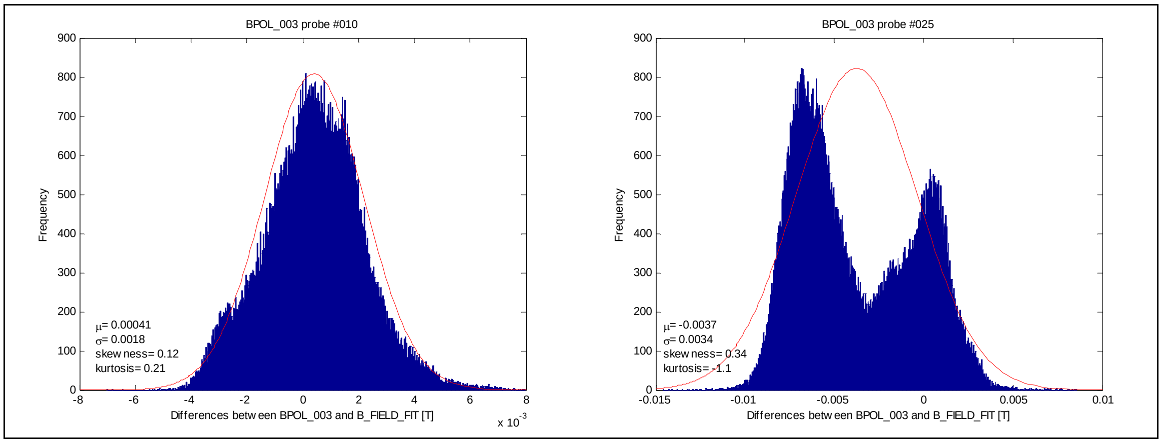

Figure 9: BPOL_003 probes #10 showing a good Gaussian distribution and #25 showing a 2 peaked distribution.

The difference distributions for BPOL_011 have the same spread of mean values and the same order of standard deviations as for the probes from BPOL_003 [appendix Figure 31]. The skewness for all the probes is closer to zero than for the BPOL_003 probes, indicating that the distributions are more symmetrical. The kurtosis values show that the peakedness of the distributions for the probes are very close to a Gaussian distribution, with probes #3, #34, #36 being much more peaked than a Gaussian [appendix Figure 32, all results in appendix Table 7].

For the RFLUX loops, the means are very close to zero (~0.001 Wb). The standard deviations are low and are of the same order [appendix Figure 33]. The skewness and the kurtosis are of the same order very close to zero indicating Gaussian distributions [appendix Figure 34]. Figure 10 shows a typical example for RFLUX loops, #15 with two peaks and #26 with a multiple number of peaks. The results for the partial loops differ from the values of the other loops, with higher values for means and standard deviations, but with the same skewness and kurtosis values. Loops #25 and #33, have means and standard deviations the same as the other loops, but compared to the other loops have abnormally large positive kurtosis and abnormally large negative skewness [all results in appendix Table 8].

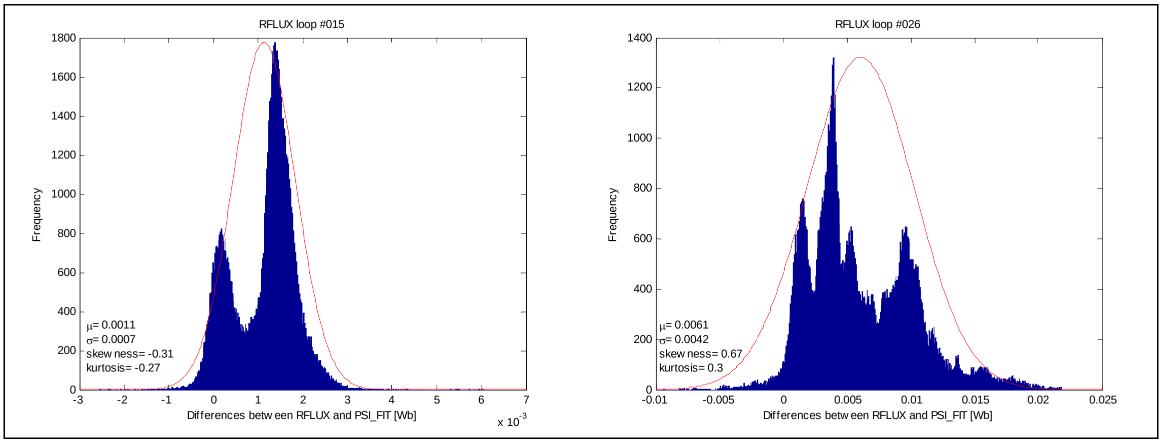

Figure 10: Typical examples for RFLUX loops, #15 a 2 peaked distribution and #26 a multiple peak distribution.

The IPOL distributions have means spread randomly within |100| A and standard deviations within the same range [appendix Figure 35]. IPOL distributions are relatively closer to a Gaussian than the other groups of sensors, with majority of skewnesses and kurtosises lying within |0.5| [appendix Figure 36]. Sensors #F_001 and #F_002 have kurtosis of about 3, much larger than the other sensors, but compared to the other groups still relatively small [all results in appendix Table 9].

For all the sensors, the distributions were close to Gaussian distributions, but it was unexpected to find so many sensors showing their error distributions as a superposition of 2 or more Gaussians. The reason for each peak must correspond to a set of shots, each characterised by some physical parameter. As a continuation to this work, it would be interesting to identify these parameters and explain why only 3 of all IPOL sensors have two peaks, why so many BPOLs have two peaked examples but some have just one peak, and why some RFLUX histograms consist of more than two peaks and the others just of 2 peaks.

3.4 Correlation Study

In the LIUQE code it is assumed that the errors between each sensor are uncorrelated. When the convergence criteria is checked by calculating the cost function χ squared [Equation 3], it is assumed that the data for which χ squared is calculated is independent. This assumption was never investigated and if studied, the results could be used to improve the code, since correlated data cannot be neglected. A cross-correlation matrix was calculated using Equation 7 for all sensors to see if the differences between the experimental and the fitted data are correlated between the sensors.

$$R(i,j) = \frac{\mathrm{cov}(i,j)}{\sqrt{\mathrm{cov}(i,i)\,\mathrm{cov}(j,j)}}, \qquad \mathrm{cov}(x_1,x_2) = E[(x_1-\mu_1)(x_2-\mu_2)]$$

Where E is the mathematical expectation and $\mu_i = E[x_i]$

Equation 7: The formula used to calculate the matrix of correlation coefficients between each sensor.

A correlation coefficient of zero between errors in two sensors would mean that there is no correlation and therefore the errors happen at different time instances. A positive or negative correlation would mean that the errors in two sensors happen at the same time.

The calculated matrix can be seen in appendix Figure 37, Figure 38 and Figure 39. The strong correlations present in this matrix were studied, and by strong correlations it is meant coefficients larger than |0.7|.

3.4.1 Correlations within each sensor group

Strong positive and negative correlations were present in the errors for the probes in the BPOL_003 group and even stronger correlations for the probes in the BPOL_011 group [appendix Figure 37]. This could be because the probes are positioned close to each other, that they measure similar magnetic fields and thus have similar errors. If the plasma for all shots was in the middle of the vessel, we would be seeing symmetry in the correlations. The symmetry however cannot be seen, since for most shots the plasma is in the upper part of the vessel. To study the correlations within the magnetic probes closer, it would be necessary to create many identical plasmas at the top of the vessel and see where the correlations are. Then moving the plasma lower, the correlations should move to the lower probes.

For the RFLUX loops [appendix Figure 39], some random but rare correlations were present. Strong positive correlations were present between the 6 partial loops. This is to be expected, since they are dominated by the magnetic flux from coil A inner board of the vessel.

For the IPOL sensors [appendix Figure 39], no correlation was present except for the seven sensors measuring the current in the E1, E2, E3, E6, E8, F7 and F8 coils. The errors in these sensors strongly correlate, some positively and some negatively between each other. The position of these coils is almost symmetrical inner board of the vessel, but sensors for coils F8 and F7 fall out of this symmetry [Figure 11]. The reason for the correlations in the errors between these coils could be that they were used more than the others to control the shape of the plasma, and perhaps produced similar fields.

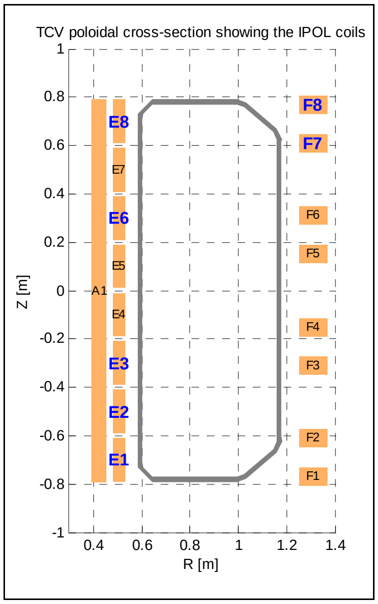

Figure 11: 7 sensors for poloidal field coils (blue), errors in which correlated strongly with each other.

3.4.2 Correlations between sensor groups

Errors in the BPOL_003 probes correlated strongly with the BPOL_011 probes [appendix Figure 37]. This is to be expected since the fitted values are only for sector 3 magnetic probes. When the fitted values are subtracted from both the BPOL_003 and BPOL_011 the trends would be similar and resultant values would correlate.

Errors in loops #15 and #24 from RFLUX correlated strongly, both positively and negatively with BPOL_003 probes [appendix Figure 38] (and obviously BPOL_011 for the reason mentioned above). Loop #15 positioned outer board on the upper part of the vessel correlated strongly with probes #5, 12, 26, 27, 28, 33, 34 and 36. While loop #24 outer board of the vessel but 1 meter lower, correlated with probes #2, 5, 6, 8, 12, 13, 20, 23, 24, 25, 26, 28, 30, 33 and 38. The probes #23-36 are at the bottom of the vessel and probes #5-16 at the top of the vessel. The flux loops #15 and #24 do not measure the full poloidal flux and no explanation can be given to why they correlate with the magnetic probes. Although it should be noted that they are positioned almost symmetrically to the midsection of the vessel, and the magnetic probes that they correlate with are in similar positions.

Looking at the correlation coefficients between BPOL_003 and IPOL [appendix Figure 38] we can see that probe #7 does not correlate with any other probes but does correlate with eleven RFLUX loops, and also strongly correlates with seven IPOL sensors, E1, E2, E3, E5, E6, E8 and F8. IPOL sensors F3, F5, F6 and F7 also show strong correlation in errors with 13, 6, 16 and 7 BPOL_003 probes respectively. This is analysed in more details in section 3.4.3.

Strong correlations occured between the RFLUX loops and the IPOL sensors [appendix Figure 39]. Each of the loops #2, 3, 5, 6, 8, 15, 21, 23, 32, 37 and 38 correlated strongly with almost half the IPOL sensors, with loop #38 correlating with the most. These loops are positioned around the midsection of the vessel, both inner and outer board of the vessel. The nature of the correlations must be the same for each loop. Loop #38 correlated with the most IPOL sensors, and if an explanation is found to the correlation, then it would also apply to the correlations by the other loops, this is studied in section 3.4.4.

3.4.3 Closer study of the BPOL_003 probe #7 correlation with IPOL sensors

The purpose of this closer analysis into the correlation between the BPOL_003 probe #7 and seven IPOL sensors was to explain it. When each IPOL coil has current in it, it creates a poloidal magnetic field to control the shape of the plasma. During each shot, the probes measure the poloidal magnetic field from the current in the plasma as well as contribution from the shaping coils. Therefore if the contribution to the 7th probe from the shaping coils is large enough, it would explain the resulting correlation in errors.

The 7th BPOL_003 probe strongly correlated with E1, E2, E3, E5, E6, E8 and F8 IPOL sensors and #2, 3, 5, 6, 8, 21, 23, 32, 35, 37 and 38 RFLUX loops [Figure 12].

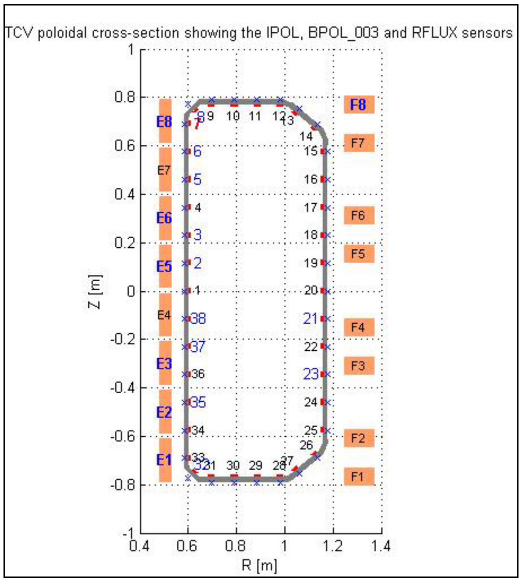

Figure 12: Position of the 7th BPOL_003 probe (red (top left of vessel)) which correlated with 11 RFLUX loops (blue) and 7 IPOL sensors (bold blue).

As can be seen from Figure 12 the probe correlates with errors in the current coils which are positioned mostly inner board of the vessel and one outer board. The positions of RFLUX loops with which it also correlates seem to be in a random order around the vacuum vessel.

One can compute the amount of magnetic field measured by each BPOL probe due to 1A current in each of the poloidal coils. These quantities were available from the TCV configuration. To compare the amount of magnetic field registered by the 7th probe and the correlations with the coils, both quantities were plotted [Figure 13].

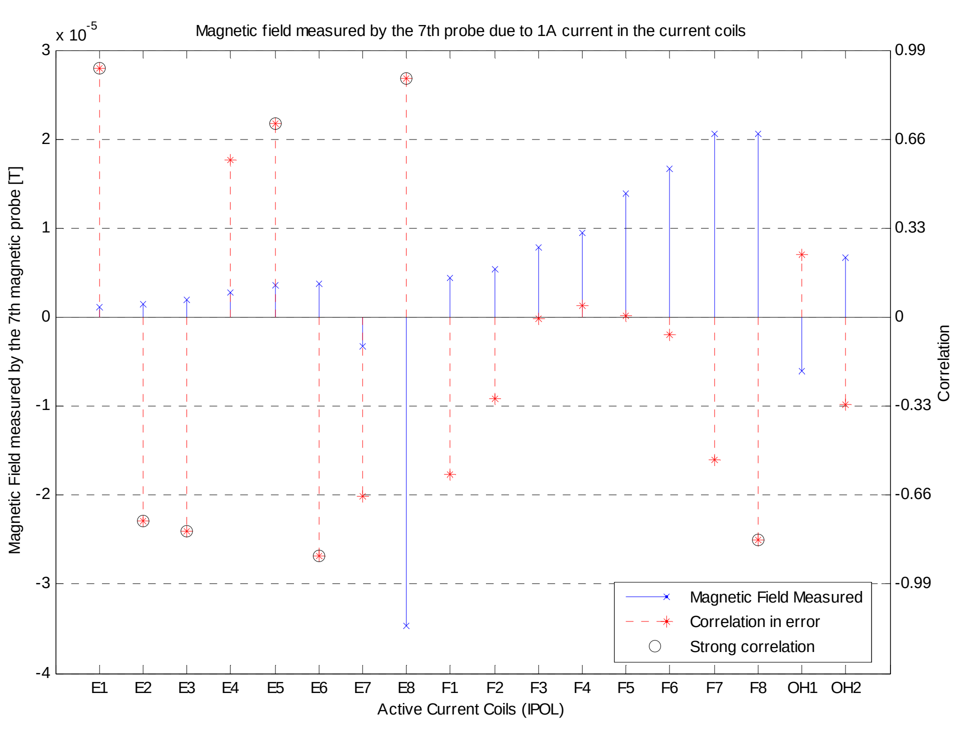

Figure 13: Graph compares the correlation coefficient between the 7th BPOL_003 probe and IPOL sensors, and the magnetic field measured by this probe due to 1A current in each of the IPOL coils.

From the graph we can see that the magnetic field measured by the probe due to the E8 IPOL coil is high and negative since they are positioned in the same locality of the vessel. The correlation between their errors however is strong but positive. This correlation cannot be explained by using the magnetic field measurement value due to coil E8, since the signs do not match.

The same is true for coil F8, where the measurement is high and positive, and the correlation is strong but negative.

The high correlations with the other 5 coils cannot be explained either, since the magnetic field registered due to those coils is very low.

To confirm that there were no physical correlations between the 7th BPOL_003 and the IPOL coils, a correlation matrix for the experimental data was calculated. Figure 14 compares the correlation matrix for the errors and for the experimental data.

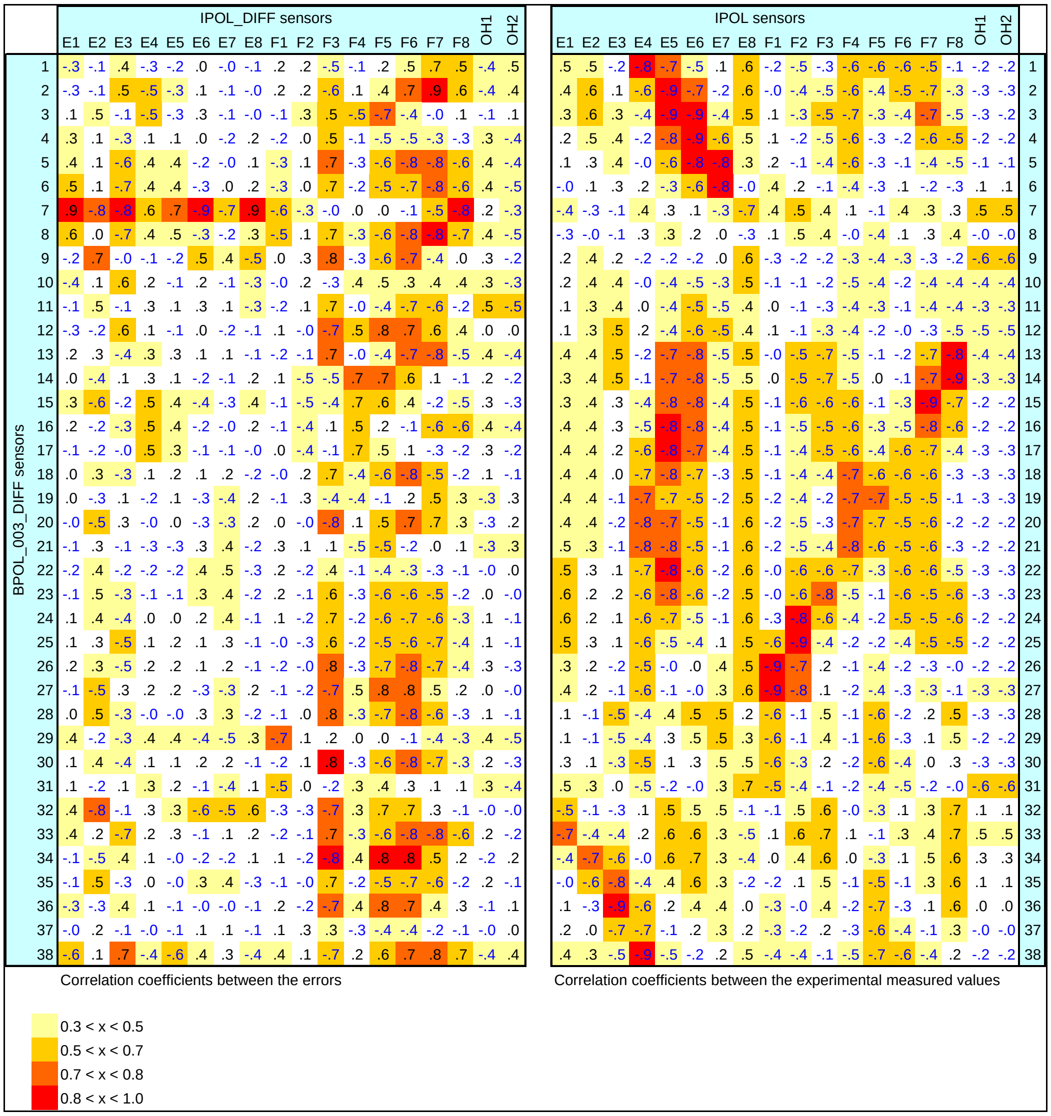

IPOL_DIFF sensors

BPOL_003_DIFF sensors	E1	E2	E3	E4	E5	E6	E7	E8	F1	F2	F3	F4	F5	F6	F7	F8	OH1	OH2
1	-.3	-.1	.4	-.3	-.2	.0	-.0	-.1	.2	.2	-.5	-.1	.2	.5	.7	.5	-.4	.5
2	-.3	-.1	.5	-.5	-.3	.1	-.1	-.0	.2	.2	-.6	.1	.4	.7	.9	.6	-.4	.4
3	.1	.5	-.1	-.5	-.3	.3	-.1	-.0	-.1	.3	.5	-.5	-.7	-.4	-.0	.1	-.1	.1
4	.3	.1	-.3	.1	.1	.0	-.2	.2	-.2	.0	.5	-.1	-.5	-.5	-.3	-.3	.3	-.4
5	.4	.1	-.6	.4	.4	-.2	-.0	.1	-.3	.1	.7	-.3	-.6	-.8	-.8	-.6	.4	-.4
6	.5	.1	-.7	.4	.4	-.3	.0	.2	-.3	.0	.7	-.2	-.5	-.7	-.8	-.6	.4	-.5
7	.9	-.8	-.8	.6	.7	-.9	-.7	.9	-.6	-.3	-.0	.0	.0	-.1	-.5	-.8	.2	-.3
8	.6	.0	-.7	.4	.5	-.3	-.2	.3	-.5	.1	.7	-.3	-.6	-.8	-.8	-.7	.4	-.5
9	-.2	.7	-.0	-.1	-.2	.5	.4	-.5	.0	.3	.8	-.3	-.6	-.7	-.4	.0	.3	-.2
10	-.4	.1	.6	.2	-.1	.2	-.1	-.3	-.0	.2	-.3	.4	.5	.3	.4	.4	.3	-.3
11	-.1	.5	-.1	.3	.1	.3	.1	-.3	-.2	.1	.7	-.0	-.4	-.7	-.6	-.2	.5	-.5
12	-.3	-.2	.6	.1	-.1	.0	-.2	-.1	.1	-.0	-.7	.5	.8	.7	.6	.4	.0	.0
13	.2	.3	-.4	.3	.3	.1	.1	-.1	-.2	-.1	.7	-.0	-.4	-.7	-.8	-.5	.4	-.4
14	.0	-.4	.1	.3	.1	-.2	-.1	.2	.1	-.5	-.5	.7	.7	.6	.1	-.1	.2	-.2
15	.3	-.6	-.2	.5	.4	-.4	-.3	.4	-.1	-.5	-.4	.7	.6	.4	-.2	-.5	.3	-.3
16	.2	-.2	-.3	.5	.4	-.2	-.0	.2	-.1	-.4	.1	.5	.2	-.1	-.6	-.6	.4	-.4
17	-.1	-.2	-.0	.5	.3	-.1	-.1	-.0	.0	-.4	-.1	.7	.5	.1	-.3	-.2	.3	-.2
18	.0	.3	-.3	.1	.2	.1	.2	-.2	-.0	.2	.7	-.4	-.6	-.8	-.5	-.2	.1	-.1
19	.0	-.3	.1	-.2	.1	-.3	-.4	.2	-.1	.3	-.4	-.4	-.1	.2	.5	.3	-.3	.3
20	-.0	-.5	.3	-.0	.0	-.3	-.3	.2	.0	-.0	-.8	.1	.5	.7	.7	.3	-.3	.2
21	-.1	.3	-.1	-.3	-.3	.3	.4	-.2	.3	.1	.1	-.5	-.5	-.2	.0	.1	-.3	.3
22	-.2	.4	-.2	-.2	-.2	.4	.5	-.3	.2	-.2	.4	-.1	-.4	-.3	-.3	-.1	-.0	.0
23	-.1	.5	-.3	-.1	-.1	.3	.4	-.2	.2	-.1	.6	-.3	-.6	-.6	-.5	-.2	.0	-.0
24	.1	.4	-.4	.0	.0	.2	.4	-.1	.1	-.2	.7	-.2	-.6	-.7	-.6	-.3	.1	-.1
25	.1	.3	-.5	.1	.2	.1	.3	-.1	-.0	-.3	.6	-.2	-.5	-.6	-.7	-.4	.1	-.1
26	.2	.3	-.5	.2	.2	.1	.2	-.1	-.2	-.0	.8	-.3	-.7	-.8	-.7	-.4	.3	-.3
27	-.1	-.5	.3	.2	.2	-.3	-.3	.2	-.1	-.2	-.7	.5	.8	.8	.5	.2	.0	-.0
28	.0	.5	-.3	-.0	-.0	.3	.3	-.2	-.1	.0	.8	-.3	-.7	-.8	-.6	-.3	.1	-.1
29	.4	-.2	-.3	.4	.4	-.4	-.5	.3	-.7	.1	.2	.0	.0	-.1	-.4	-.3	.4	-.5
30	.1	.4	-.4	.1	.1	.2	.2	-.1	-.2	.1	.8	-.3	-.6	-.8	-.7	-.3	.2	-.3
31	.1	-.2	.1	.3	.2	-.1	-.4	.1	-.5	.0	-.2	.3	.4	.3	.1	.1	.3	-.4
32	.4	-.8	-.1	.3	.3	-.6	-.5	.6	-.3	-.3	-.7	.3	.7	.7	.3	-.1	-.0	-.0
33	.4	.2	-.7	.2	.3	-.1	.1	.2	-.2	-.1	.7	-.3	-.6	-.8	-.8	-.6	.2	-.2
34	-.1	-.5	.4	.1	-.0	-.2	-.2	.1	.1	-.2	-.8	.4	.8	.8	.5	.2	-.2	.2
35	-.1	.5	-.3	.0	-.0	.3	.4	-.3	-.1	-.0	.7	-.2	-.5	-.7	-.6	-.2	.2	-.1
36	-.3	-.3	.4	.1	-.1	-.0	-.0	-.1	.2	-.2	-.7	.4	.8	.7	.4	.3	-.1	.1
37	-.0	.2	-.1	-.0	-.1	.1	.1	-.1	.1	.3	.3	-.3	-.4	-.4	-.2	-.1	-.0	.0
38	-.6	.1	.7	-.4	-.6	.4	.3	-.4	.4	.1	-.7	.2	.6	.7	.8	.7	-.4	.4

Correlation coefficients between the errors

IPOL sensors

E1	E2	E3	E4	E5	E6	E7	E8	F1	F2	F3	F4	F5	F6	F7	F8	OH1	OH2	
.5	.5	-.2	-.8	-.7	-.5	.1	.6	-.2	-.5	-.3	-.6	-.6	-.6	-.5	-.1	-.2	-.2	1
.4	.6	.1	-.6	-.9	-.7	-.2	.6	-.0	-.4	-.5	-.6	-.4	-.5	-.7	-.3	-.3	-.3	2
.3	.6	.3	-.4	-.9	-.9	-.4	.5	.1	-.3	-.5	-.7	-.3	-.4	-.7	-.5	-.3	-.2	3
.2	.5	.4	-.2	-.8	-.9	-.6	.5	.1	-.2	-.5	-.6	-.3	-.2	-.6	-.5	-.2	-.2	4
.1	.3	.4	-.0	-.6	-.8	-.8	.3	.2	-.1	-.4	-.6	-.3	-.1	-.4	-.5	-.1	-.1	5
-.0	.1	.3	.2	-.3	-.6	-.8	-.0	.4	.2	-.1	-.4	-.3	.1	-.2	-.3	.1	.1	6
-.4	-.3	-.1	.4	.3	.1	-.3	-.7	.4	.5	.4	.1	-.1	.4	.3	.3	.5	.5	7
-.3	-.0	-.1	.3	.3	.2	.0	-.3	.1	.5	.4	-.0	-.4	.1	.3	.4	-.0	-.0	8
.2	.4	.2	-.2	-.2	-.2	.0	.6	-.3	-.2	-.2	-.3	-.4	-.3	-.3	-.2	-.6	-.6	9
.2	.4	.4	-.0	-.4	-.5	-.3	.5	-.1	-.1	-.2	-.5	-.4	-.2	-.4	-.4	-.4	-.4	10
.1	.3	.4	.0	-.4	-.5	-.5	.4	.0	-.1	-.3	-.4	-.3	-.1	-.4	-.4	-.3	-.3	11
.1	.3	.5	.2	-.4	-.6	-.5	.4	.1	-.1	-.3	-.4	-.2	-.0	-.3	-.5	-.5	-.5	12
.4	.4	.5	-.2	-.7	-.8	-.5	.5	-.0	-.5	-.7	-.5	-.1	-.2	-.7	-.8	-.4	-.4	13
.3	.4	.5	-.1	-.7	-.8	-.5	.5	.0	-.5	-.7	-.5	.0	-.1	-.7	-.9	-.3	-.3	14
.3	.4	.3	-.4	-.8	-.8	-.4	.5	-.1	-.6	-.6	-.6	-.1	-.3	-.9	-.7	-.2	-.2	15
.4	.4	.3	-.5	-.8	-.8	-.4	.5	-.1	-.5	-.5	-.6	-.3	-.5	-.8	-.6	-.2	-.2	16
.4	.4	.2	-.6	-.8	-.7	-.4	.5	-.1	-.4	-.5	-.6	-.4	-.6	-.7	-.4	-.3	-.3	17
.4	.4	.0	-.7	-.8	-.7	-.3	.5	-.1	-.4	-.4	-.7	-.6	-.6	-.6	-.3	-.3	-.3	18
.4	.4	-.1	-.7	-.7	-.5	-.2	.5	-.2	-.4	-.2	-.7	-.7	-.5	-.5	-.1	-.3	-.3	19
.4	.4	-.2	-.8	-.7	-.5	-.1	.6	-.2	-.5	-.3	-.7	-.7	-.5	-.6	-.2	-.2	-.2	20
.5	.3	-.1	-.8	-.8	-.5	-.1	.6	-.2	-.5	-.4	-.8	-.6	-.5	-.6	-.3	-.2	-.2	21
.5	.3	.1	-.7	-.8	-.6	-.2	.6	-.0	-.6	-.6	-.7	-.3	-.6	-.6	-.5	-.3	-.3	22
.6	.2	.2	-.6	-.8	-.6	-.2	.5	-.0	-.6	-.8	-.5	-.1	-.6	-.5	-.6	-.3	-.3	23
.6	.2	.1	-.6	-.7	-.5	-.1	.6	-.3	-.8	-.6	-.4	-.2	-.5	-.5	-.6	-.2	-.2	24
.5	.3	.1	-.6	-.5	-.4	.1	.5	-.6	-.9	-.4	-.2	-.2	-.4	-.5	-.5	-.2	-.2	25
.3	.2	-.2	-.5	-.0	.0	.4	.5	-.9	-.7	.2	-.1	-.4	-.2	-.3	-.0	-.2	-.2	26
.4	.2	-.1	-.6	-.1	-.0	.3	.6	-.9	-.8	.1	-.2	-.4	-.3	-.3	-.1	-.3	-.3	27
.1	-.1	-.5	-.4	.4	.5	.5	.2	-.6	-.1	.5	-.1	-.6	-.2	.2	.5	-.3	-.3	28
.1	-.1	-.5	-.4	.3	.5	.5	.3	-.6	-.1	.4	-.1	-.6	-.3	.1	.5	-.2	-.2	29
.3	.1	-.3	-.5	.1	.3	.5	.5	-.6	-.3	.2	-.2	-.6	-.4	.0	.3	-.3	-.3	30
.5	.3	.0	-.5	-.2	-.0	.3	.7	-.5	-.4	-.1	-.2	-.4	-.5	-.2	-.0	-.6	-.6	31
-.5	-.1	-.3	.1	.5	.5	.5	-.1	-.1	.5	.6	-.0	-.3	.1	.3	.7	.1	.1	32
-.7	-.4	-.4	.2	.6	.6	.3	-.5	.1	.6	.7	.1	-.1	.3	.4	.7	.5	.5	33
-.4	-.7	-.6	-.0	.6	.7	.3	-.4	.0	.4	.6	.0	-.3	.1	.5	.6	.3	.3	34
-.0	-.6	-.8	-.4	.4	.6	.3	-.2	-.2	.1	.5	-.1	-.5	-.1	.3	.6	.1	.1	35
.1	-.3	-.9	-.6	.2	.4	.4	.0	-.3	-.0	.4	-.2	-.7	-.3	.1	.6	.0	.0	36
.2	.0	-.7	-.7	-.1	.2	.3	.2	-.3	-.2	.2	-.3	-.6	-.4	-.1	.3	-.0	-.0	37
.4	.3	-.5	-.9	-.5	-.2	.2	.5	-.4	-.4	-.1	-.5	-.7	-.6	-.4	.2	-.2	-.2	38

Correlation coefficients between the experimental measured values

0.3 < x < 0.5
0.5 < x < 0.7
0.7 < x < 0.8
0.8 < x < 1.0

Figure 14: Correlation matrix in the errors between the BPOL_003 and IPOL sensors, and correlation matrix in the measurements.

The correlation matrix confirms that physical correlations between the 7th probe and the coils are not present. A physical correlation exists however with coil E8 as it is in the exact same locality as the magnetic probe, but it cannot be used to explain the high correlation coefficient as they have different signs.

This means that the correlations are of different origins for which no viable explanation is available, but hypotheses can be drawn.

For example, these correlations could be due to misalignment of the probe. A thorough study was made of the positions and alignments of all the probes [3] and nothing abnormal was found for probe #7. But it is possibile that some time after the study was carried out, due to some maintenance work inside the vessel, the probe was knocked. When that happens, LIUQE will keep trying to minimise the error for that probe by fitting different fields. But this would lead to the probes around #7 having same correlations. In this case, the probes around #7 do not have any strong correlations with IPOLs making this reason possible but not likely.

Perhaps the data could be biased towards that probe, because plasma was mostly in that area, but this is not a good explanation since the probes adjacent to the 7th probe do not share high correlation values with the IPOL sensors. So again this reason is not likely.

The correlations are normalised [Equation 7], such that if the covariance between these values is very small, then the normalised correlation would be large. The covariance values were calculated, and they were found to be very small. Therefore it could be due to normalisation in Equation 7 that the correlations are strong. However, once again this is not a firm reason since it would not explain the pattern of the correlations.

There is no obvious explanation for these correlations and new techniques will need to be found for further analysis. If it is a case of something stopping working properly (misalignment), then by analysing different chunks of shots it could be possible to find when the correlations started happening.

The correlation with this probe and the 11 RFLUX loops cannot be explained either. It would be interesting to see, what correlations would occur if instead of using BPOL_003 probes for reconstruction, BPOL_011 probes were used, which could help in explaining the correlations.

For the IPOL coils F3, F5, F6 and F7 which correlate with 13, 6, 16 and 7 BPOL_003 probes respectively an explanation can be provided. The correlations are due to the mutual positions of the magnetic probes and the corresponding coils. F6 coil correlates with the most of the magnetic probes. The position of F6 is where the centre of most plasmas occurred, so in this area the higher magnetic field is needed to confine the shape of plasma to the vessel. Thus more probes picked up the magnetic field produced by the coil F6.

3.4.4 Closer study of the correlation between the #38 RFLUX loop and the IPOL sensors

The RFLUX loop #38, wound around the midsection inner board of the vessel, correlated strongly with IPOL sensors E1, E2, E3, E5, E6, E8 and F8. The E coils are inner board of the vessel, and the F coil outer board [Figure 15]. First of all it should be noted that this 38th loop correlates strongly with exactly the same IPOL coils as the 7th BPOL_003 probe studied above. By comparing the correlativity coefficients it is clear that the degree is almost the same, as well as the polarity of correlations.

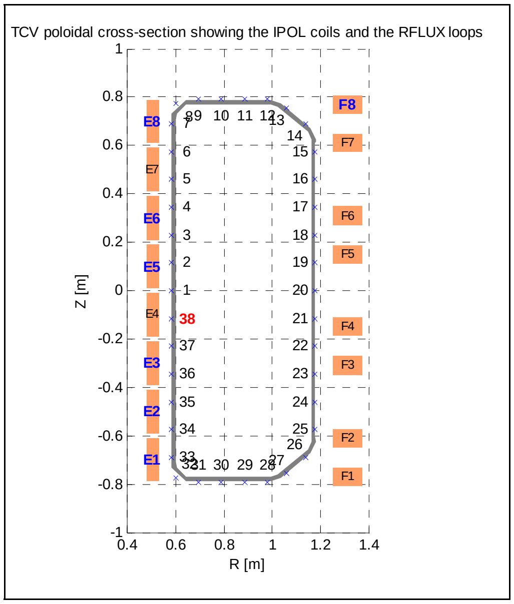

Figure 15: Position of the 38th RFLUX loop (red) which correlates with the 7 IPOL sensors (blue).

Similarly to how the magnetic probes pick up the additional contribution of the poloidal magnetic field from the IPOL coils [section 3.4.3], the flux loops measure the poloidal magnetic flux from the plasma and contribution from the IPOL coils which produce magnetic field to shape the plasma. The amount of magnetic flux measured by each loop due to 1A current in each of the IPOL coils is known. To compare the amount of magnetic flux measured by the 38th loop with the correlations, both quantities were plotted in Figure 16.

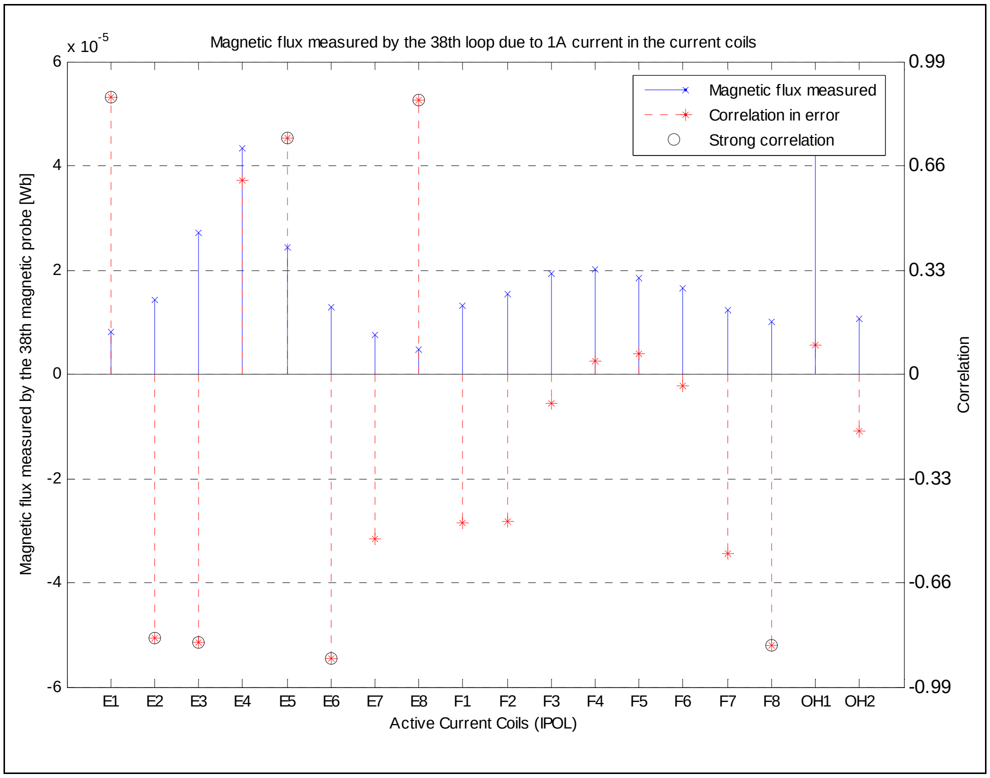

Figure 16: Graph compares the correlation coefficients for the errors in 38th RFLUX loop and the IPOL sensors with the magnetic flux measured due to 1A current in each of the IPOL coils.

From the results above, it is again unclear what the reason for the strong correlations is. However in this case, unlike for the case of the 7th BPOL_003 probe, we have eleven RFLUX loops that show strong correlations with almost the same set of IPOL coils, therefore the reason should be easier to find, but still difficult.

Once again it could be that because the values for these loops are so small, that when the covariance is normalised it creates a strong correlation. The covariance between the RFLUX loops and IPOL sensors was calculated, and was found to be very small. Therefore it is a possibility that the normalisation is the reason for these strong correlations. However this explanation is not ultimate and further analysis is required.

3.5 Data normalisation

The errors for each sensor group were studied in section 3.3 but error comparison between the groups was not possible, because of their different physical meanings. Therefore it was necessary to normalise the data. Data normalisation can be complicated and several approaches were tried.

The first step taken towards error comparison between different sensor groups was to normalise each difference between the measurement and the fitted value by dividing the difference by the absolute measurement value. This approach did not work well, because of divisions by zeros. To fix this a lot of data with zeros as measurements had to be removed. The means and standard deviations were plotted for the new normalised data for each sensor in each group. The results were not very promising because of large scale differences between groups which did not allow quantitative comparison. The removal of data was also not a good step, since the new smaller data set would need to be studied from the beginning.

The second step was to normalise the data by its weight used in the reconstruction. For the reconstruction a weight is set for each group, BERR, FERR and CERR, for magnetic probes, flux loops and current sensors respectively. In the standard reconstruction, one and the same weight is given to each sensor within the group in order to minimise the errors. To normalise the data each difference between the experimental and fitted data was divided by the weight for its sensor group. To see the results, error-bar graph was plotted showing all the sensors with their means and standard deviations [Figure 17].

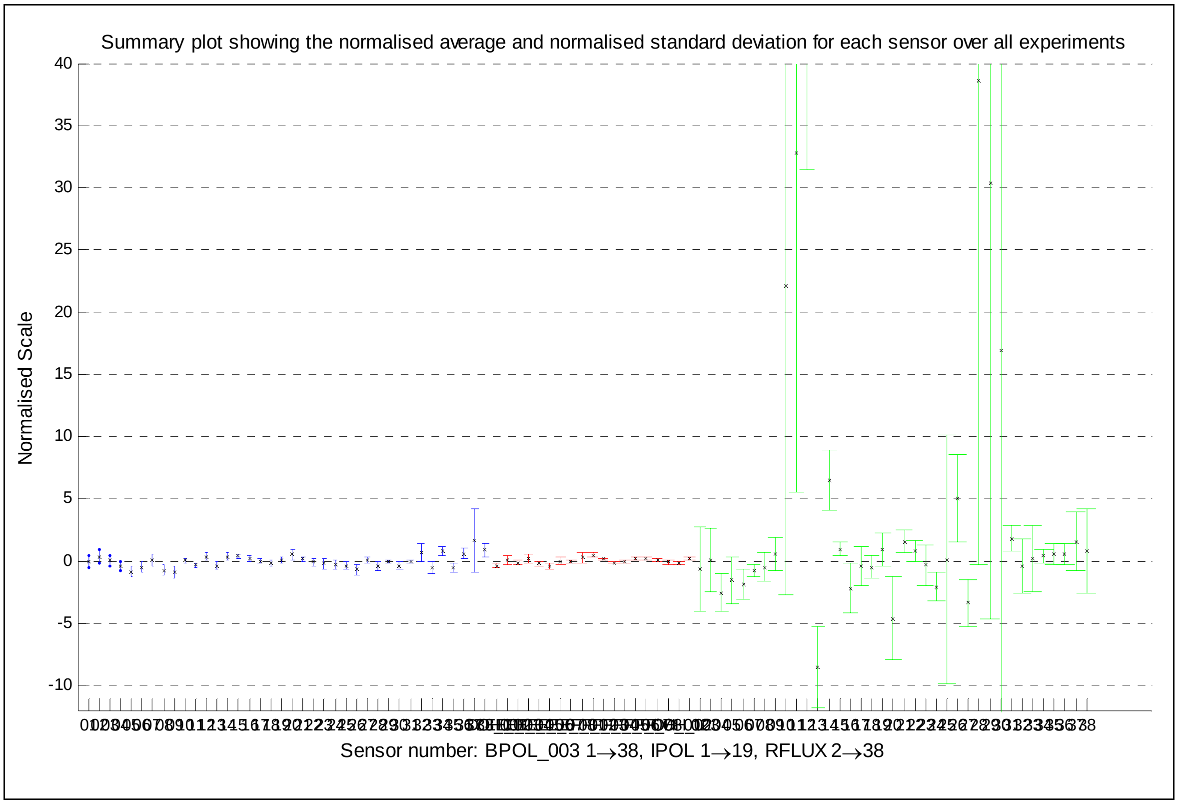

Figure 17: Summary error-bar graph showing the normalised means and standard deviations for each sensor.

From the graph we can see that the normalised differences in BPOL and IPOL are rather well fitted and give us small differences between each sensor and small standard deviations. With RFLUX loops we can see that the standard deviations are larger and we can see the values for 6 partial loops being well outside the range compared to the other values.

To compare the normalised standard deviations of the errors for each sensor, they were plotted on a logarithmic scale [Figure 18]. This allowed to see the differences in standard deviations for each sensor more clearly, being able to distinguish between small and large standard deviations on the same plot.

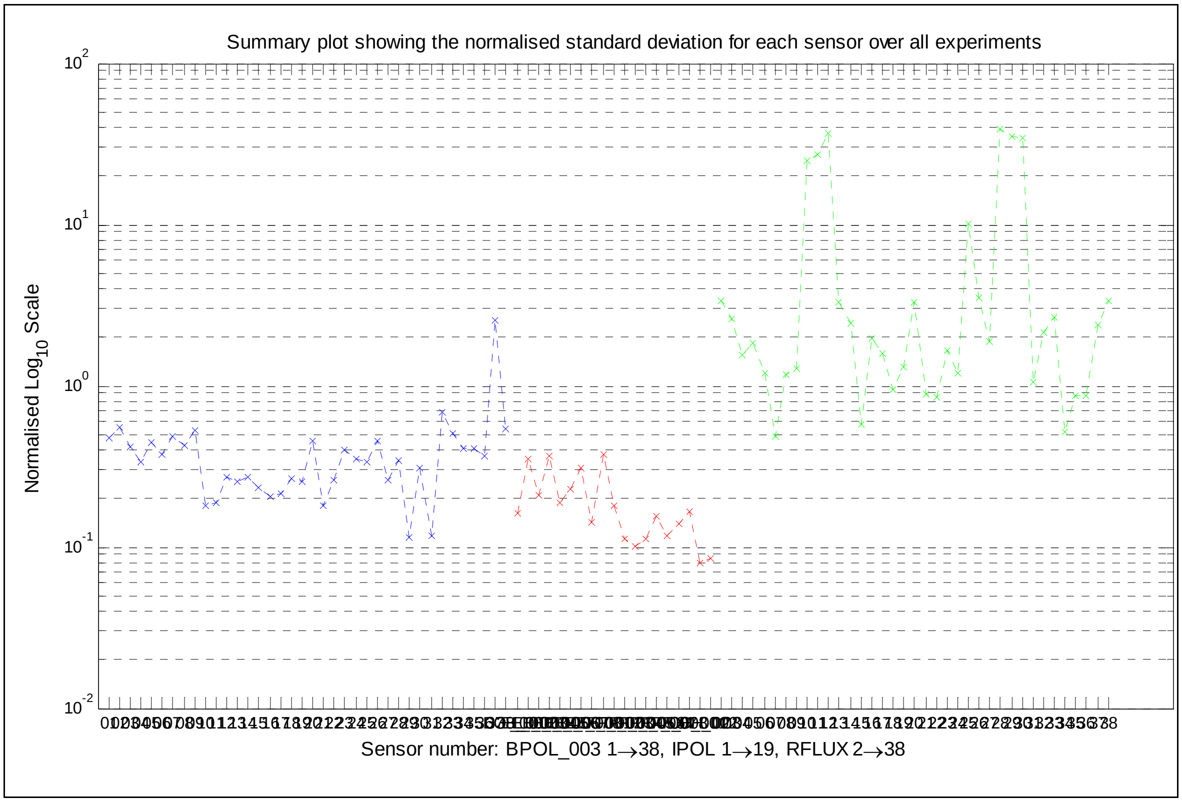

Figure 18: Summary plot showing the normalised standard deviations for each sensor.

From the plot we can see 3 groups of points, relating to each sensor group, with BPOL and IPOL being on the same level, and RFLUX higher up. We can see that the value of standard deviation for magnetic probe #37 is too large, which was expected as it was found in section 3.1 that this probe is malfunctioning. The values for the 6 partial loops, along with loop #25 (the loop that did not fit the Gaussian distribution in section 3.3) are too large too.

This graph can be used to adjust the weights such that the level of standard deviations is about the same, and this should lead to the improvement of errors in the reconstruction.

3.6 Improvement to the reconstruction

3.6.1 Step one reconstruction

Figure 18 shows the effect the weights have on the errors of the sensors. The graph shows the sensors whose errors are too large, data from which shouldn't be used for reconstruction, as it could lead to inaccuracies.

RFLUX loops #10-12, #25 and #28-30 lie far out from the standard deviations for the other loops. Loops #10-12 are the partial loops at the top of the vessel and are not used for the reconstruction. Loops #28-30 are also the partial loops at the bottom of the vessel but are still included in the reconstruction. These loops are still used, because it is considered that their measurements do not affect the reconstruction since most plasmas are nearer the top of the vessel than the bottom. Loop #25 has a large error too and should not be used either.

From the above analysis the malfunctioning probe #37 should be removed from the reconstruction. It would be better to replace it by the probe #37 from the 11th sector, but this would require a lot of reprogramming to the LIUQE code, and thus will not be done here.

The removal of loops #25, #28-30 and probe #37 would be the first way to improve the reconstruction. It is also necessary to change the weights, to take into account that the data from RFLUX should be weighted heavier, to expect a larger error. Also slight improvements for the weights for BPOL and IPOL could be made.

The values of the new weights were calculated by taking the average of the standard deviations for each sensor group (excluding the sensors that I will remove from reconstruction) [Figure 19]. The averages were then un-normalised by multiplying them by the old weights to get the new weights [Table 2].

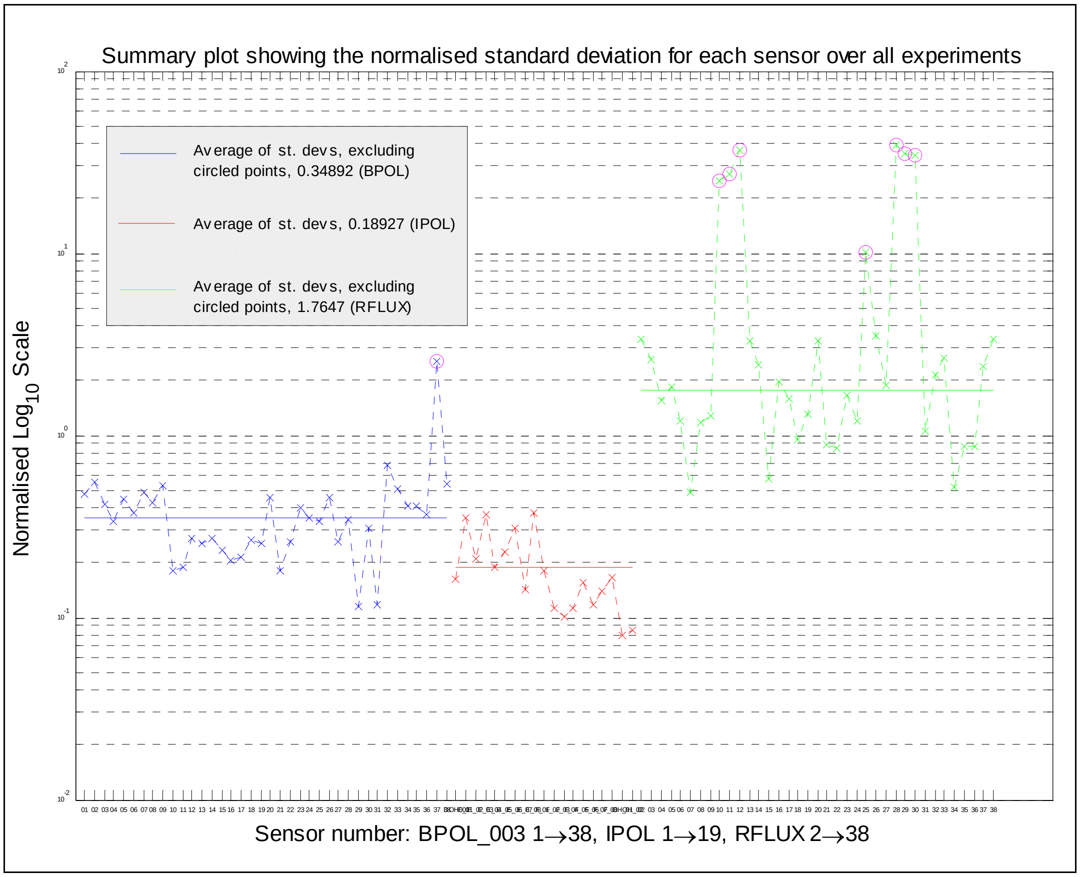

Figure 19: Graph showing the sensors that should be removed from the reconstruction (circled points), and showing the average standard deviations for each group.

Table 2: Showing the old and the new proposed weights for the sensor groups to be used in reconstruction.

	Average σ for the group	Old weight	New weight
BERR [T]	0.349	0.01	0.00349
CERR [kA]	0.189	0.2	0.0379
FERR [Wb]	1.765	0.0012	0.00212

The new weights were used to reconstruct a selection of shots covering different plasma conditions [Table 3]. The results for a number of key variables [Table 4] obtained using the standard reconstruction and step one reconstruction are compared in Table 5.

Table 3: A selection of shots that were reconstructed by the new parameters.

Shot number	Description
16752	High core confinement
18532	Fully non-inductive ECCD shot
19043	Standard shot
19592	H-mode
19645	High kappa

Table 4: Plasma variables used for comparing the standard reconstruction to the new reconstruction.

Variable	Description
z-axis	Z position of the plasma's magnetic axis
κ_{edge}	Plasma elongation at the plasma boundary
δ_{edge}	Plasma triangularity at the plasma boundary
L_I	Internal inductance per unit length
q_0	Safety factor at the magnetic axis
q_{95}	Safety factor at the 95% of the flux
χ	Overall root mean squared relative error of the reconstruction

The differences for the plasma variables were noticeable but very small. The difference for the z position of the plasma's magnetic axis was of 0.4 cm for the duration of shots #16752 and #18532 [Figure 20], and zero for the shot #19043. The differences in the other variables were present, but disagreed only at some time instances during the shots, while the other times they matched the standard reconstruction nicely. The greatest discrepancy was obtained for the overall root mean squared relative error of the reconstruction χ for each shot. The χ value has risen towards 1 for each shot, while the standard was always much less than 1 [Figure 20]. When χ is too low, the errors are being underestimated, when it is too high the errors are overestimated, however when it is around 1 it means that the errors are judged about right.

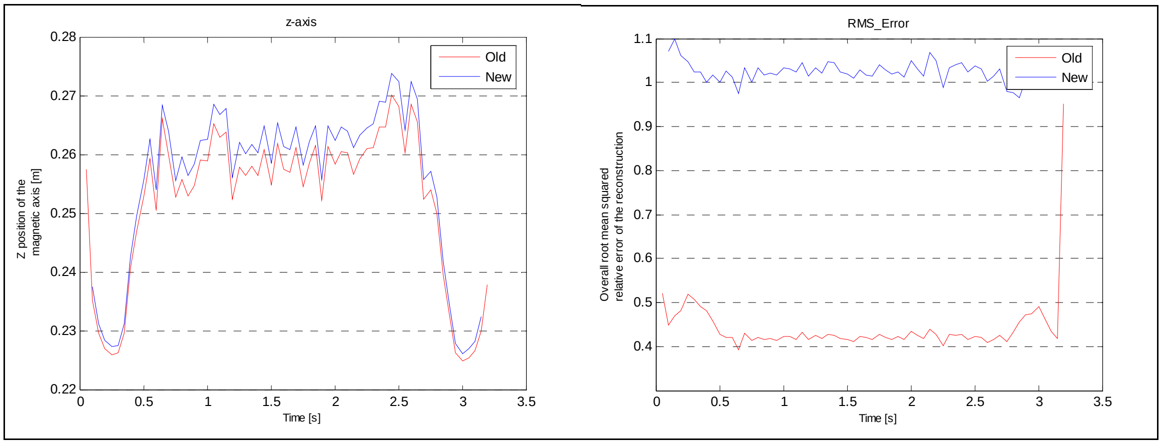

Figure 20: Comparison of the z-axis position of the magnetic axis and the RMS error (χ) between the standard parameters and the step one parameters for shot #18532.

For discharges #19592 [Figure 21] and #19645 the points in the middle of the shot failed to reconstruct. When the points are not being reconstructed it means that the convergence values are very erratic such that the reconstruction code LIUQE discards them. To reconstruct these points, the convergence acceptability was increased, but the reconstruction still failed. This is not a good result, since the standard parameterisation was able to reconstruct these shots.

3.6.2 Step two reconstruction

In step one as in standard reconstruction one weight was used for all the sensors in the group. From Figure 19 it can be seen that different sensors have different standard deviations for the errors. One weight is insufficient to minimise the errors for all sensors within a group. To improve this, the same weight was used as in step one but also each sensor was given a ratio to reflect the difference of its standard deviation to the average standard deviation seen in Figure 19. The reconstruction was run for the same shots as before [Table 3]. The results for same key variables [Table 4] were compared in Table 5 for the standard and step two reconstructions.

For all shots the χ value was evenly between 1 (value for step one reconstruction) and the χ value for standard reconstruction. The other variables were not changed much compared to step one parameterisation, the z axis positions were still different by about the same amount of 0.4 cm and were shifted in the same direction.

However this time the values for shot #19592 converged and all variables were successfully reconstructed [Figure 22]. The z position of the magnetic axis was about 0.4 cm lower than for the standard reconstruction and the value for χ was higher, starting at 0.75 and rising towards 0.9 at the end of the shot. The successful reconstruction is a good sign meaning that the errors were judged more correctly. But it is difficult to say if this reconstruction was more accurate, it can only be said that it should be more accurate because the χ value was closer to 1 compared to the standard parameterisation.

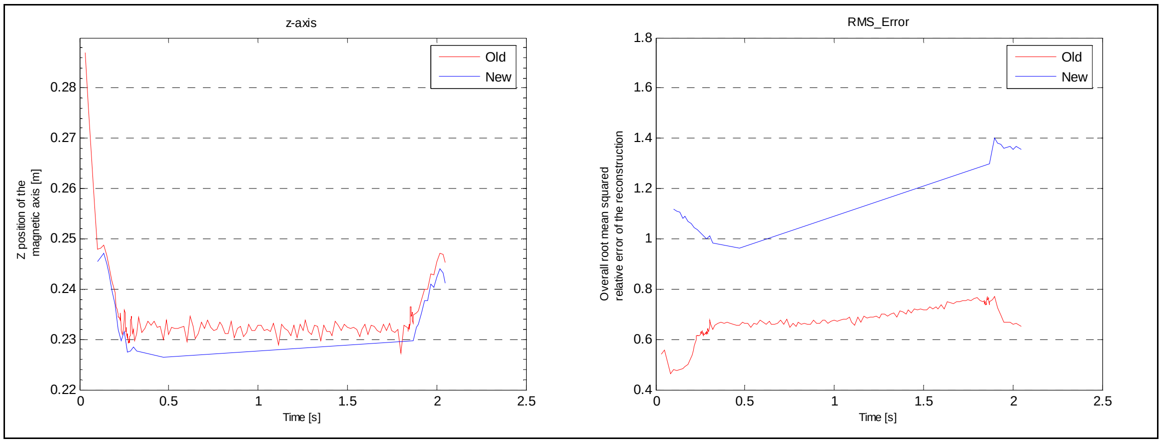

Figure 21: Step one improvement to the parameterisation failed to reconstruct the values for shot #19592. A straight line can be seen where points should have been reconstructed.

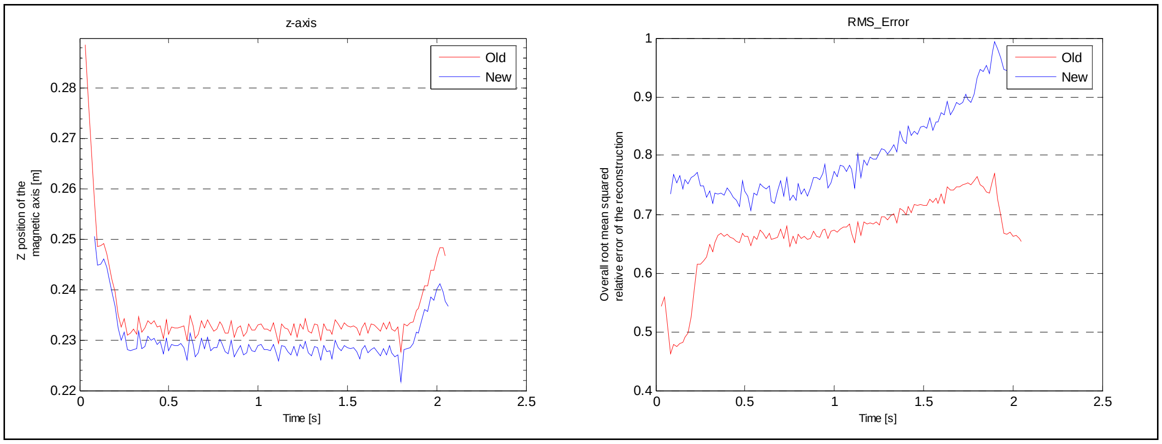

Figure 22: Step two improvement to the parameterisation succeeded in reconstructing all the values for shot #19592.

Similarly to step one reconstruction, in step two reconstruction the values failed to converge for the duration of the shot #19645, giving only an extra 4 points [Figure 23]. The reason it failed must be the same as to why the reconstruction for step one improvement to the parameterisation failed for the shots #19592 and #19645. The main difference between shots #19592, #19645 and the other 3 shots is the magnitude of current induced inside the plasma. For the 3 shots, the current is less than 350kA, while for shot #19592 400kA of current is induced inside the plasma, and for shot #19645 the current induced inside the plasma reached 600kA. For step two parameterisation the only improvement done, was to give relative weights to each sensor, and already the shot #19592 was successfully reconstructed. That means that even though the errors grew bigger, they were judged and weighed correctly. However for shot #19592 the current inside the plasma is significantly higher and the errors are still not judged properly. It is necessary to find a new way to set the weights for high currents.

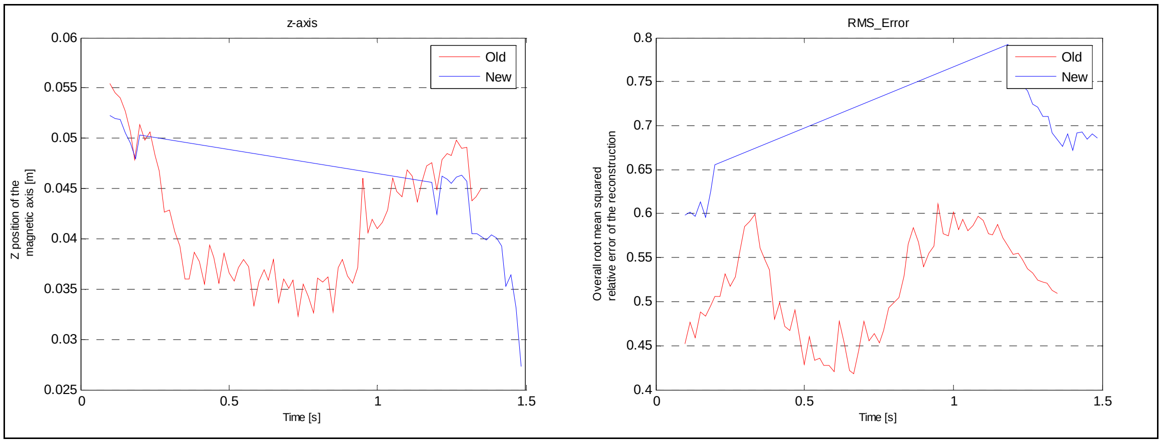

Figure 23: Failed reconstruction for shot #19645 using step two improvement to the parameterisation.

Table 5: Summary for the differences in plasma variables for the standard, step one and step two reconstructions.

Shot#	Standard						Step one						Step two					
	z [cm]	κ	δ	LI	q_0	q_{95}	Δz [cm]	Δκ	Δδ	ΔLI	Δq_0	Δq_{95}	Δz [cm]	Δκ	Δδ	ΔLI	Δq_0	Δq_{95}
16752 @1.5s	13.5	1.42	0.42	1.27	0.65	3.53	-0.5	0.05	0.08	0	0.02	0.29	-0.5	0.02	0.05	0.02	0.01	0.15
18532 @1s	25.9	1.66	0.40	1.43	0.83	5.26	0.4	0.01	0	0.04	-0.03	-0.02	0.3	0.01	0.01	0.01	0	0.02
19043 @1s	24.6	1.65	0.52	1.03	0.87	3.56	0	-0.02	-0.01	0.09	-0.11	-0.05	-0.2	-0.02	0	0.05	-0.06	-0.04
19592 @1.5s	23.3	1.73	0.58	0.79	0.91	2.69	-	-	-	-	-	-	-0.4	-0.01	-0.01	0.02	-0.05	-0.04
19645 @0.5s	3.61	2.34	0.39	0.75	0.75	2.33	-	-	-	-	-	-	-	-	-	-	-	-

3.6.3 Plasma current dependence

The shot #19645 that failed to reconstruct had a very high current inside the plasma. To see if weights could be set by the current magnitude inside the plasma, the correlation between the magnitude of current in the plasma and the errors in the IPOL coils was calculated. It was expected to see that as the current in the plasma gets large, the difference between the experimental and fitted measurements for IPOL gets large too, which would be a good explanation why LIUQE did not converge with the proposed parameters. Finding a correlation would lead to a possibility of finding different parameters for different magnitudes of current inside the plasma.

The current inside the plasma was plotted against the difference between the experimental and fitted data of each IPOL sensor, but no correlation was observed [Figure 24]. It was checked to see if correlation was present for BPOL_003 and RFLUX sensors, but again no correlation was observed.

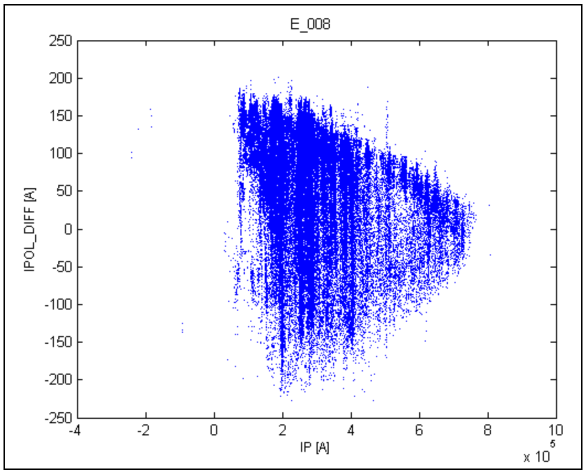

Figure 24: Scatter plot between the current inside the plasma (Ip) on the x-axis and the errors in the E8 IPOL coil on the y-axis.

It is interesting to notice from Figure 24, which is similar to all the other plots produced, that as the current inside the plasma increases, the error spread decreases.

The reason however that the error spread decreases as current increases could be due to amount of shots available. For low current plasmas a lot of shots were present in my database, but for high currents much less shots might have been present. To check this, for all the shots where current inside the plasma was between 280 kA and 320 kA, the errors between the IPOL experimental and fitted data were plotted as a histogram. For currents between 580 kA and 620 kA, the errors in IPOL were plotted as histogram too [Figure 25].

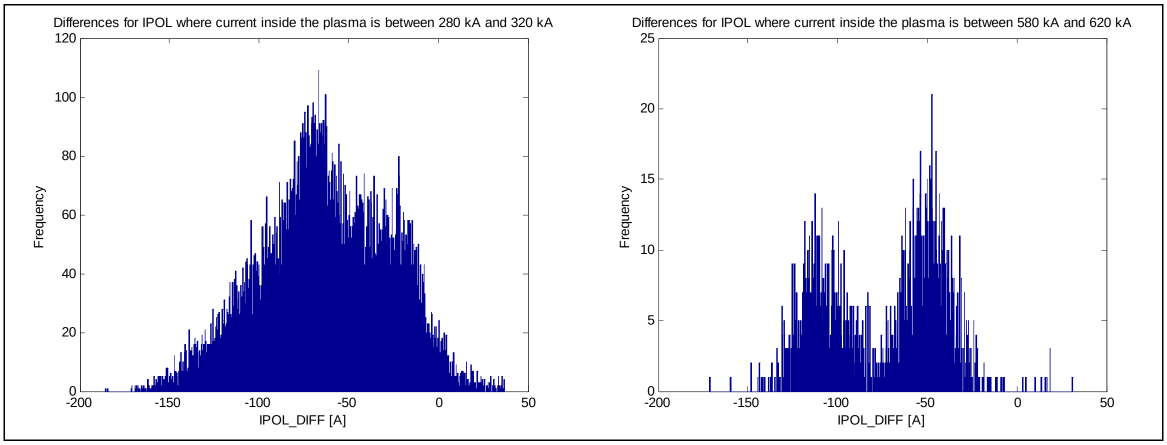

Figure 25: Histograms for difference between experimental and fitted data for IPOL, for currents inside the plasma between 280 kA and 320 kA, and 580 kA and 620 kA.

In the two histograms above, from the frequencies it can be clearly seen that much more data is available for lower plasma currents than for high plasma currents, which explains the shape of Figure 24. It can also be seen that the errors in the IPOL coils stay the same both for low and high plasma currents.

Since the errors are not dependent on the current as expected and stay similar between low and high plasma currents, it is unclear why the high current inside the plasma stops the shots from being reconstructed. It could mean that the error is high for that shot, that it is not being reconstructed, but the reason for this error needs to be investigated further.

Weights could be optimised for shots which have different errors. Such weights can be found by creating a database which contains shots based on some specific magnitude of error. Such that a selection of weights is available, ranging from low to high error and each new reconstruction starts by using the low error weights. If it fails to reconstruct then a set of weights for higher error is used, until the shot is successfully reconstructed.

3.6.4 BPOL_003 and BPOL_011

After seeing the standard deviations of the differences between experimental and fitted data for BPOL_003 probes normalised [Figure 18], it was interesting to compare that to the BPOL_011 probes. This would enable us to see if it would be worth adding the measurements from BPOL_011 to the reconstruction as well as having BPOL_003.

The difference was taken between the BPOL_011 measurements and the fitted data from B_FIELD_FIT, which is data fitted for the magnetic probes in the 3rd sector, not the 11th. The difference calculated in section 3.1 and pre-processed in section 3.2 was used. Then this difference was normalised by dividing it by the weight BERR that is given to the magnetic probes in sector 3 of the vessel (BPOL_003) in the reconstruction. The difference and the normalisation are not specific to the magnetic probes in the 11th sector since they are for the 3rd sector, and thus if large discrepancies between magnetic measurements in the 3rd and 11th sectors occur, they would be easily spotted. If large discrepancies between the two are found then it will be a good idea to use the measurements from BPOL_011 in the reconstruction too. However if everything is working normally, large discrepancies should not be found, as the magnetic field from the plasma is toroidally symmetric, and thus the only discrepancies would be due to errors or some misconfigurations in the probes. The standard deviations for the normalised differences of BPOL_003 and BPOL_011 were plotted [Figure 26].

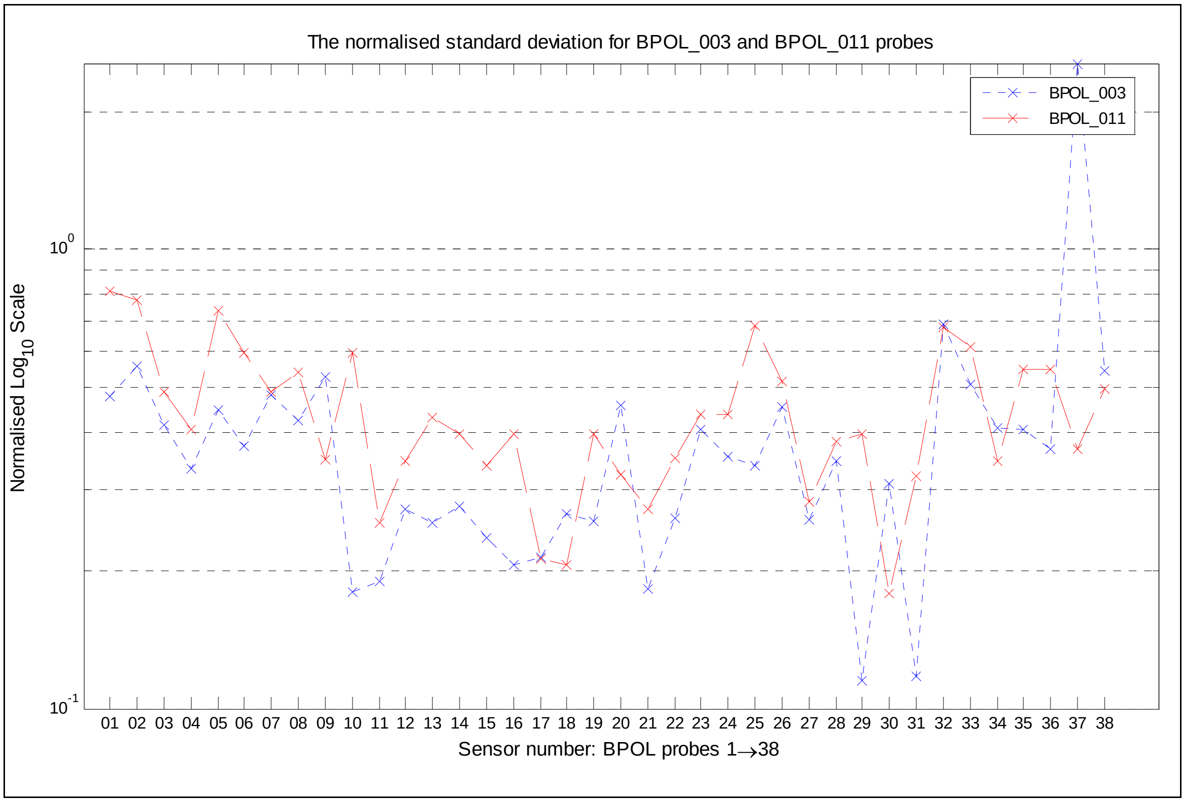

Figure 26: Normalised standard deviations of differences between experimental and fitted data to compare the measurements between magnetic probes BPOL_003 and BPOL_011.

The scale was set to logarithmic, which enabled us to see both the small and large differences. The malfunctioning probe #37 in the 3rd sector has a much higher standard deviation in the error than from the 11th sector. The other probes have good agreement with each other in the way that their standard deviations of the errors are equally small. From this data it can be seen that B_FIELD_FIT fits quite well to BPOL_011 probes and therefore it is not necessary to include BPOL_011 in the reconstruction, as no significant improvement will be achieved. However, since probe #37 is malfunctioning, it would be a good idea to replace its data by probe #37 in the 11th sector.

3.6.5 Shot #20792

It was interesting to run two reconstructions, using my step one parameters, and the step two parameters, on shot #20792. It has been complained that the standard reconstruction gets the z-axis position of the plasma's magnetic axis wrong. Tim Goodman re-checked the z-axis position by studying the soft x-ray emissions from the plasma for this shot and has concluded that on the basis of the x-ray symmetry the magnetic axis could be off by as much as 1 cm, which is a very significant shift.

The reconstruction using my first set of parameters showed a shift of 0.1 cm for the position of the magnetic axis, which is rather insignificant compared to 1 cm. Using the second set of parameters for the reconstruction, the z-axis position was 0.3 cm higher than for the parameters in the standard reconstruction [Figure 27]. The 0.3 cm difference is not very significant on the scale of the vessel size [Figure 28]. It is significant though when for example the ECRH beam is aligned. The beam is aligned by sweeping across the up-down symmetry of the vessel and measuring the symmetry from the plasma. The mirrors aligning the beam have precision of millimetres therefore it is necessary to have high precision in the position of the plasma's magnetic axis. Otherwise the plasma will be heated in the wrong place.

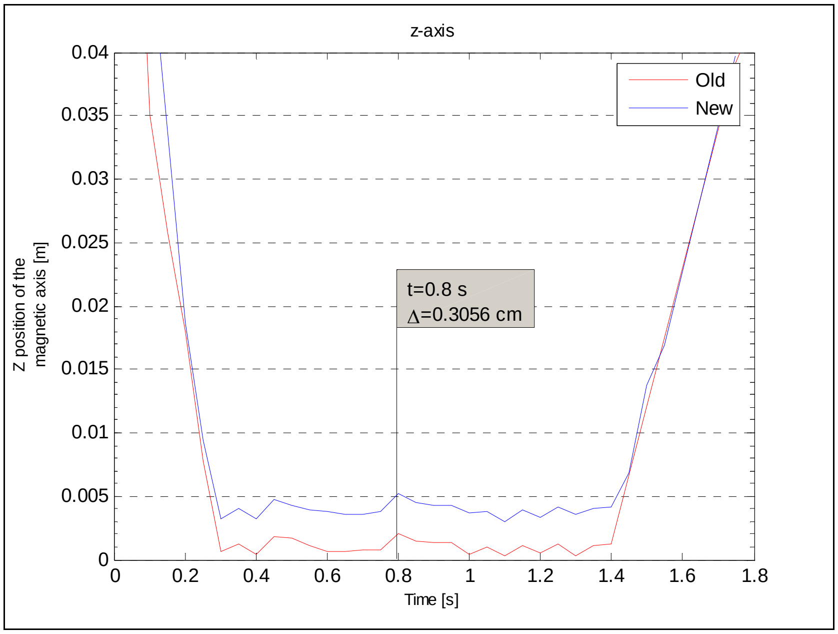

Figure 27: Difference in the z-axis position of the plasma's magnetic axis for the standard reconstruction, and reconstruction using my 2^{nd} set of parameters.

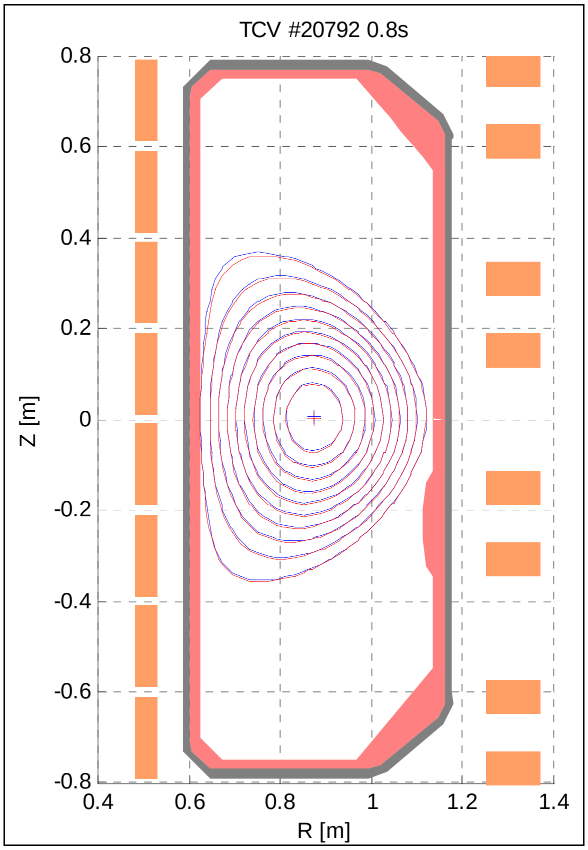

Figure 28: Reconstruction of the plasma flux contours in the shot #20792 at 0.8s. Blue are the contours for step two reconstruction, and red are the contours for the standard reconstruction. Pink shading inside the vessel are the tiles which line the vessel wall protecting the sensors.

Step two reconstruction gives us 0.3 cm in the difference for the z position for a shot whose difference in z position is supposed to be 1 cm. It can be argued that the shots studied earlier, where differences reached 0.5 cm, could have real position of plasma's magnetic axis more than 1 cm off than the value given by the standard reconstruction.

4. Conclusion

The aim of this project was to improve the accuracy of the reconstruction of the plasma equilibrium. The analysis carried out studied the errors between the experimental measurements and the fitted data. It was proposed to take magnetic probe #37 and RFLUX loops #25 and #28-30 out of the reconstruction and new weights optimised for each sensor were calculated. The step two parameters reconstructed the data giving a shift of about 0.4 cm for the z-axis position compared to the standard reconstruction, the other variables had a similar magnitude of difference, and the value for χ was closer to 1. However the shot #19645 failed to reconstruct because the convergence values were not satisfied. The reason why shot #19645 failed was thought to be due to high current induced inside the plasma which reached 600kA. The correlation between plasma current and errors was studied and no dependence was found. The shot failed to reconstruct because the optimised weights did not judge the errors well enough and thus it is necessary to do further work into weights optimisation. Weights could be calculated for a database with shots containing some specific high errors. Those weights could be used for shots that fail to reconstruct, such that a selection of weights would be available for different magnitudes of errors. Weights could also be optimised by feeding the LIUQE code into a neural network, where the weights would be adjusted automatically to get the best possible fit.

The distributions of errors for each sensor were compared to Gaussian distributions. It was found that for more than half magnetic probes in sector 3 and sector 11 the distributions were superposition of two Gaussians rather than just one. For relative flux loops the distributions had 2 peaks and some had several peaks. For poloidal coils only 3 coils were 2 peaked. Each peak must correspond to a group of shots which must be characterised by some different physical parameters. To understand the nature of the errors better it would be necessary to identify these parameters.

The correlations in errors were studied between all the sensors. A lot of strong correlations were present that did not have firm explanations. It was found that almost the same poloidal coil sensors correlated strongly with both magnetic probes, relative flux loops and with each other.

The unexplained correlations for probe #7, could be investigated further by changing the input of the reconstruction from magnetic probes in sector 3 to magnetic probes in sector 11. This would allow us to see if the same correlations happen, and if they do not happen then it would be better to leave magnetic probes from sector 11 as the input. Also if the reason for that correlation is based on some physical error, then studying correlations for different chunks of shots would allow us to pinpoint exactly when the change was introduced.

In the end, if the correlations do occur, it would be necessary to adjust LIUQE to take into account the correlations when evaluating the cost function χ.

5. Formal acknowledgements

I would like to thank my supervisor Jean-Marc Moret, Stefano Coda and Stefano Alberti for the excellent help they gave me throughout this project.

6. References

[1] J.-M. Moret, F. Buhlmann, G. Tonetti, Rev. of Scientific Instrum. 74, Num. 11 (2003) 4634

[2] M. Anton et al, Plasma Phys. Control. Fusion 38 (1996) 1849.

[3] J.-M. Moret, F. Buhlmann, D. Fasel, F. Hofmann, G. Tonetti, Rev. of Scientific Instrum. 69, Num. 6 (1998) 2333

[4] J. Lister et al, Fusion Tech. 32 (Nov 1997) 321

[5] F. Hofmann, G. Tonetti, Nucl. Fusion 28 (1988) 1871

[6] F. Hofmann, G. Tonetti, Nucl. Fusion 28 (1988) 519

[7] W. Feneberg, K. Lackner, P. Martin, Comput. Phys. Commun. 31 (1984) 143

7. Appendix

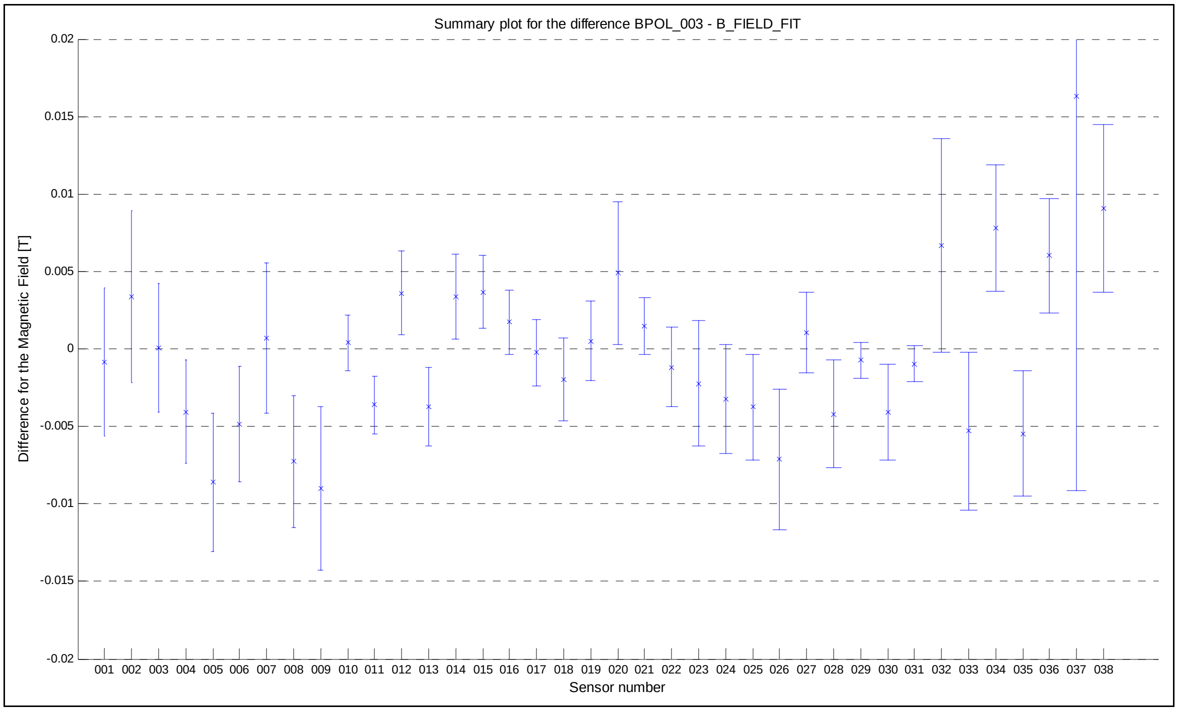

Figure 29: Means and standard deviations of the difference between experimental and reconstructed data for the magnetic probes in the 3rd sector (BPOL_003 probes).

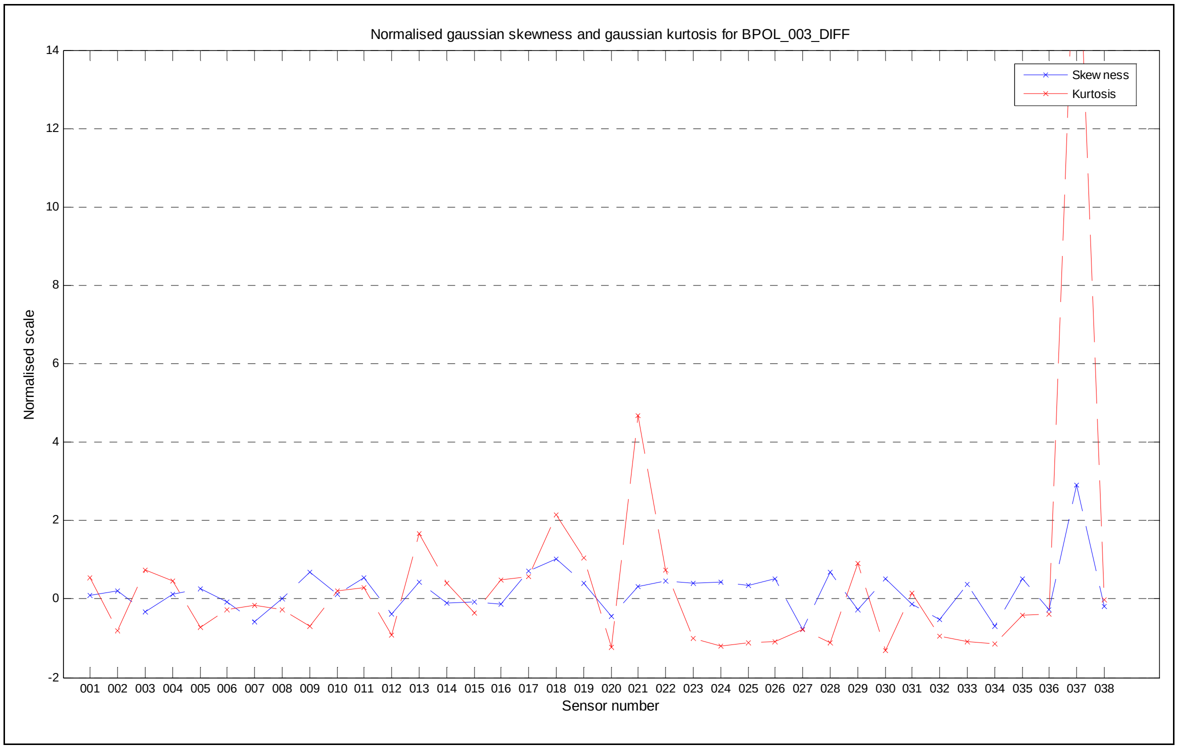

Figure 30: Skewness and kurtosis of the difference between experimental and reconstructed data for the magnetic probes in the 3rd sector (BPOL_003 probes).

Table 6: Summary of the difference between experimental and reconstructed data for the magnetic probes in the 3rd sector (BPOL_003 probes).

Probe number	Mean [T]	St. Deviation [T]	Skewness	Kurtosis
1	-0.001	0.005	0.08	0.53
2	0.003	0.006	0.20	-0.80
3	0.000	0.004	-0.33	0.74
4	-0.004	0.003	0.11	0.45
5	-0.009	0.004	0.26	-0.72
6	-0.005	0.004	-0.08	-0.26
7	0.001	0.005	-0.59	-0.17
8	-0.007	0.004	0.02	-0.28
9	-0.009	0.005	0.69	-0.68
10	0.000	0.002	0.12	0.21
11	-0.004	0.002	0.53	0.30
12	0.004	0.003	-0.39	-0.91
13	-0.004	0.003	0.42	1.66
14	0.003	0.003	-0.09	0.41
15	0.004	0.002	-0.08	-0.36
16	0.002	0.002	-0.12	0.48
17	0.000	0.002	0.70	0.56
18	-0.002	0.003	1.03	2.16
19	0.001	0.003	0.41	1.06
20	0.005	0.005	-0.43	-1.22
21	0.001	0.002	0.32	4.69
22	-0.001	0.003	0.45	0.73
23	-0.002	0.004	0.40	-0.99
24	-0.003	0.004	0.42	-1.19
25	-0.004	0.003	0.34	-1.12
26	-0.007	0.005	0.52	-1.10
27	0.001	0.003	-0.77	-0.78
28	-0.004	0.003	0.69	-1.13
29	-0.001	0.001	-0.27	0.90
30	-0.004	0.003	0.52	-1.31
31	-0.001	0.001	-0.14	0.16
32	0.007	0.007	-0.51	-0.95
33	-0.005	0.005	0.37	-1.08
34	0.008	0.004	-0.70	-1.15
35	-0.005	0.004	0.51	-0.41
36	0.006	0.004	-0.27	-0.39
37	0.016	0.025	2.92	18.22
38	0.009	0.005	-0.19	-0.01

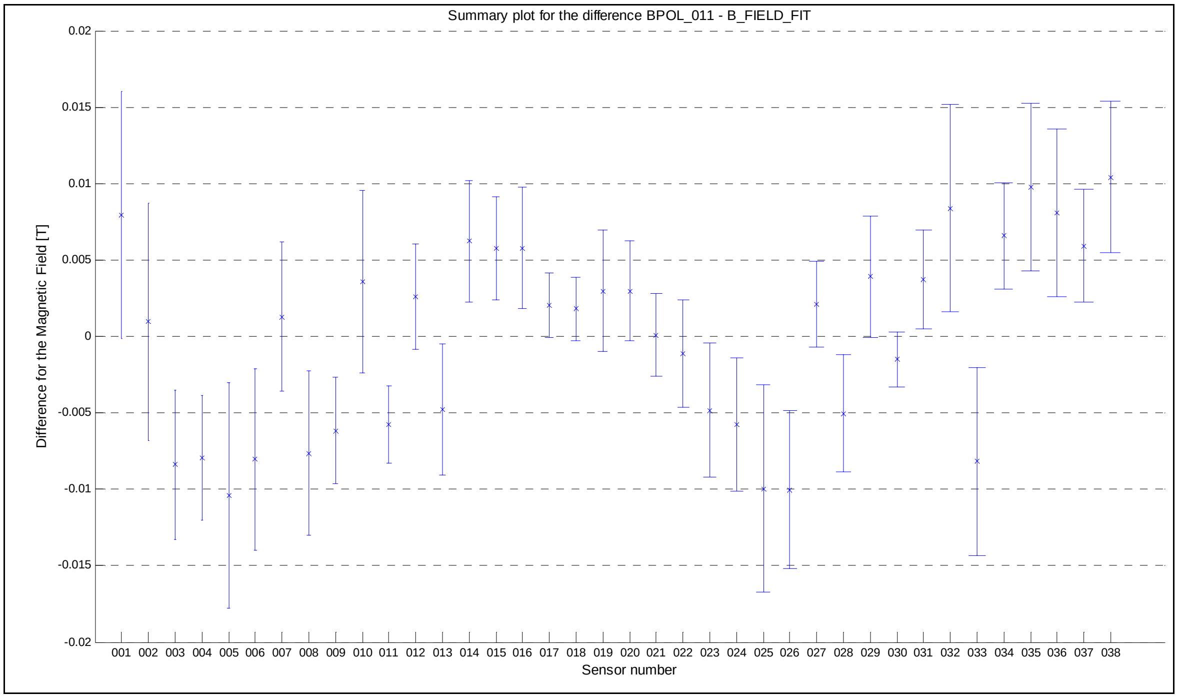

Figure 31: Means and standard deviations of the difference between experimental and reconstructed data for the magnetic probes in the 11th sector (BPOL_011 probes).

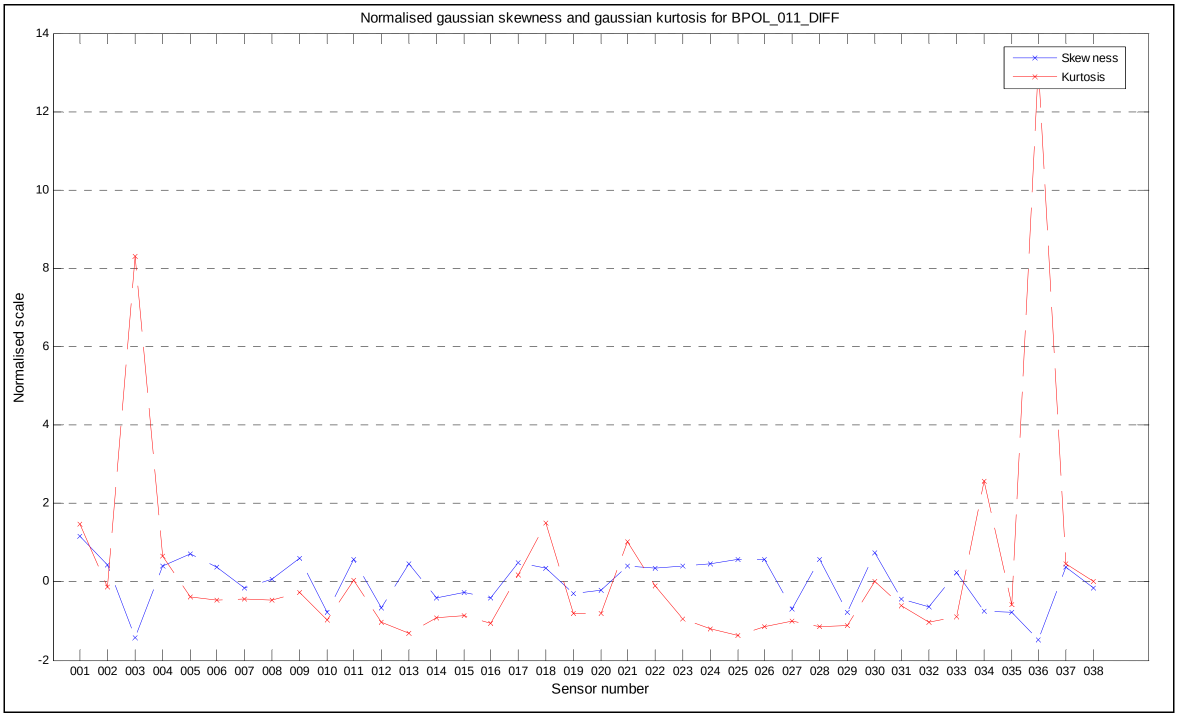

Figure 32: Skewness and kurtosis of the difference between experimental and reconstructed data for the magnetic probes in the 11th sector (BPOL_011 probes).

Table 7: Summary of the difference between experimental and reconstructed data for the magnetic probes in the 11th sector (BPOL_011 probes).

Probe number	Mean [T]	St. Deviation [T]	Skewness	Kurtosis
1	0.008	0.008	1.17	1.47
2	0.001	0.008	0.42	-0.12
3	-0.008	0.005	-1.42	8.30
4	-0.008	0.004	0.39	0.67
5	-0.010	0.007	0.70	-0.38
6	-0.008	0.006	0.37	-0.45
7	0.001	0.005	-0.16	-0.44
8	-0.008	0.005	0.05	-0.46
9	-0.006	0.003	0.59	-0.27
10	0.004	0.006	-0.78	-0.96
11	-0.006	0.003	0.58	0.05
12	0.003	0.003	-0.66	-1.04
13	-0.005	0.004	0.45	-1.32
14	0.006	0.004	-0.42	-0.93
15	0.006	0.003	-0.28	-0.85
16	0.006	0.004	-0.42	-1.05
17	0.002	0.002	0.50	0.17
18	0.002	0.002	0.35	1.50
19	0.003	0.004	-0.30	-0.80
20	0.003	0.003	-0.22	-0.81
21	0.000	0.003	0.40	1.03
22	-0.001	0.004	0.35	-0.10
23	-0.005	0.004	0.41	-0.93
24	-0.006	0.004	0.47	-1.20
25	-0.010	0.007	0.57	-1.35
26	-0.010	0.005	0.56	-1.15
27	0.002	0.003	-0.70	-1.01
28	-0.005	0.004	0.58	-1.13
29	0.004	0.004	-0.77	-1.11
30	-0.002	0.002	0.75	0.02
31	0.004	0.003	-0.45	-0.62
32	0.008	0.007	-0.63	-1.02
33	-0.008	0.006	0.23	-0.89
34	0.007	0.003	-0.75	2.56
35	0.010	0.005	-0.79	-0.58
36	0.008	0.005	-1.47	13.16
37	0.006	0.004	0.36	0.45
38	0.010	0.005	-0.16	0.01

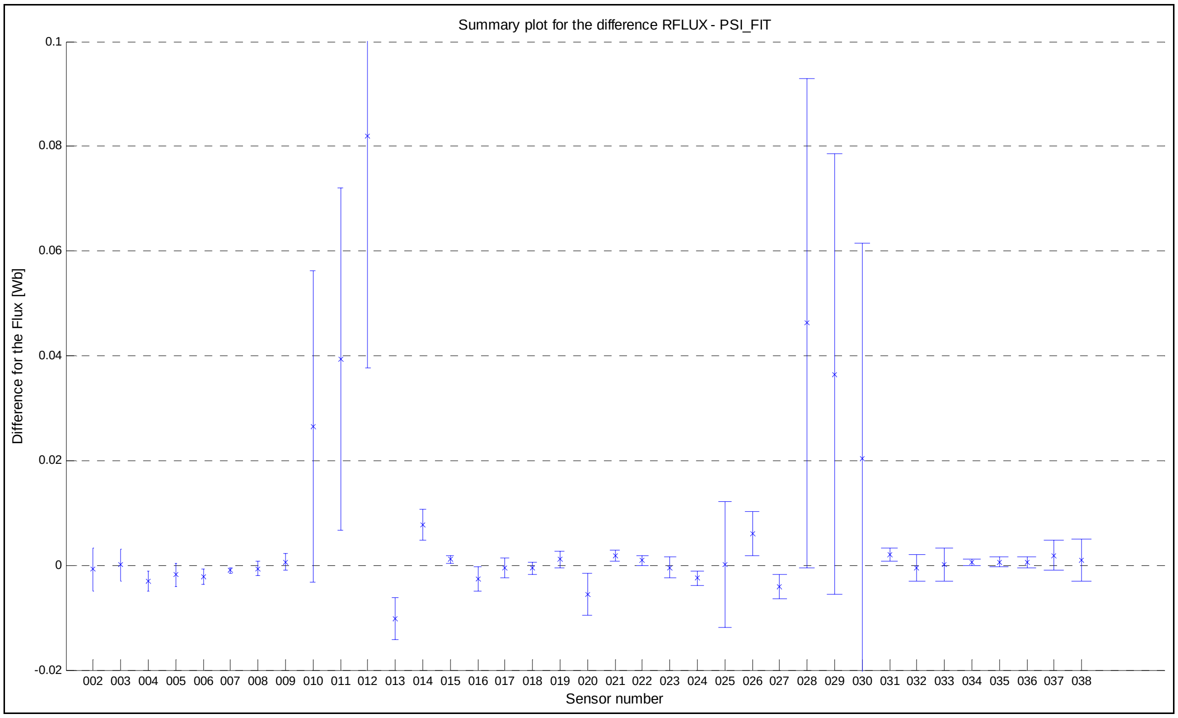

Figure 33: Means and standard deviations of the difference between experimental and reconstructed data for the relative flux loops (RFLUX loops).

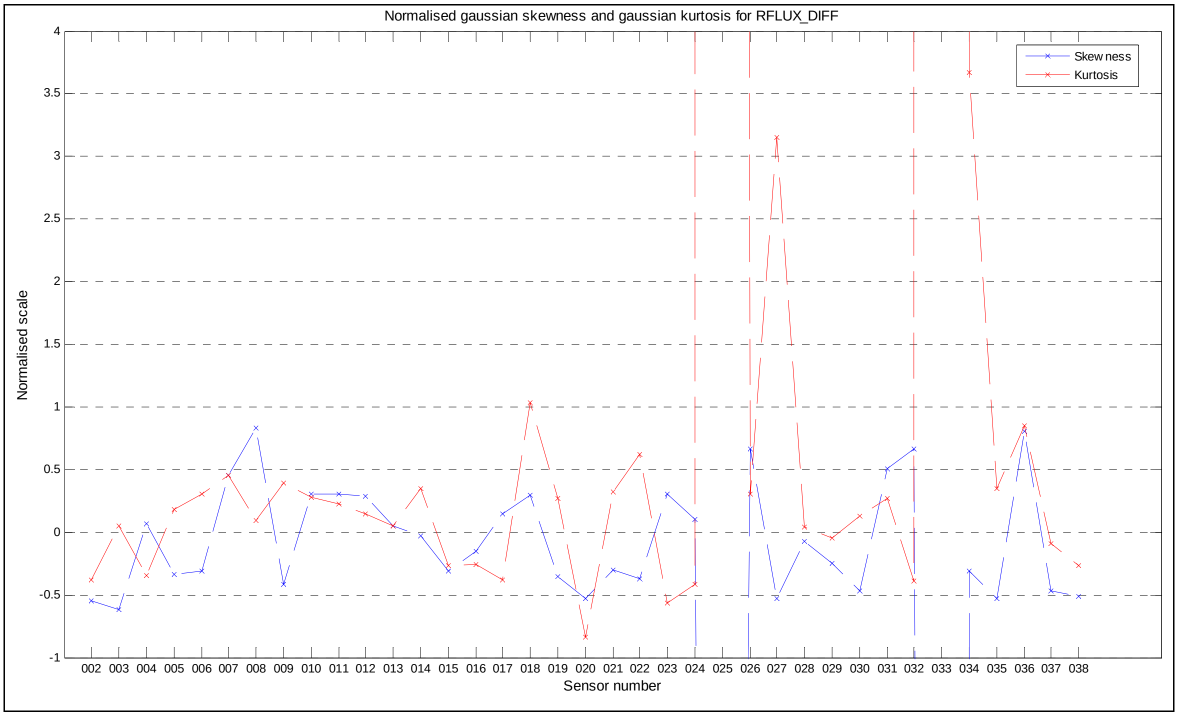

Figure 34: Skewness and kurtosis of the difference between experimental and reconstructed data for the relative flux loops (RFLUX loops).

Table 8: Summary of the difference between experimental and reconstructed data for the relative flux loops (RFLUX loops).

Loop number	Mean [Wb]	St. Deviation [Wb]	Skewness	Kurtosis
2	-0.001	0.004	-0.55	-0.38
3	0.000	0.003	-0.62	0.05
4	-0.003	0.002	0.07	-0.34
5	-0.002	0.002	-0.34	0.18
6	-0.002	0.001	-0.31	0.31
7	-0.001	0.001	0.45	0.45
8	-0.001	0.001	0.83	0.09
9	0.001	0.002	-0.42	0.39
10	0.026	0.030	0.30	0.28
11	0.039	0.033	0.30	0.22
12	0.082	0.044	0.29	0.15
13	-0.010	0.004	0.05	0.05
14	0.008	0.003	-0.03	0.35
15	0.001	0.001	-0.31	-0.27
16	-0.003	0.002	-0.15	-0.26
17	-0.001	0.002	0.15	-0.38
18	-0.001	0.001	0.30	1.03
19	0.001	0.002	-0.35	0.27
20	-0.006	0.004	-0.53	-0.84
21	0.002	0.001	-0.30	0.32
22	0.001	0.001	-0.38	0.62
23	0.000	0.002	0.31	-0.56
24	-0.002	0.001	0.10	-0.42
25	0.000	0.012	-26.81	746.46
26	0.006	0.004	0.67	0.30
27	-0.004	0.002	-0.53	3.15
28	0.046	0.047	-0.08	0.04
29	0.036	0.042	-0.25	-0.05
30	0.020	0.041	-0.47	0.13
31	0.002	0.001	0.50	0.27
32	0.000	0.003	0.66	-0.39
33	0.000	0.003	-52.25	4173.70
34	0.000	0.001	-0.31	3.67
35	0.001	0.001	-0.53	0.34
36	0.001	0.001	0.81	0.85
37	0.002	0.003	-0.47	-0.09
38	0.001	0.004	-0.52	-0.27

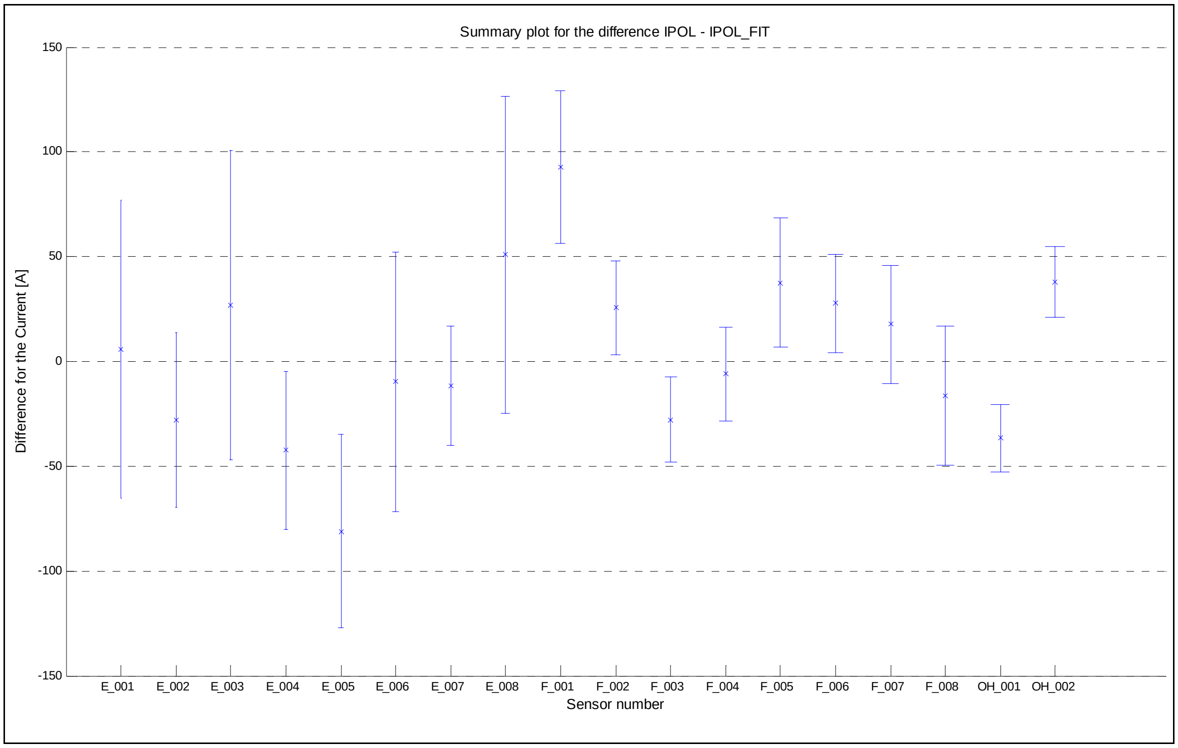

Figure 35: Means and standard deviations of the difference between experimental and reconstructed data for the current sensors (IPOL sensors).

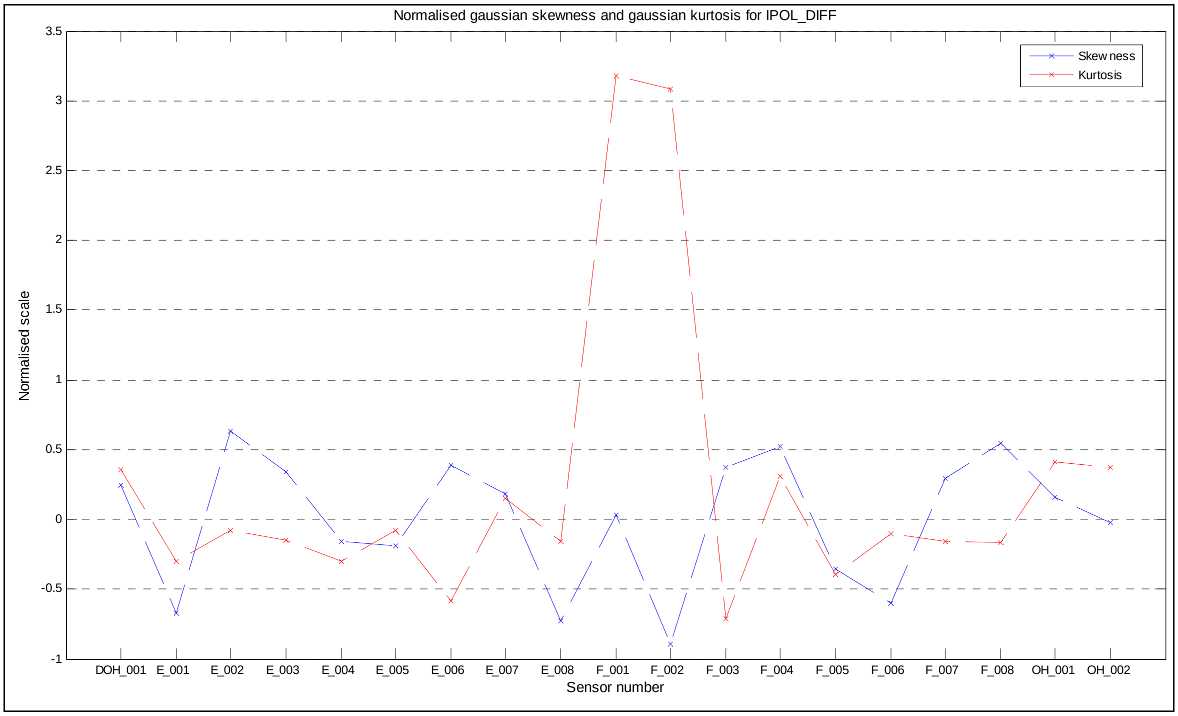

Figure 36: Skewness and kurtosis of the difference between experimental and reconstructed data for the current sensors (IPOL sensors).

Table 9: Summary of the difference between experimental and reconstructed data for the current sensors (IPOL sensors).

Sensor number	Mean [A]	St. Deviation [A]	Skewness	Kurtosis
E_001	6	71	-0.67	-0.30
E_002	-28	42	0.64	-0.08
E_003	27	74	0.34	-0.15
E_004	-42	38	-0.16	-0.30
E_005	-81	46	-0.19	-0.08
E_006	-10	62	0.38	-0.58
E_007	-12	28	0.18	0.15
E_008	51	76	-0.73	-0.16
F_001	93	36	0.03	3.18
F_002	26	23	-0.89	3.08
F_003	-28	20	0.37	-0.71
F_004	-6	22	0.52	0.31
F_005	38	31	-0.35	-0.40
F_006	28	24	-0.60	-0.10
F_007	18	28	0.29	-0.16
F_008	-16	33	0.54	-0.17
OH_001	-37	16	0.16	0.41
OH_002	38	17	-0.02	0.38

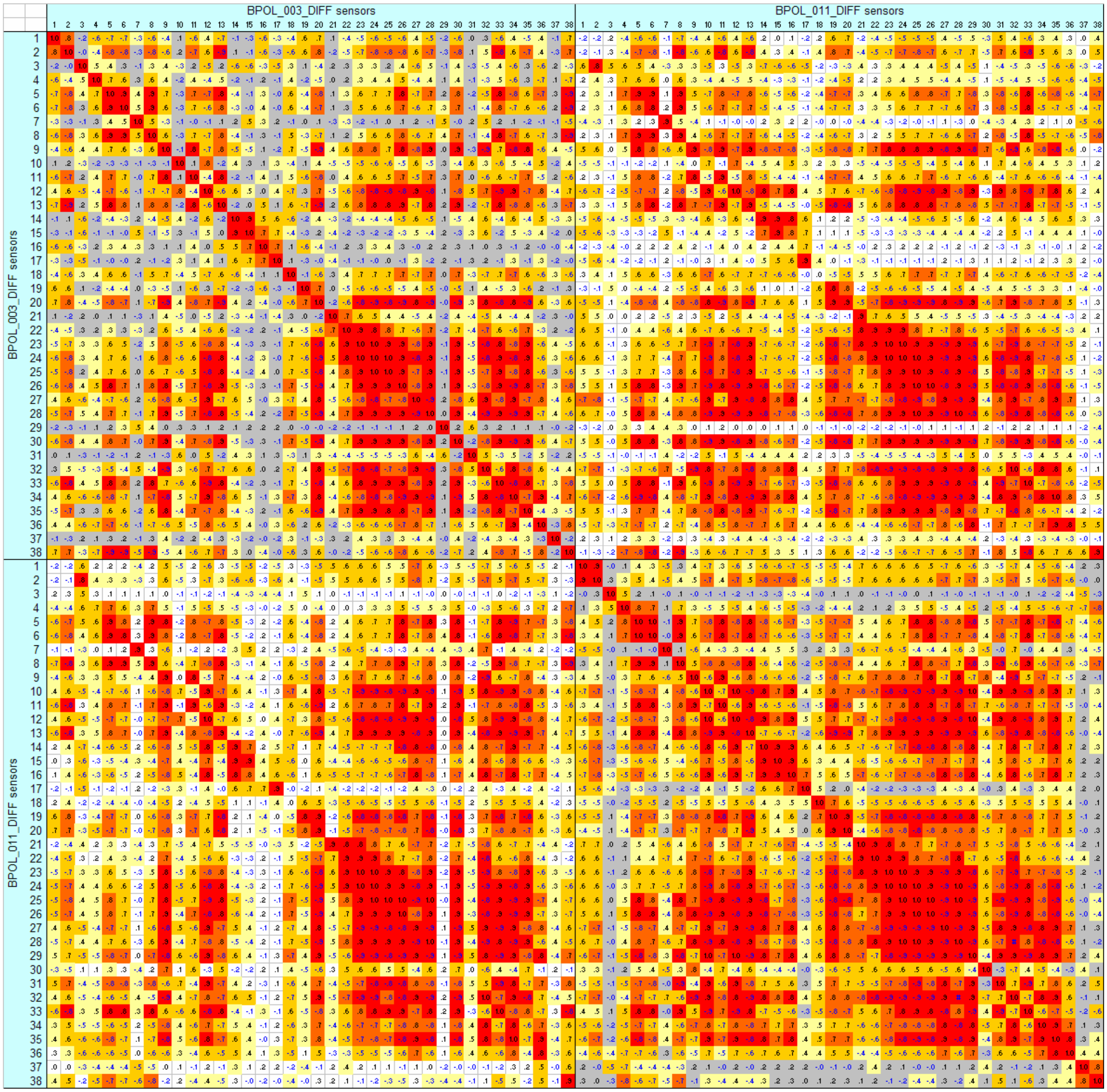

Figure 37: Correlation matrix between the errors in BPOL_003, BPOL_0011 and BPOL_003 and BPOL_011.

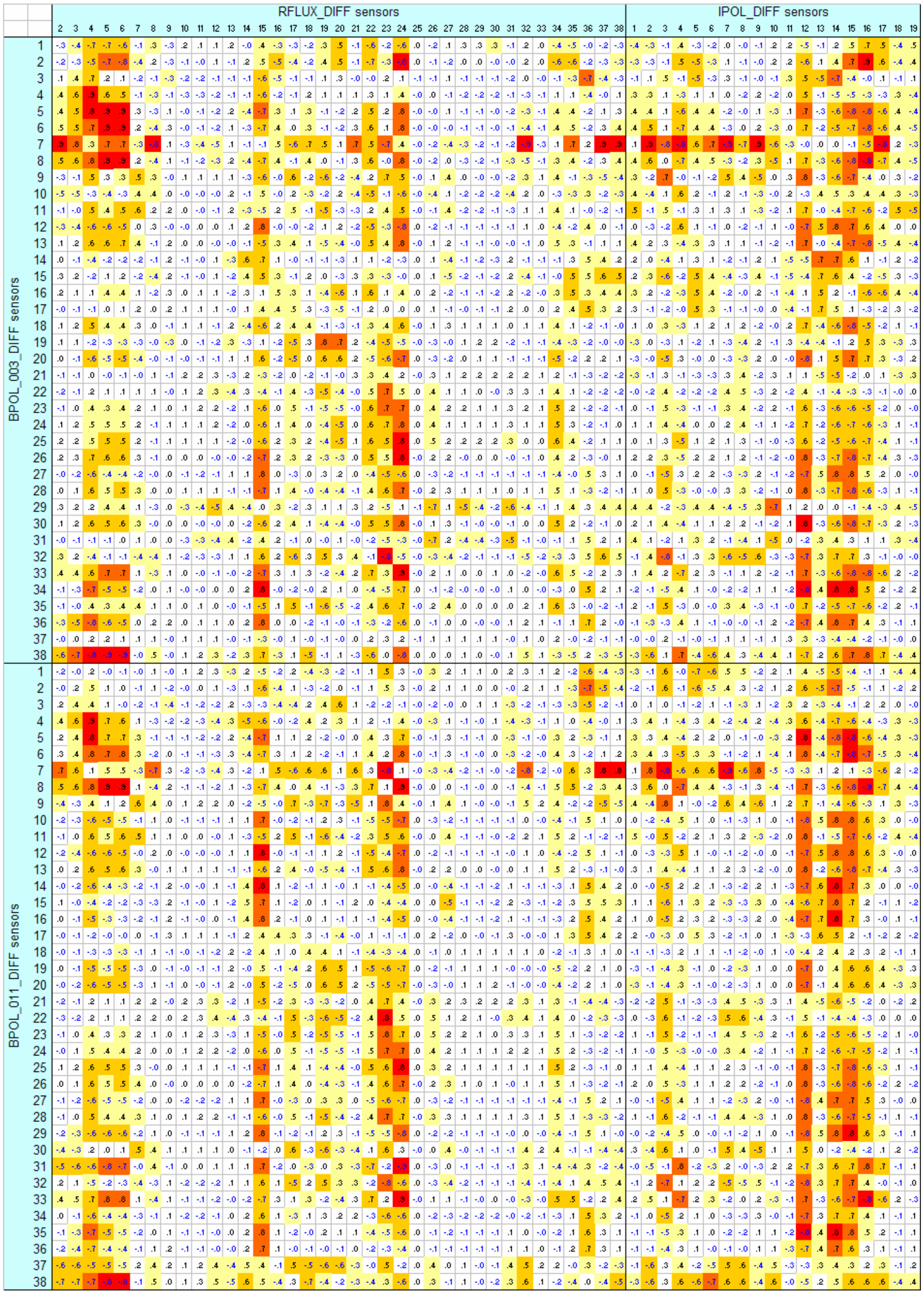

		RFLUX_DIFF sensors																																			IPOL_DIFF sensors																		
		2	3	4	5	6	7	8	9	10	11	12	13	14	15	16	17	18	19	20	21	22	23	24	25	26	27	28	29	30	31	32	33	34	35	36	37	38	1	2	3	4	5	6	7	8	9	10	11	12	13	14	15	16	17	18	19
BPOL_003_DIFF sensors	1	-.3	-.4	-.7	-.7	-.6	-.1	.3	-.3	.2	.1	.1	.2	-.0	.4	-.3	-.3	-.2	.3	.5	-.1	-.6	-.2	-.6	.0	-.2	.1	.3	.3	.3	-.1	.2	.0	-.4	-.5	-.0	-.2	-.3	-.4	-.3	-.1	.4	-.3	-.2	.0	-.0	-.1	.2	.2	-.5	-.1	.2	.5	.7	.5	-.4	.5
	2	-.2	-.3	-.5	-.7	-.8	-.4	.2	-.3	-.1	-.0	.1	-.1	.2	.5	-.5	-.4	-.2	.4	.5	-.1	-.7	-.3	-.8	.0	-.1	-.2	.0	.0	-.0	-.0	.2	.0	-.6	-.6	-.2	-.3	-.3	-.3	-.3	-.1	.5	-.5	-.3	.1	-.1	-.0	.2	.2	-.6	.1	.4	.7	.9	.6	-.4	.4
	3	.1	.4	.7	.2	.1	-.2	-.1	-.3	-.2	-.2	-.1	-.1	-.1	-.6	-.5	-.1	-.1	.1	.3	-.0	-.0	.2	.1	-.1	-.1	.1	-.1	-.1	-.1	-.2	.0	-.0	-.1	-.3	-.7	-.4	-.3	-.1	.1	.5	-.1	-.5	-.3	.3	-.1	-.0	-.1	.3	.5	-.5	-.7	-.4	-.0	.1	-.1	.1
	4	.4	.6	.9	.6	.5	-.1	-.3	-.1	-.3	-.3	-.2	-.1	-.1	-.6	-.2	-.1	.2	.1	.1	.1	.3	.1	.4	-.0	.0	-.1	-.2	-.2	-.2	-.1	-.3	-.1	.1	.1	-.4	-.0	.1	.3	.3	.1	-.3	.1	.1	.0	-.2	.2	-.2	.0	.5	-.1	-.5	-.5	-.3	-.3	.3	-.4
	5	.4	.5	.8	.9	.9	.3	-.3	.1	-.0	-.1	-.2	.2	-.4	-.7	.3	.1	.3	-.1	-.2	.2	.5	.2	.8	-.0	-.0	.1	-.1	-.1	-.0	-.2	-.3	-.1	.4	.4	-.2	.1	.3	.4	.4	.1	-.6	.4	.4	-.2	-.0	.1	-.3	.1	.7	-.3	-.6	-.8	-.8	-.6	.4	-.4
	6	.5	.5	.7	.9	.9	.2	-.4	.3	-.0	-.1	-.2	.1	-.3	-.7	.4	.0	.3	-.1	-.2	.3	.6	.1	.8	-.0	-.0	-.0	-.1	-.1	-.0	-.1	-.4	-.1	.4	.5	-.2	.3	.4	.4	.5	.1	-.7	.4	.4	-.3	.0	.2	-.3	.0	.7	-.2	-.5	-.7	-.8	-.6	.4	-.5
	7	.9	.8	.3	.7	.7	-.3	-.8	.1	-.3	-.4	-.5	.1	-.1	-.1	.5	-.6	.7	.5	.1	.7	.5	-.7	.4	-.0	-.2	-.4	-.3	-.2	-.1	-.2	-.9	-.3	.1	.7	.2	.9	.9	.1	.9	-.8	-.8	.6	.7	-.9	-.7	.9	-.6	-.3	-.0	.0	.0	-.1	-.5	-.8	.2	-.3
	8	.5	.6	.8	.9	.9	.2	-.4	.1	-.1	-.2	-.3	.2	-.4	-.7	.4	-.1	.4	.0	-.1	.3	.6	-.0	.8	-.0	-.2	.0	-.3	-.2	-.1	-.3	-.5	-.1	.3	.4	-.2	.3	.4	.4	.6	.0	-.7	.4	.5	-.3	-.2	.3	-.5	.1	.7	-.3	-.6	-.8	-.8	-.7	.4	-.5
	9	-.3	-.1	.5	.3	.3	.5	.3	-.0	.1	.1	.1	.1	-.3	-.6	-.0	.6	-.2	-.6	-.2	-.4	.2	.7	.5	-.0	.1	.4	.0	-.0	-.0	-.2	.3	.1	.4	-.1	-.3	-.5	-.4	.3	-.2	.7	-.0	-.1	-.2	.5	.4	-.5	.0	.3	.8	-.3	-.6	-.7	-.4	.0	.3	-.2
	10	-.5	-.5	-.3	-.4	-.3	.4	.4	.0	-.0	-.0	-.0	.2	-.1	.5	-.0	.2	-.3	-.2	.2	-.4	-.5	-.1	-.6	-.0	-.4	.1	-.2	-.2	-.2	-.4	.2	.0	-.3	-.3	.3	-.2	-.3	.4	-.4	.1	.6	.2	-.1	.2	-.1	-.3	-.0	.2	-.3	.4	.5	.3	.4	.4	.3	-.3
	11	-.1	-.0	.5	.4	.5	.6	.2	.2	.0	-.0	-.1	.2	-.3	-.5	.2	.5	-.1	-.5	-.3	-.3	.2	.4	.5	-.0	-.1	.4	-.2	-.2	-.1	-.3	.1	.1	.4	.1	-.0	-.2	-.1	.5	-.1	.5	-.1	.3	.1	.3	.1	-.3	-.2	.1	.7	-.0	-.4	-.7	-.6	-.2	.5	-.5
	12	-.3	-.4	-.6	-.6	-.5	.0	.3	-.0	-.0	.0	.0	.1	.2	.8	-.0	-.0	-.2	.1	.2	-.2	-.5	-.3	-.8	.0	-.2	-.1	-.1	-.1	-.1	-.1	.1	.0	-.4	-.2	.4	.0	-.1	.0	-.3	-.2	.6	.1	-.1	.0	-.2	-.1	.1	-.0	-.7	.5	.8	.7	.6	.4	.0	.0
	13	.1	.2	.6	.6	.7	.4	-.1	.2	.0	.0	-.0	-.0	-.1	-.5	.3	.4	.1	-.5	-.4	-.0	.5	.4	.8	-.0	.1	.2	-.1	-.1	-.0	-.0	-.1	.0	.5	.3	-.1	.1	.1	.4	.2	.3	-.4	.3	.3	.1	.1	-.1	-.2	-.1	.7	-.0	-.4	-.7	-.8	-.5	.4	-.4
	14	.0	-.1	-.4	-.2	-.2	-.2	-.1	.2	-.1	-.0	.1	-.3	.6	.7	.1	-.0	-.1	-.1	-.3	.1	.1	-.2	-.3	.0	.1	-.4	-.1	-.2	-.3	.2	-.1	-.1	-.1	.3	.5	.4	.2	.2	.0	-.4	.1	.3	.1	-.2	-.1	.2	.1	-.5	-.5	.7	.7	.6	.1	-.1	.2	-.2
	15	.3	.2	-.2	.1	.2	-.2	-.4	.2	-.1	-.0	.1	-.2	.4	.5	.3	-.1	.2	.0	-.3	.3	.3	-.3	-.0	.0	.1	-.5	-.2	-.1	-.2	.2	-.4	-.1	-.0	.5	.5	.6	.5	.2	.3	-.6	-.2	.5	.4	-.4	-.3	.4	-.1	-.5	-.4	.7	.6	.4	-.2	-.5	.3	-.3
	16	.2	.1	.1	.4	.4	.1	-.2	.3	.0	.1	.1	-.2	.3	.1	.5	.3	.1	-.4	-.6	.1	.6	.1	.4	.0	.2	-.2	-.1	-.1	-.2	.2	-.2	-.0	.3	.5	.3	.4	.4	.3	.2	-.2	-.3	.5	.4	-.2	-.0	.2	-.1	-.4	.1	.5	.2	-.1	-.6	-.6	.4	-.4
	17	-.0	-.1	-.1	.0	.1	.2	.0	.2	.1	.1	.1	-.0	.1	.4	.4	.5	.3	-.3	-.5	-.1	.2	.0	.0	.0	.1	-.1	-.0	-.1	-.1	.2	.0	.0	.2	.4	.5	.3	.2	.3	-.1	-.2	-.0	.5	.3	-.1	-.1	-.0	.0	-.4	-.1	.7	.5	.1	-.3	-.2	.3	-.2
	18	.1	.2	.5	.4	.4	.3	.0	-.1	.1	.1	-.1	.2	-.4	-.6	.2	.4	.4	-.1	-.3	-.1	.3	.4	.6	-.0	.1	.3	.1	.1	.1	.0	.1	.1	.4	.1	-.2	-.1	-.0	.1	.0	.3	-.3	.1	.2	.1	.2	-.2	-.0	.2	.7	-.4	-.6	-.8	-.5	-.2	.1	-.1
	19	.1	.1	-.2	-.3	-.3	-.3	-.0	-.3	.0	-.1	-.2	.3	-.3	.1	-.2	-.5	.3	.8	.7	.2	-.4	-.5	-.5	-.0	-.3	-.0	.1	.2	.2	-.2	-.1	-.1	-.4	-.3	-.2	-.0	-.0	-.3	.0	-.3	.1	-.2	.1	-.3	-.4	.2	-.1	.3	-.4	-.4	-.1	.2	.5	.3	-.3	.3
	20	.0	-.1	-.6	-.5	-.5	-.4	-.0	-.1	-.0	-.1	-.1	.1	.1	.6	-.2	-.5	.0	.6	.6	.2	-.5	-.6	-.7	.0	-.3	-.2	.0	.1	.1	-.1	-.1	-.1	-.5	-.2	.2	.2	.1	-.3	-.0	-.5	.3	-.0	.0	-.3	-.3	.2	.0	-.0	-.8	.1	.5	.7	.7	.3	-.3	.2
	21	-.1	-.1	.0	-.0	-.1	-.0	.1	-.1	.2	.2	.3	-.3	.2	-.3	-.2	.0	-.2	-.1	-.0	.3	.3	.4	.2	-.0	.3	.1	.2	.2	.2	.2	.2	.1	.2	-.1	-.3	-.2	-.2	-.3	-.1	.3	-.1	-.3	-.3	.3	.4	-.2	.3	.1	.1	-.5	-.5	-.2	.0	.1	-.3	.3
	22	-.2	-.1	.2	.1	.1	.1	.1	-.0	.1	.2	.3	-.4	.3	-.4	-.1	.4	-.3	-.5	-.4	-.0	.5	.7	.5	.0	.4	.1	.1	.0	-.0	.3	.3	.1	.4	.1	-.2	-.2	-.2	-.0	-.2	.4	-.2	-.2	-.2	.4	.5	-.3	.2	-.2	.4	-.1	-.4	-.3	-.3	-.1	-.0	.0
	23	-.1	.0	.4	.3	.4	.2	.1	.0	.1	.2	.2	-.2	.1	-.6	.0	.5	-.1	-.5	-.5	-.0	.6	.7	.7	.0	.4	.2	.2	.1	.1	.3	.2	.1	.5	.2	-.2	-.2	-.1	.0	-.1	.5	-.3	-.1	-.1	.3	.4	-.2	.2	-.1	.6	-.3	-.6	-.6	-.5	-.2	.0	-.0
	24	.1	.2	.5	.5	.5	.2	-.1	.1	.1	.1	.2	-.2	.0	-.6	.1	.4	.0	-.4	-.5	.0	.6	.7	.8	.0	.4	.1	.1	.1	.1	.3	.1	.1	.5	.3	-.2	-.1	.0	.1	.1	.4	-.4	.0	.0	.2	.4	-.1	.1	-.2	.7	-.2	-.6	-.7	-.6	-.3	.1	-.1
	25	.2	.2	.5	.5	.5	.2	-.1	.1	.1	.1	.1	-.2	-.0	-.6	.2	.3	.2	-.4	-.5	.1	.6	.5	.8	.0	.5	.2	.2	.2	.2	.3	.0	.0	.6	.4	-.2	.1	.1	.0	.1	.3	-.5	.1	.2	.1	.3	-.1	-.0	-.3	.6	-.2	-.5	-.6	-.7	-.4	.1	-.1
	26	.2	.3	.7	.6	.6	.3	-.1	.0	.0	.0	-.0	-.0	-.2	-.7	.2	.3	.2	-.3	-.3	.0	.5	.5	.8	-.0	.2	.2	-.0	.0	.0	-.0	-.1	.0	.4	.2	-.3	-.0	.1	.2	.2	.3	-.5	.2	.2	.1	.2	-.1	-.2	-.0	.8	-.3	-.7	-.8	-.7	-.4	.3	-.3
	27	-.0	-.2	-.6	-.4	-.4	-.2	-.0	.0	-.1	-.2	-.1	.1	.1	.8	.0	-.3	.0	.3	.2	.0	-.4	-.5	-.6	.0	-.3	-.2	-.1	-.1	-.1	-.1	-.1	-.1	-.4	-.0	.5	.3	.1	.0	-.1	-.5	.3	.2	.2	-.3	-.3	.2	-.1	-.2	-.7	.5	.8	.8	.5	.2	.0	-.0
	28	.0	.1	.6	.5	.5	.3	.0	.0	.1	.1	.1	-.1	-.1	-.7	.1	.4	-.0	-.4	-.4	-.1	.4	.6	.7	-.0	.2	.3	.1	.1	.1	.0	.1	.1	.5	.1	-.3	-.2	-.1	.1	.0	.5	-.3	-.0	-.0	.3	.3	-.2	-.1	.0	.8	-.3	-.7	-.8	-.6	-.3	.1	-.1
	29	.3	.2	.2	.4	.4	.1	-.3	.0	-.3	-.4	-.5	.4	-.4	.0	.3	-.2	.3	.1	.1	.3	.2	-.5	.1	-.1	-.7	.1	-.5	-.4	-.2	-.6	-.4	-.1	.1	.4	.3	.4	.4	.4	.4	-.2	-.3	.4	.4	-.4	-.5	.3	-.7	.1	.2	.0	.0	-.1	-.4	-.3	.4	-.5
	30	.1	.2	.6	.5	.6	.3	-.0	.0	.0	-.0	-.0	.0	-.2	-.6	.2	.4	.1	-.4	-.4	-.0	.5	.5	.8	-.0	.1	.3	-.1	-.0	-.0	-.1	.0	.0	.5	.2	-.2	-.1	.0	.2	.1	.4	-.4	.1	.1	.2	.2	-.1	-.2	.1	.8	-.3	-.6	-.8	-.7	-.3	.2	-.3
	31	-.0	-.1	-.1	-.1	.0	.1	.0	.0	-.3	-.3	-.4	.4	-.2	.4	.2	-.1	.0	-.0	.1	-.0	-.2	-.5	-.3	-.0	-.7	.2	-.4	-.4	-.3	-.5	-.1	-.0	-.1	.1	.5	.2	.1	.4	.1	-.2	.1	.3	.2	-.1	-.4	.1	-.5	.0	-.2	.3	.4	.3	.1	.1	.3	-.4
	32	.3	.2	-.4	-.1	-.1	-.4	-.4	.1	-.2	-.3	-.3	.1	.1	.6	.2	-.6	.3	.5	.3	.4	-.1	-.8	-.5	-.0	-.3	-.4	-.2	-.1	-.1	-.1	-.5	-.2	-.3	.3	.5	.6	.5	-.1	.4	-.8	-.1	.3	.3	-.6	-.5	.6	-.3	-.3	-.7	.3	.7	.7	.3	-.1	-.0	-.0
	33	.4	.4	.6	.7	.7	.1	-.3	.1	.0	-.0	-.1	-.0	-.2	-.7	.3	.1	.3	-.2	-.4	.2	.7	.3	.9	-.0	.2	.1	.0	.0	.1	.0	-.2	-.0	.6	.5	-.2	.2	.3	.1	.4	.2	-.7	.2	.3	-.1	.1	.2	-.2	-.1	.7	-.3	-.6	-.8	-.8	-.6	.2	-.2
	34	-.1	-.3	-.7	-.5	-.5	-.2	.0	.1	-.0	-.0	.0	.0	.2	.8	-.0	-.2	-.0	.2	.1	.0	-.4	-.5	-.7	.0	-.1	-.2	-.0	-.0	-.0	.1	.0	-.0	-.3	.0	.5	.2	.1	-.2	-.1	-.5	.4	.1	-.0	-.2	-.2	.1	.1	-.2	-.8	.4	.8	.8	.5	.2	-.2	.2
	35	-.1	-.0	.4	.3	.4	.4	.1	.1	.0	.1	.0	-.0	-.1	-.5	.1	.5	-.1	-.6	-.5	-.2	.4	.6	.7	-.0	.2	.4	.0	.0	.0	.0	.2	.1	.6	.3	-.0	-.2	-.1	.2	-.1	.5	-.3	.0	-.0	.3	.4	-.3	-.1	-.0	.7	-.2	-.5	-.7	-.6	-.2	.2	-.1
	36	-.3	-.5	-.8	-.6	-.5	.0	.2	.2	.0	.1	.1	.0	.2	.8	.0	.0	-.2	-.1	-.0	-.1	-.3	-.2	-.6	.0	-.1	.0	.0	-.0	-.0	.1	.2	.1	-.1	.1	.7	.2	-.0	-.1	-.3	-.3	.4	.1	-.1	-.0	-.0	-.1	.2	-.2	-.7	.4	.8	.7	.4	.3	-.1	.1
	37	-.0	.0	.2	.2	.1	.1	.1	-.0	.1	.1	.1	-.0	-.1	-.3	-.0	.1	-.0	-.1	-.0	.0	.2	.3	.2	-.1	.1	.1	.1	.1	.1	-.0	.1	.0	.2	-.0	-.2	-.1	-.1	-.0	-.0	.2	-.1	-.0	-.1	.1	.1	-.1	.1	.3	.3	-.3	-.4	-.4	-.2	-.1	-.0	.0
	38	-.6	-.7	-.8	-.9	-.9	-.0	.5	-.0	.1	.2	.3	-.2	.3	.7	-.3	.1	-.5	-.1	.1	-.3	-.6	.0	-.8	.0	.0	.0	.1	.0	-.0	.1	.5	.1	-.3	-.5	.2	-.3	-.5	-.3	-.6	.1	.7	-.4	-.6	.4	.3	-.4	.4	.1	-.7	.2	.6	.7	.8	.7	-.4	.4
BPOL_011_DIFF sensors	1	-.2	-.0	.2	-.0	-.1	-.0	.1	-.0	.1	.2	.3	-.3	.2	-.5	-.2	.2	-.4	-.3	-.2	-.1	.1	.5	.3	-.0	.3	.2	.1	.1	.0	.2	.3	.1	.2	-.2	-.6	-.4	-.3	-.3	-.1	.6	-.0	-.7	-.6	.5	.5	-.2	.2	.1	.4	-.5	-.5	-.4	-.1	.1	-.4	.4
	2	-.0	.2	.5	.1	.0	-.1	.1	-.2	-.0	.0	.1	-.3	.1	-.6	-.4	.1	-.3	-.2	.0	-.1	.1	.5	.3	-.0	.2	.1	.1	.0	.0	-.0	.2	.1	.1	-.3	-.7	-.5	-.4	-.2	-.1	.6	-.1	-.6	-.5	.4	.3	-.2	.1	.2	.6	-.5	-.7	-.5	-.1	.1	-.2	.2
	3	.2	.4	.4	.1	-.0	-.2	-.1	-.4	-.1	-.2	-.2	.2	-.3	-.3	-.4	-.4	.2	.4	.6	.1	-.2	-.2	-.1	-.0	-.2	-.0	.0	.1	.1	-.3	-.2	-.1	-.3	-.3	-.5	-.2	-.1	.0	.1	.0	-.1	-.2	.1	-.1	-.3	.1	-.2	.3	.2	-.3	-.4	-.1	.2	.2	.0	-.0
	4	.4	.6	.9	.7	.6	.1	-.3	-.2	-.2	-.3	-.4	.3	-.5	-.6	-.0	-.2	.4	.2	.3	.1	.2	-.1	.4	-.0	-.3	.1	-.1	-.0	.1	-.4	-.3	-.1	.1	.0	-.4	-.0	.1	.3	.4	.1	-.4	.3	.4	-.2	-.4	.2	-.4	.3	.6	-.4	-.7	-.6	-.4	-.3	.3	-.3
	5	.2	.4	.8	.7	.7	.3	-.1	-.1	-.1	-.2	-.2	.2	-.4	-.7	.1	.1	.2	-.2	-.0	.0	.4	.3	.7	-.0	-.1	.3	-.1	-.1	.0	-.3	-.1	-.0	.3	.2	-.3	-.1	.1	.3	.3	.4	-.4	.2	.2	.0	-.1	-.0	-.3	.2	.8	-.4	-.8	-.8	-.6	-.4	.3	-.3
	6	.3	.4	.8	.7	.8	.3	-.2	.0	-.1	-.1	-.3	.3	-.4	-.7	.3	.1	.2	-.2	-.1	.1	.4	.2	.8	-.0	-.1	.3	-.1	-.0	.0	-.3	-.2	-.0	.4	.3	-.2	.1	.2	.3	.4	.3	-.5	.3	.3	-.1	-.2	.1	-.4	.1	.8	-.4	-.7	-.8	-.7	-.5	.3	-.4
	7	.7	.6	.1	.5	.5	-.3	-.7	.3	-.2	-.3	-.4	.3	-.2	.1	.5	-.6	.6	.6	.1	.6	.3	-.8	.1	-.0	-.3	-.4	-.2	-.1	-.0	-.2	-.8	-.2	-.0	.6	.3	.8	.8	.1	.8	-.8	-.6	.6	.6	-.9	-.6	.8	-.5	-.3	-.3	.1	.2	.1	-.3	-.6	.2	-.2
	8	.5	.6	.8	.9	.9	.1	-.4	.2	-.1	-.1	-.2	.1	-.3	-.7	.4	.0	.4	-.1	-.3	.3	.7	.1	.9	-.0	.0	.0	-.1	-.0	.0	-.1	-.4	-.1	.5	.5	-.2	.3	.4	.3	.6	.0	-.7	.4	.4	-.3	-.1	.3	-.4	-.1	.7	-.3	-.6	-.8	-.9	-.7	.4	-.4
	9	-.4	-.3	.4	.1	.2	.6	.4	.0	.1	.2	.2	.0	-.2	-.5	-.0	.7	-.3	-.7	-.3	-.5	.1	.8	.4	-.0	.1	.4	.1	-.0	-.0	-.1	.5	.2	.4	-.2	-.2	-.5	-.5	.4	-.4	.8	.1	-.0	-.2	.6	.4	-.6	.1	.2	.7	-.1	-.4	-.6	-.3	.1	.3	-.3
	10	-.2	-.3	-.6	-.5	-.5	-.1	.1	.0	-.1	-.1	-.1	.1	.1	.7	-.0	-.2	-.1	.2	.3	-.1	-.5	-.5	-.7	.0	-.3	-.2	-.1	-.1	-.1	-.1	.0	-.0	-.4	-.1	.5	.1	.0	.0	-.2	-.4	.5	.1	.0	-.1	-.3	.1	.0	-.1	-.8	.5	.8	.8	.6	.3	.0	-.0
	11	-.1	.0	.6	.5	.6	.5	.1	.1	.0	.0	-.0	.1	-.3	-.5	.2	.5	-.1	-.6	-.4	-.2	.3	.5	.6	-.0	.0	.4	-.1	-.1	-.0	-.2	.2	.1	.5	.2	-.1	-.2	-.1	.5	-.0	.5	-.2	.2	.1	.3	.2	-.3	-.2	.0	.8	-.1	-.5	-.7	-.6	-.2	.4	-.4
	12	-.2	-.4	-.6	-.6	-.5	-.0	.2	.0	-.0	-.0	-.0	.1	.1	.8	-.0	-.1	-.1	.1	.2	-.1	-.5	-.4	-.7	.0	-.2	-.1	-.1	-.1	-.1	-.0	.1	.0	-.4	-.2	.5	.1	-.1	.0	-.3	-.3	.5	.1	-.0	-.1	-.2	-.0	.0	-.1	-.7	.5	.8	.8	.6	.3	-.0	.0
	13	.0	.2	.6	.5	.6	.3	-.0	.1	.1	.1	.1	-.1	-.1	-.6	.2	.4	-.0	-.5	-.4	-.1	.5	.6	.8	-.0	.2	.2	.0	.0	-.0	.0	.1	.1	.5	.2	-.3	-.1	-.0	.3	.1	.4	-.4	.1	.1	.2	.3	-.2	-.0	.0	.8	-.2	-.6	-.8	-.7	-.4	.3	-.3
	14	-.0	-.2	-.6	-.4	-.3	-.2	-.1	.2	-.0	-.0	.1	-.1	.4	.8	.1	-.2	-.1	.1	-.0	.1	-.1	-.4	-.5	.0	-.0	-.4	-.1	-.1	-.2	.1	-.1	-.1	-.3	.1	.5	.4	.2	.0	-.0	-.5	.2	.2	.1	-.3	-.2	.2	.1	-.3	-.7	.6	.8	.7	.3	.0	.0	-.0
	15	.1	-.0	-.4	-.2	-.2	-.3	-.3	.2	-.1	-.0	.1	-.2	.5	.7	.1	-.2	.0	.1	-.1	.2	.0	-.4	-.4	.0	.0	-.5	-.1	-.1	-.2	.2	-.3	-.1	-.2	.3	.5	.5	.3	.1	.1	-.6	.1	.3	.2	-.3	-.3	.3	.0	-.4	-.6	.7	.8	.7	.2	-.1	.1	-.2
	16	.0	-.1	-.5	-.3	-.3	-.2	-.1	.2	-.1	-.0	.0	-.1	.4	.8	.2	-.1	.0	.1	-.1	.1	-.1	-.4	-.5	.0	-.0	-.4	-.1	-.1	-.2	.1	-.1	-.1	-.3	.2	.5	.4	.2	.1	.0	-.5	.2	.3	.2	-.3	-.3	.2	.0	-.4	-.7	.7	.8	.7	.3	-.0	.1	-.1
	17	-.0	-.1	-.2	-.0	-.0	.0	-.1	.3	.1	.1	.1	-.1	.2	.4	.4	.3	.3	-.1	-.4	-.0	.1	-.1	-.1	.0	.2	-.2	.0	-.0	-.1	.3	-.0	-.0	.1	.3	.5	.4	.2	.2	-.0	-.3	.0	.5	.3	-.2	-.1	.0	.1	-.3	-.3	.6	.5	.2	-.1	-.2	.2	-.2
	18	-.0	-.1	-.3	-.3	-.3	-.1	.1	-.1	-.0	-.1	-.2	.2	-.2	.4	.1	.0	.4	.4	.1	-.1	-.4	-.3	-.4	.0	-.1	.0	.1	.1	.1	.1	.1	.0	-.2	-.1	.3	.1	.0	-.1	-.1	-.3	.2	.1	.1	-.1	-.2	-.0	.1	-.0	-.4	.2	.4	.2	.3	.2	-.1	.1
	19	.0	-.1	-.5	-.5	-.5	-.3	.0	-.1	-.0	-.1	-.1	.2	-.0	.5	-.1	-.4	.2	.6	.5	.1	-.5	-.6	-.7	.0	-.2	-.1	.1	.1	.1	-.0	-.0	-.0	-.5	-.2	.2	.1	.0	-.3	-.1	-.4	.3	-.1	.0	-.2	-.3	.1	.0	.0	-.7	.0	.4	.6	.6	.4	-.3	.3
	20	-.0	-.2	-.6	-.5	-.5	-.3	.1	-.1	.0	-.0	-.1	.2	-.0	.5	-.2	-.5	.0	.6	.5	.2	-.5	-.5	-.7	-.0	-.3	-.0	.1	.1	.2	-.1	-.0	-.0	-.4	-.2	.2	.1	.0	-.3	-.1	-.4	.3	-.1	-.0	-.2	-.3	.1	.0	.0	-.7	-.1	.4	.6	.6	.4	-.3	.3
	21	-.2	-.1	.2	.1	.1	.2	.2	-.0	.2	.3	.3	-.2	.1	-.5	-.2	.3	-.3	-.3	-.2	.0	.4	.7	.4	-.0	.3	.2	.3	.2	.2	.2	.3	.1	.3	-.1	-.4	-.4	-.3	-.2	-.2	.5	-.1	-.3	-.3	.4	.5	-.3	.3	.1	.4	-.5	-.6	-.5	-.2	.0	-.2	.2
	22	-.3	-.2	.2	.1	.1	.2	.2	.0	.2	.3	.4	-.4	.3	-.4	-.1	.5	-.3	-.6	-.5	-.2	.4	.8	.5	.0	.5	.1	.2	.1	-.0	.3	.4	.1	.4	.0	-.2	-.3	-.3	.0	-.3	.6	-.1	-.2	-.3	.5	.6	-.4	.3	-.1	.5	-.1	-.4	-.4	-.3	.0	.0	.0
	23	-.1	.0	.4	.3	.3	.2	.1	.0	.1	.2	.3	-.3	.1	-.5	-.0	.5	-.2	-.5	-.5	-.1	.5	.8	.7	.0	.5	.2	.2	.1	.0	.3	.3	.1	.5	.1	-.3	-.2	-.2	.1	-.1	.5	-.2	-.1	-.1	.4	.5	-.3	.2	-.1	.6	-.2	-.5	-.6	-.5	-.2	.1	-.0
	24	-.0	.1	.5	.4	.4	.2	.0	.0	.1	.2	.2	-.2	.0	-.6	.0	.5	-.1	-.5	-.5	-.1	.5	.7	.7	.0	.4	.2	.1	.1	.1	.2	.2	.1	.5	.2	-.3	-.2	-.1	.1	-.0	.5	-.3	-.0	-.0	.3	.4	-.2	.1	-.1	.7	-.2	-.6	-.7	-.5	-.2	.1	-.1
	25	.1	.2	.6	.5	.5	.3	-.0	.0	.1	.1	.1	-.1	-.1	-.7	.1	.4	.1	-.4	-.4	-.0	.5	.6	.8	.0	.3	.2	.1	.1	.1	.1	.1	.1	.5	.2	-.3	-.1	.0	.1	.1	.4	-.4	.1	.1	.2	.3	-.1	-.0	-.1	.8	-.3	-.7	-.8	-.6	-.3	.1	-.1
	26	.0	.1	.6	.5	.5	.4	.0	-.0	.0	.0	.0	.0	-.2	-.7	.1	.4	.0	-.4	-.3	-.1	.4	.6	.7	-.0	.2	.3	.1	.0	.1	-.0	.1	.1	.5	.1	-.3	-.2	-.1	.2	.0	.5	-.3	.1	.1	.2	.2	-.2	-.1	.0	.8	-.3	-.6	-.8	-.6	-.2	.2	-.2
	27	-.1	-.2	-.6	-.5	-.5	-.2	.0	.0	-.2	-.2	-.2	.1	.1	.7	-.0	-.3	.0	.3	.3	.0	-.5	-.6	-.7	.0	-.3	-.2	-.1	-.1	-.1	-.1	-.1	-.1	-.4	-.1	.5	.2	.1	-.0	-.1	-.5	.4	.1	.1	-.2	-.3	.2	-.0	-.1	-.8	.4	.7	.7	.5	.3	-.0	.0
	28	-.1	.0	.5	.4	.4	.3	.1	.0	.1	.2	.2	-.1	-.1	-.6	-.0	.5	-.1	-.5	-.4	-.2	.4	.7	.7	-.0	.3	.3	.1	.1	.1	.1	.3	.1	.5	.1	-.3	-.3	-.2	.1	-.1	.6	-.2	-.1	-.1	.4	.4	-.3	.1	.0	.8	-.3	-.6	-.7	-.5	-.1	.1	-.1
	29	-.2	-.3	-.6	-.6	-.6	-.2	.1	.0	-.1	-.1	-.1	.1	.2	.8	-.1	-.2	-.1	.2	.3	-.1	-.5	-.5	-.8	.0	-.2	-.2	-.1	-.1	-.1	-.0	.0	-.0	-.4	-.1	.5	.1	-.0	-.0	-.2	-.4	.5	.0	-.0	-.1	-.2	.1	.0	-.1	-.8	.5	.8	.8	.6	.3	-.1	.1
	30	-.4	-.3	.2	.0	.1	.5	.4	.1	.1	.1	.1	.0	-.1	-.2	.0	.6	-.3	-.6	-.3	-.4	.1	.6	.3	-.0	.0	.4	-.0	-.1	-.1	-.1	.4	.2	.4	-.1	-.1	-.4	-.4	.3	-.4	.6	.1	.0	-.1	.5	.4	-.5	.1	.1	.5	.0	-.2	-.4	-.2	.1	.2	-.2
	31	-.5	-.6	-.6	-.8	-.7	-.0	.4	-.1	.0	.0	.1	.1	.1	.7	-.2	.0	-.3	.0	.3	-.3	-.7	-.2	-.9	.0	-.3	.0	-.1	-.1	-.1	-.1	.3	.1	-.4	-.4	.3	-.2	-.4	-.0	-.5	-.1	.8	-.2	-.3	.2	-.0	-.3	.2	.2	-.7	.3	.6	.7	.8	.7	-.1	.1
	32	.2	.1	-.5	-.2	-.3	-.4	-.3	.1	-.2	-.2	-.2	.1	.1	.6	.1	-.5	.2	.5	.3	.3	-.2	-.8	-.6	.0	-.3	-.4	-.2	-.1	-.1	-.1	-.4	-.1	-.4	.1	.4	.5	.4	-.1	.2	-.7	.1	.2	.2	-.5	-.5	.5	-.1	-.2	-.8	.3	.7	.7	.4	-.0	-.1	.0
	33	.4	.5	.7	.8	.8	.1	-.4	.1	-.1	-.1	-.2	-.0	-.2	-.7	.3	.1	.3	-.2	-.4	.3	.7	.2	.9	-.0	.1	.1	-.1	-.0	.0	-.0	-.3	-.0	.5	.5	-.2	.2	.4	.2	.5	.1	-.7	.2	.3	-.2	.0	.2	-.3	-.1	.7	-.3	-.6	-.7	-.8	-.6	.2	-.3
	34	.0	-.1	-.6	-.4	-.4	-.3	-.1	.1	-.2	-.2	-.1	.0	.2	.6	.1	-.3	.1	.3	.2	.2	-.3	-.6	-.6	.0	-.2	-.3	-.2	-.2	-.2	-.0	-.2	-.1	-.3	.1	.5	.3	.2	-.1	.0	-.5	.2	.1	.0	-.3	-.3	.3	-.0	-.1	-.7	.3	.7	.7	.4	.1	-.1	.1
	35	-.1	-.3	-.7	-.5	-.5	-.2	.0	.1	-.1	-.1	-.0	.0	.2	.8	.1	-.2	-.0	.2	.1	.1	-.4	-.5	-.6	.0	-.1	-.2	-.1	-.1	-.1	.1	.0	-.0	-.2	.1	.6	.3	.1	-.1	-.1	-.5	.3	.1	.0	-.2	-.2	.1	.1	-.2	-.8	.4	.8	.8	.5	.2	-.1	.1
	36	-.2	-.4	-.7	-.4	-.4	-.1	.1	.2	-.1	-.1	-.0	-.0	.2	.7	.1	-.0	-.1	-.0	-.1	.0	-.2	-.3	-.4	.0	-.1	-.1	-.1	-.1	-.1	.1	.1	.0	-.1	.2	.7	.3	.1	-.1	-.1	-.4	.3	.1	-.0	-.1	-.0	.1	.1	-.3	-.7	.4	.7	.6	.3	.1	-.1	.1
	37	-.6	-.6	-.5	-.5	-.5	.2	.4	.2	.1	.2	.4	-.4	.5	.4	-.1	.5	-.5	-.6	-.6	-.3	-.0	.5	-.2	.0	.4	.0	.1	-.0	-.1	.4	.5	.2	.2	-.0	.3	-.2	-.3	-.1	-.6	.3	.4	-.2	-.5	.5	.6	-.4	.5	-.3	-.3	.3	.4	.3	.2	.3	-.1	.2
	38	-.7	-.7	-.7	-.8	-.8	-.1	.5	.0	.1	.3	.5	-.5	.6	.5	-.4	.3	-.7	-.4	-.2	-.3	-.4	.3	-.6	.0	.3	-.1	.1	-.0	-.2	.3	.6	.1	-.2	-.4	.0	-.4	-.5	-.3	-.6	.3	.6	-.6	-.7	.6	.6	-.4	.6	-.0	-.5	.2	.5	.6	.6	.6	-.4	.4

Figure 38: Correlation matrix between the errors in BPOL_003, BPOL_011 and RFLUX and IPOL.

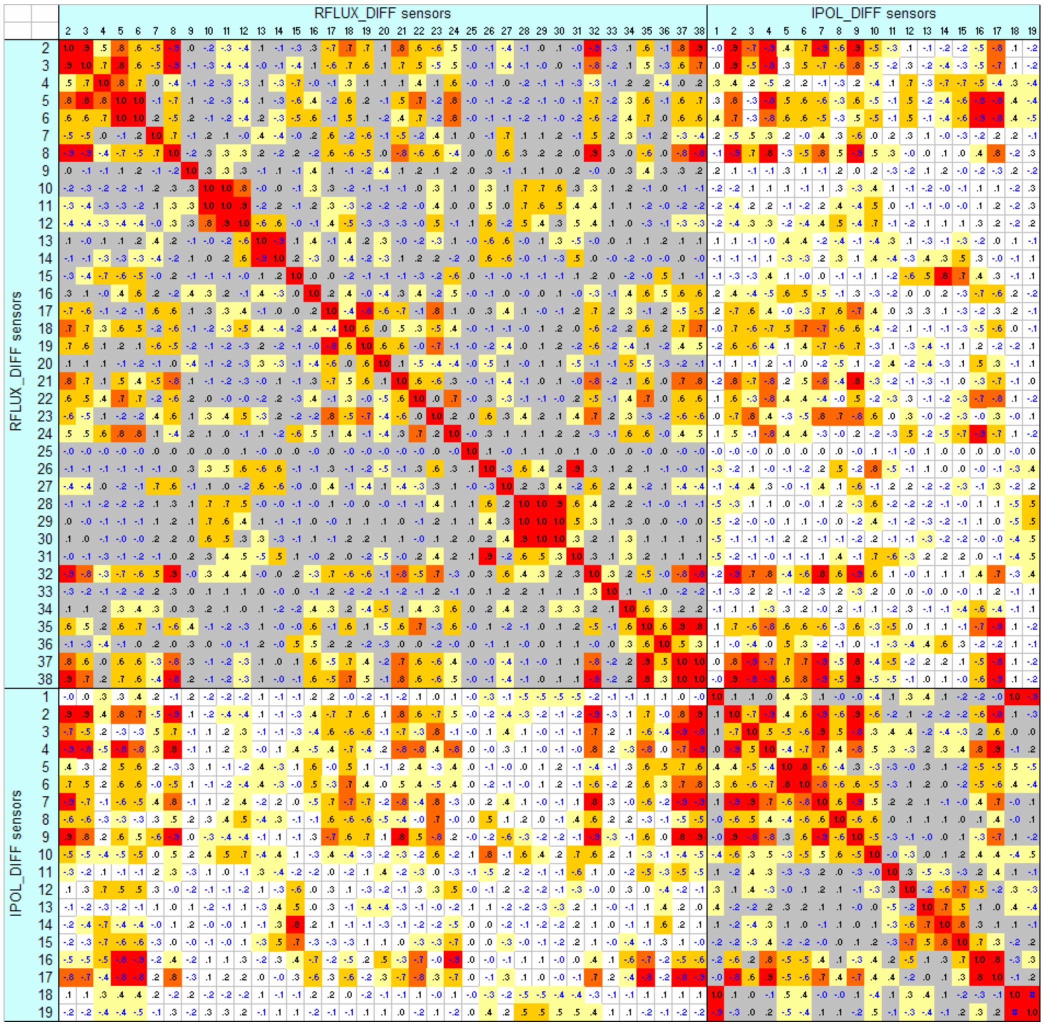

		RFLUX_DIFF sensors																																				IPOL_DIFF sensors																		
		2	3	4	5	6	7	8	9	10	11	12	13	14	15	16	17	18	19	20	21	22	23	24	25	26	27	28	29	30	31	32	33	34	35	36	37	38	1	2	3	4	5	6	7	8	9	10	11	12	13	14	15	16	17	18	19
RFLUX_DIFF sensors	2	1.0	.9	.5	.8	.6	-.5	-.9	.0	-.2	-.3	-.4	.1	-.1	-.3	.3	-.7	.7	.7	.1	.8	.6	-.6	.5	-.0	-.1	-.4	-.1	.0	.1	-.0	-.9	-.3	.1	.6	-.1	.8	.9	-.0	.9	-.7	-.9	.4	.7	-.9	-.6	.9	-.5	-.3	.1	-.1	-.2	-.2	-.5	-.8	.1	-.2
	3	.9	1.0	.7	.8	.6	-.5	-.9	-.1	-.3	-.4	-.4	-.0	-.1	-.4	.1	-.6	.7	.6	.1	.7	.5	-.5	.5	-.0	-.1	-.4	-.1	-.0	.0	-.1	-.8	-.2	.1	.5	-.3	.6	.7	.0	.9	-.5	-.8	.3	.5	-.7	-.6	.8	-.5	-.2	.3	-.2	-.4	-.3	-.5	-.7	.1	-.2
	4	.5	.7	1.0	.8	.7	.0	-.4	-.1	-.2	-.3	-.3	.1	-.3	-.7	-.0	-.1	.3	.1	.1	.1	.4	.1	.6	-.0	-.1	.0	-.2	-.1	-.1	-.3	-.3	-.1	.2	.2	-.4	.0	.2	.3	.4	.2	-.5	.2	.2	-.1	-.3	.2	-.4	.1	.7	-.3	-.7	-.7	-.5	-.4	.3	-.4
	5	.8	.8	.8	1.0	1.0	-.1	-.7	.1	-.2	-.3	-.4	.1	-.3	-.6	.4	-.2	.6	.2	-.1	.5	.7	-.2	.8	-.0	-.1	-.2	-.2	-.1	-.0	-.1	-.7	-.2	.3	.6	-.1	.6	.7	.3	.8	-.3	-.8	.5	.6	-.6	-.3	.6	-.5	-.1	.5	-.2	-.4	-.6	-.8	-.8	.4	-.4
	6	.6	.6	.7	1.0	1.0	.2	-.5	.2	-.1	-.2	-.4	.2	-.3	-.5	.6	-.1	.5	.1	-.2	.4	.7	-.2	.8	-.0	-.1	-.1	-.2	-.1	-.0	-.2	-.6	-.2	.4	.7	.0	.6	.6	.4	.7	-.3	-.8	.6	.6	-.5	-.3	.5	-.5	-.1	.5	-.1	-.4	-.6	-.9	-.8	.4	-.5
	7	-.5	-.5	.0	-.1	.2	1.0	.7	-.1	.2	.1	-.0	.4	-.4	-.0	.2	.6	-.2	-.6	-.1	-.5	-.2	.4	.1	.0	-.1	.7	.1	.1	.2	-.1	.5	.2	.3	-.1	.2	-.3	-.4	.2	-.5	.5	.3	.2	-.0	.4	.3	-.6	.0	.2	.3	.1	-.0	-.3	-.2	.2	.2	-.1
	8	-.9	-.9	-.4	-.7	-.5	.7	1.0	-.2	.3	.3	.3	.2	-.2	.2	-.2	.6	-.6	-.5	.0	-.8	-.6	.6	-.4	.0	.0	.6	.3	.2	.2	.0	.9	.3	.0	-.6	.0	-.8	-.8	-.1	-.9	.7	.8	-.3	-.5	.8	.5	-.9	.5	.3	-.0	.0	.1	.0	.4	.8	-.2	.3
	9	.0	-.1	-.1	.1	.2	-.1	-.2	1.0	.3	.3	.3	-.1	.1	-.1	.4	.1	-.1	-.2	-.4	.1	.2	.1	.2	.0	.3	-.1	.1	.1	.0	.2	-.0	.0	.3	.4	.3	.3	.2	.2	.1	-.1	-.1	.3	.1	-.1	.2	.0	.2	-.3	-.2	.1	.2	-.0	-.2	-.3	.2	-.2
	10	-.2	-.3	-.2	-.2	-.1	.2	.3	.3	1.0	1.0	.8	-.0	.0	-.1	.3	.3	-.2	-.1	-.1	-.1	.0	.3	.1	.0	.3	.1	.7	.7	.6	.3	.3	.1	.2	-.1	.0	-.1	-.1	-.2	-.2	.1	.1	.1	-.1	.1	.3	-.3	.4	.1	-.1	-.2	-.0	-.1	.1	.1	-.2	.3
	11	-.3	-.4	-.3	-.3	-.2	.1	.3	.3	1.0	1.0	.9	-.2	.2	-.1	.2	.3	-.3	-.2	-.2	-.2	-.0	.4	.0	.0	.5	.0	.7	.6	.5	.4	.4	.1	.1	-.2	-.0	-.2	-.2	-.2	-.4	.2	.2	-.1	-.2	.2	.4	-.4	.5	.0	-.1	-.1	-.0	-.0	.1	.2	-.2	.3
	12	-.4	-.4	-.3	-.4	-.4	-.0	.3	.3	.8	.9	1.0	-.6	.6	-.0	-.1	.4	-.5	-.3	-.3	-.3	-.0	.5	-.1	.1	.6	-.2	.5	.4	.3	.5	.4	.1	.0	-.3	-.1	-.3	-.3	-.2	-.4	.3	.3	-.2	-.4	.4	.5	-.4	.7	-.1	-.2	.1	.1	.1	.3	.2	-.2	.2
	13	.1	-.0	.1	.1	.2	.4	.2	-.1	-.0	-.2	-.6	1.0	-.9	.1	.4	-.1	.4	.2	.3	-.0	-.2	-.3	.1	-.0	-.6	.6	-.0	.1	.3	-.5	-.0	.0	.1	.1	.2	.1	.1	.1	.1	-.1	-.0	.4	.4	-.2	-.4	-.1	-.4	.3	.1	-.3	-.1	-.3	-.2	.0	.1	-.1
	14	-.1	-.1	-.3	-.3	-.3	-.4	-.2	.1	.0	.2	.6	-.9	1.0	.2	-.3	.0	-.4	-.2	-.3	.1	.2	.2	-.2	.0	.6	-.6	-.0	-.1	-.3	.5	.0	-.0	-.2	-.0	-.0	.0	-.0	-.1	-.1	-.1	.1	-.3	-.3	.2	.3	.1	.4	-.4	-.3	.4	.3	.5	.3	-.0	-.1	.1
	15	-.3	-.4	-.7	-.6	-.5	-.0	.2	-.1	-.1	-.1	-.0	.1	.2	1.0	.0	.0	-.2	-.1	-.1	-.1	-.3	-.2	-.6	.0	-.1	-.0	-.1	-.1	-.1	.1	.2	.0	-.2	-.0	.5	.1	-.1	-.1	-.3	-.3	.4	.1	-.0	.0	-.1	-.1	.1	-.2	-.6	.5	.8	.7	.4	.3	-.1	.1
	16	.3	.1	-.0	.4	.6	.2	-.2	.4	.3	.2	-.1	.4	-.3	.0	1.0	.2	.4	-.0	-.4	.3	.4	-.2	.5	-.0	-.1	.0	-.0	.0	.1	-.0	-.3	-.1	.4	.6	.5	.6	.6	.2	.4	-.4	-.5	.6	.5	-.5	-.1	.3	-.3	-.2	.0	.0	.2	-.3	-.7	-.6	.2	-.2
	17	-.7	-.6	-.1	-.2	-.1	.6	.6	.1	.3	.3	.4	-.1	.0	.0	.2	1.0	-.4	-.8	-.6	-.7	-.1	.8	.1	.0	.3	.4	.1	-.0	-.1	.2	.7	.2	.3	-.1	.2	-.5	-.5	.2	-.7	.6	.4	-.0	-.3	.7	.6	-.7	.4	.0	.3	.3	.1	-.3	-.2	.3	.2	-.1
	18	.7	.7	.3	.6	.5	-.2	-.6	-.1	-.2	-.3	-.5	.4	-.4	-.2	.4	-.4	1.0	.6	.0	.5	.3	-.5	.4	-.0	-.1	-.1	-.0	.1	.2	.0	-.6	-.2	.2	.6	.2	.7	.7	-.0	.7	-.6	-.7	.5	.7	-.7	-.6	.6	-.4	-.2	.1	-.1	-.1	-.3	-.5	-.6	.0	-.1
	19	.7	.6	.1	.2	.1	-.6	-.5	-.2	-.1	-.2	-.3	.2	-.2	-.1	-.0	-.8	.6	1.0	.6	.6	-.0	-.7	-.1	-.0	-.2	-.4	.0	.1	.2	-.2	-.6	-.2	-.4	.1	-.2	.4	.5	-.2	.6	-.6	-.4	.1	.4	-.7	-.6	.7	-.3	.1	-.3	-.4	-.1	.1	.2	-.2	-.2	.1
	20	.1	.1	.1	-.1	-.2	-.1	.0	-.4	-.1	-.2	-.3	.3	-.3	-.1	-.4	-.6	.0	.6	1.0	.1	-.5	-.4	-.4	-.0	-.5	.1	-.0	.1	.1	-.5	-.1	-.1	-.5	-.5	-.3	-.2	-.1	-.1	.1	-.1	.2	-.1	.0	-.2	-.5	.1	-.2	.4	-.2	-.4	-.3	.1	.5	.3	-.1	.1
	21	.8	.7	.1	.5	.4	-.5	-.8	.1	-.1	-.2	-.3	-.0	.1	-.1	.3	-.7	.5	.6	.1	1.0	.6	-.6	.3	-.0	-.1	-.4	-.1	.0	.1	-.0	-.8	-.2	.1	.6	.0	.7	.8	-.2	.8	-.7	-.8	.2	.5	-.8	-.4	.8	-.3	-.2	-.1	-.3	-.1	.0	-.3	-.7	-.1	.0
	22	.6	.5	.4	.7	.7	-.2	-.6	.2	.0	-.0	-.0	-.2	.2	-.3	.4	-.1	.3	-.0	-.5	.6	1.0	.0	.7	-.0	.3	-.3	-.1	-.1	-.0	.2	-.5	-.1	.4	.7	.0	.6	.6	.1	.6	-.3	-.8	.4	.4	-.4	-.0	.5	-.2	-.3	.3	-.1	-.2	-.3	-.7	-.8	.1	-.2
	23	-.6	-.5	.1	-.2	-.2	.4	.6	.1	.3	.4	.5	-.3	.2	-.2	-.2	.8	-.5	-.7	-.4	-.6	.0	1.0	.2	.0	.6	.3	.4	.2	.1	.4	.7	.2	.3	-.3	-.2	-.6	-.6	.0	-.7	.8	.4	-.3	-.5	.8	.7	-.8	.6	.0	.3	-.0	-.2	-.3	-.0	.3	-.0	.1
	24	.5	.5	.6	.8	.8	.1	-.4	.2	.1	.0	-.1	.1	-.2	-.6	.5	.1	.4	-.1	-.4	.3	.7	.2	1.0	-.0	.3	.1	.1	.1	.2	.2	-.3	-.1	.6	.6	-.0	.4	.5	.1	.5	-.1	-.8	.4	.4	-.3	-.0	.2	-.2	-.3	.5	-.2	-.5	-.7	-.9	-.7	.1	-.2
	25	-.0	-.0	-.0	-.0	-.0	.0	.0	.0	.0	.0	.1	-.0	.0	.0	-.0	.0	-.0	-.0	-.0	-.0	-.0	.0	-.0	1.0	.1	-.0	.1	.1	.0	.1	.0	.0	.0	-.0	.0	-.0	-.0	-.0	-.0	-.0	.0	.0	.0	.0	.0	-.0	.1	-.1	-.0	.1	.0	.0	.0	.0	-.0	.0
	26	-.1	-.1	-.1	-.1	-.1	-.1	.0	.3	.3	.5	.6	-.6	.6	-.1	-.1	.3	-.1	-.2	-.5	-.1	.3	.6	.3	.1	1.0	-.3	.6	.4	.2	.9	.3	.1	.2	.1	-.1	-.0	-.1	-.3	-.2	.1	-.0	-.1	-.2	.2	.5	-.2	.8	-.5	-.1	.1	.0	.0	-.0	-.1	-.3	.4
	27	-.4	-.4	.0	-.2	-.1	.7	.6	-.1	.1	.0	-.2	.6	-.6	-.0	.0	.4	-.1	-.4	.1	-.4	-.3	.3	.1	-.0	-.3	1.0	.2	.3	.4	-.2	.6	.2	.4	-.2	.1	-.4	-.4	-.1	-.4	.4	.3	-.0	-.1	.4	.1	-.6	-.1	.2	.2	-.2	-.2	-.3	-.1	.3	-.2	.2
	28	-.1	-.1	-.2	-.2	-.2	.1	.3	.1	.7	.7	.5	-.0	-.0	-.1	-.0	.1	-.0	.0	-.0	-.1	-.1	.4	.1	.1	.6	.2	1.0	1.0	.9	.6	.4	.2	.2	-.1	-.0	-.1	-.1	-.5	-.3	.1	.1	.0	-.0	.1	.2	-.3	.6	-.2	-.2	-.2	-.1	-.0	.1	.1	-.5	.5
	29	.0	-.0	-.1	-.1	-.1	.1	.2	.1	.7	.6	.4	.1	-.1	-.1	.0	-.0	.1	.1	.1	.0	-.1	.2	.1	.1	.4	.3	1.0	1.0	1.0	.5	.3	.1	.3	.0	.0	-.0	.0	-.5	-.2	-.0	-.0	.1	.1	-.0	.0	-.2	.4	-.1	-.2	-.3	-.2	-.1	.1	.0	-.5	.5
	30	.1	.0	-.1	-.0	-.0	.2	.2	.0	.6	.5	.3	.3	-.3	-.1	.1	-.1	.2	.2	.1	.1	-.0	.1	.2	.0	.2	.4	.9	1.0	1.0	.3	.2	.1	.3	.1	.1	.1	.1	-.5	-.1	-.1	-.1	.2	.2	-.1	-.1	-.2	.2	-.1	-.1	-.3	-.2	-.2	-.0	-.0	-.4	.5
	31	-.0	-.1	-.3	-.1	-.2	-.1	.0	.2	.3	.4	.5	-.5	.5	.1	-.0	.2	.0	-.2	-.5	-.0	.2	.4	.2	.1	.9	-.2	.6	.5	.3	1.0	.3	.1	.3	.2	.1	.1	.1	-.5	-.2	-.1	-.0	-.1	-.1	.1	.4	-.1	.7	-.6	-.3	.2	.2	.2	.0	-.1	-.4	.5
	32	-.9	-.8	-.3	-.7	-.6	.5	.9	-.0	.3	.4	.4	-.0	.0	.2	-.3	.7	-.6	-.6	-.1	-.8	-.5	.7	-.3	.0	.3	.6	.4	.3	.2	.3	1.0	.3	.2	-.5	-.0	-.8	-.8	-.2	-.9	.7	.8	-.4	-.6	.8	.6	-.9	.6	.1	-.0	.1	.1	.1	.4	.7	-.3	.4
	33	-.3	-.2	-.1	-.2	-.2	.2	.3	.0	.1	.1	.1	.0	-.0	.0	-.1	.2	-.2	-.2	-.1	-.2	-.1	.2	-.1	.0	.1	.2	.2	.1	.1	.1	.3	1.0	.1	-.1	.0	-.2	-.2	-.1	-.3	.2	.2	-.1	-.2	.3	.2	-.3	.2	.0	.0	-.0	.0	-.0	.1	.2	-.1	.1
	34	.1	.1	.2	.3	.4	.3	.0	.3	.2	.1	.0	.1	-.2	-.2	.4	.3	.2	-.4	-.5	.1	.4	.3	.6	.0	.2	.4	.2	.3	.3	.3	.2	.1	1.0	.6	.3	.2	.2	-.1	.1	.1	-.3	.3	.2	-.0	.2	-.1	.1	-.2	.3	-.1	-.1	-.4	-.6	-.4	-.1	.1
	35	.6	.5	.2	.6	.7	-.1	-.6	.4	-.1	-.2	-.3	.1	-.0	-.0	.6	-.1	.6	.1	-.5	.6	.7	-.3	.6	-.0	.1	-.2	-.1	.0	.1	.2	-.5	-.1	.6	1.0	.6	.9	.8	.1	.7	-.6	-.8	.6	.6	-.6	-.3	.6	-.3	-.5	.0	.1	.1	-.1	-.7	-.8	.1	-.2
	36	-.1	-.3	-.4	-.1	.0	.2	.0	.3	.0	-.0	-.1	.2	-.0	.5	.5	.2	.2	-.2	-.3	.0	.0	-.2	-.0	.0	-.1	.1	-.0	.0	.1	.1	-.0	.0	.3	.6	1.0	.5	.3	.1	-.0	-.4	.0	.5	.3	-.2	-.1	.0	-.1	-.3	-.4	.4	.6	.3	-.2	-.2	.1	-.1
	37	.8	.6	.0	.6	.6	-.3	-.8	.3	-.1	-.2	-.3	.1	.0	.1	.6	-.5	.7	.4	-.2	.7	.6	-.6	.4	-.0	-.0	-.4	-.1	-.0	.1	.1	-.8	-.2	.2	.9	.5	1.0	1.0	.0	.8	-.9	-.7	.7	.7	-.9	-.5	.8	-.4	-.5	-.2	.2	.2	.1	-.5	-.8	.1	-.2
	38	.9	.7	.2	.7	.6	-.4	-.8	.2	-.1	-.2	-.3	.1	-.0	-.1	.6	-.5	.7	.5	-.1	.8	.6	-.6	.5	-.0	-.1	-.4	-.1	.0	.1	.1	-.8	-.2	.2	.8	.3	1.0	1.0	-.0	.9	-.8	-.9	.6	.8	-.9	-.5	.9	-.5	-.5	-.1	.0	.1	-.0	-.6	-.9	.1	-.2
IPOL_DIFF sensors	1	-.0	.0	.3	.3	.4	.2	-.1	.2	-.2	-.2	-.2	.1	-.1	-.1	.2	.2	-.0	-.2	-.1	-.2	.1	.0	.1	-.0	-.3	-.1	-.5	-.5	-.5	-.5	-.2	-.1	-.1	.1	.1	.0	-.0	1.0	.1	.1	.0	.4	.3	.1	-.0	-.0	-.4	.1	.3	.4	.1	-.2	-.2	-.0	1.0	-.9
	2	.9	.9	.4	.8	.7	-.5	-.9	.1	-.2	-.4	-.4	.1	-.1	-.3	.4	-.7	.7	.6	.1	.8	.6	-.7	.5	-.0	-.2	-.4	-.3	-.2	-.1	-.2	-.9	-.3	.1	.7	-.0	.8	.9	.1	1.0	-.7	-.9	.4	.6	-.9	-.6	.9	-.6	-.2	.1	-.2	-.2	-.2	-.6	-.8	.1	-.3
	3	-.7	-.5	.2	-.3	-.3	.5	.7	-.1	.1	.2	.3	-.1	-.1	-.3	-.4	.6	-.6	-.6	-.1	-.7	-.3	.8	-.1	-.0	.1	.4	.1	-.0	-.1	-.1	.7	.2	.1	-.6	-.4	-.9	-.8	.1	-.7	1.0	.5	-.5	-.6	.9	.5	-.8	.3	.4	.4	-.2	-.4	-.3	.2	.6	.0	.0
	4	-.9	-.8	-.5	-.8	-.8	.3	.8	-.1	.1	.2	.3	-.0	.1	.4	-.5	.4	-.7	-.4	.2	-.8	-.8	.4	-.8	.0	-.0	.3	.1	-.0	-.1	-.0	.8	.2	-.3	-.8	.0	-.7	-.9	.0	-.9	.5	1.0	-.4	-.7	.7	.4	-.8	.5	.3	-.3	.2	.3	.4	.8	.9	-.1	.2
	5	.4	.3	.2	.5	.6	.2	-.3	.3	.1	-.1	-.2	.4	-.3	.1	.6	-.0	.5	.1	-.1	.2	.4	-.3	.4	.0	-.1	-.0	.0	.1	.2	-.1	-.4	-.1	.3	.6	.5	.7	.6	.4	.4	-.5	-.4	1.0	.8	-.6	-.4	.3	-.3	-.3	-.0	.3	.1	-.2	-.5	-.5	.5	-.5
	6	.7	.5	.2	.6	.6	-.0	-.5	.1	-.1	-.2	-.4	.4	-.3	-.0	.5	-.3	.7	.4	.0	.5	.4	-.5	.4	.0	-.2	-.1	-.0	.1	.2	-.1	-.6	-.2	.2	.6	.3	.7	.8	.3	.6	-.6	-.7	.8	1.0	-.8	-.6	.6	-.5	-.3	.1	.2	.0	-.2	-.5	-.6	.4	-.4
	7	-.9	-.7	-.1	-.6	-.5	.4	.8	-.1	.1	.2	.4	-.2	.2	.0	-.5	.7	-.7	-.7	-.2	-.8	-.4	.8	-.3	.0	.2	.4	.1	-.0	-.1	.1	.8	.3	-.0	-.6	-.2	-.9	-.9	.1	-.9	.9	.7	-.6	-.8	1.0	.6	-.9	.5	.2	.2	.1	-.1	-.0	.4	.7	-.0	.1
	8	-.6	-.6	-.3	-.3	-.3	.3	.5	.2	.3	.4	.5	-.4	.3	-.1	-.1	.6	-.6	-.6	-.5	-.4	-.0	.7	-.0	.0	.5	.1	.2	.0	-.1	.4	.6	.2	.2	-.3	-.1	-.5	-.5	-.0	-.6	.5	.4	-.4	-.6	.6	1.0	-.6	.6	.0	.1	.1	.1	.0	.1	.4	-.0	.1
	9	.9	.8	.2	.6	.5	-.6	-.9	.0	-.3	-.4	-.4	-.1	.1	-.1	.3	-.7	.6	.7	.1	.8	.5	-.8	.2	-.0	-.2	-.6	-.3	-.2	-.2	-.1	-.9	-.3	-.1	.6	.0	.8	.9	-.0	.9	-.8	-.8	.3	.6	-.9	-.6	1.0	-.5	-.3	-.1	-.0	.0	.1	-.3	-.7	.1	-.2
	10	-.5	-.5	-.4	-.5	-.5	.0	.5	.2	.4	.5	.7	-.4	.4	.1	-.3	.4	-.4	-.3	-.2	-.3	-.2	.6	-.2	.1	.8	-.1	.6	.4	.2	.7	.6	.2	.1	-.3	-.1	-.4	-.5	-.4	-.6	.3	.5	-.3	-.5	.5	.6	-.5	1.0	-.0	-.3	.0	.1	.2	.4	.4	-.4	.5
	11	-.3	-.2	.1	-.1	-.1	.2	.3	-.3	.1	.0	-.1	.3	-.4	-.2	-.2	.0	-.2	.1	.4	-.2	-.3	.0	-.3	-.1	-.5	.2	-.2	-.1	-.1	-.6	.1	.0	-.2	-.5	-.3	-.5	-.5	.1	-.2	.4	.3	-.3	-.3	.2	.0	-.3	-.0	1.0	.3	-.5	-.3	-.3	.2	.4	.1	-.1
	12	.1	.3	.7	.5	.5	.3	-.0	-.2	-.1	-.1	-.2	.1	-.3	-.6	.0	.3	.1	-.3	-.2	-.1	.3	.3	.5	-.0	-.1	.2	-.2	-.2	-.1	-.3	-.0	.0	.3	.0	-.4	-.2	-.1	.3	.1	.4	-.3	-.0	.1	.2	.1	-.1	-.3	.3	1.0	-.2	-.6	-.7	-.5	-.2	.3	-.3
	13	-.1	-.2	-.3	-.2	-.1	.1	.0	.1	-.2	-.1	.1	-.3	.4	.5	.0	.3	-.1	-.4	-.4	-.3	-.1	-.0	-.2	.1	.1	-.2	-.2	-.3	-.3	.2	.1	-.0	-.1	.1	.4	.2	.0	.4	-.2	-.2	.2	.3	.2	.1	.1	-.0	.0	-.5	-.2	1.0	.7	.5	.1	.0	.4	-.4
	14	-.2	-.4	-.7	-.4	-.4	-.0	.1	.2	-.0	-.0	.1	-.1	.3	.8	.2	.1	-.1	-.1	-.3	-.1	-.2	-.2	-.5	.0	.0	-.2	-.1	-.2	-.2	.2	.1	.0	-.1	.1	.6	.2	.1	.1	-.2	-.4	.3	.1	.0	-.1	.1	.0	.1	-.3	-.6	.7	1.0	.8	.3	.1	.1	-.1
	15	-.2	-.3	-.7	-.6	-.6	-.3	.0	-.0	-.1	-.0	.1	-.3	.5	.7	-.3	-.3	-.3	.1	.1	.0	-.3	-.3	-.7	.0	.0	-.3	-.0	-.1	-.2	.2	.1	-.0	-.4	-.1	.3	.1	-.0	-.2	-.2	-.3	.4	-.2	-.2	-.0	.0	.1	.2	-.3	-.7	.5	.8	1.0	.7	.3	-.2	.2
	16	-.5	-.5	-.5	-.8	-.9	-.2	.4	-.2	.1	.1	.3	-.2	.3	.4	-.7	-.2	-.5	.2	.5	-.3	-.7	-.0	-.9	.0	-.0	-.1	.1	.1	-.0	.0	.4	.1	-.6	-.7	-.2	-.5	-.6	-.2	-.6	.2	.8	-.5	-.5	.4	.1	-.3	.4	.2	-.5	.1	.3	.7	1.0	.8	-.3	.3
	17	-.8	-.7	-.4	-.8	-.8	.2	.8	-.3	.1	.2	.2	.0	-.0	.3	-.6	.3	-.6	-.2	.3	-.7	-.8	.3	-.7	.0	-.1	.3	.1	.0	-.0	-.1	.7	.2	-.4	-.8	-.2	-.8	-.9	-.0	-.8	.6	.9	-.5	-.6	.7	.4	-.7	.4	.4	-.2	.0	.1	.3	.8	1.0	-.1	.2
	18	.1	.1	.3	.4	.4	.2	-.2	.2	-.2	-.2	-.2	.1	-.1	-.1	.2	.2	.0	-.2	-.1	-.1	.1	-.0	.1	-.0	-.3	-.2	-.5	-.5	-.4	-.4	-.3	-.1	-.1	.1	.1	.1	.1	1.0	.1	.0	-.1	.5	.4	-.0	-.0	.1	-.4	.1	.3	.4	.1	-.2	-.3	-.1	1.0	#
	19	-.2	-.2	-.4	-.4	-.5	-.1	.3	-.2	.3	.3	.2	-.1	.1	.1	-.2	-.1	-.1	.1	.1	.0	-.2	.1	-.2	.0	.4	.2	.5	.5	.5	.5	.4	.1	.1	-.2	-.1	-.2	-.2	-.9	-.3	.0	.2	-.5	-.4	.1	.1	-.2	.5	-.1	-.3	-.4	-.1	.2	.3	.2	#	1.0

Figure 39: Correlation matrix between the errors in RFLUX, IPOL and RFLUX and IPOL.